Numerical Modeling for the Prediction of Primary Blast Injury to the Lung

by

Alexander D. Greer

A thesis
presented to the University of Waterloo
In fulfillment of the
thesis requirement for the degree of

Master of Applied Science

in

Mechanical Engineering

Waterloo, Ontario, Canada, 2006

I hereby declare that I am the sole author of this thesis. This is a true copy of the thesis, including any required final revisions, as accepted by my examiners.

I understand that my thesis may be made electronically available to the public.

ABSTRACT

As explosive blasts continue to cause casualties in both civil and military environments, there is a need for increased understanding of the mechanisms of blast trauma at the organ level and a need for a more detailed predictive methodology. A fundamental understanding of blast injury will lead to the development of improved protective equipment and ultimately reduce the severity of injury. Models capable of predicting injury to varied blast loading will also reduce the emphasis on animal blast testing. To provide some historical context, this research was begun shortly after the U.S. led invasion of Iraq, and came to a close while there continues to be daily loss of life from blast injuries in the Middle East, as well as continued threats of terrorism throughout the world. In addition to industrial accidents, it is clear that blast injury is far more than just a military concern.

Simplified finite element models of the human and sheep thoraces were created in order to provide practical and flexible models for the prediction of primary blast injury in simple and complex blast environments, and subsequently for the development of improved protective equipment. The models were created based on actual human and sheep geometries and published material properties. The fluid-structure interaction of the models compared well with experimental blast studies carried out during the course of the research, as shown by comparing actual and predicted overpressures in the free field and at the thorax.

By comparing the models to published experimental data from simple blasts, trends in the results were verified and peak lung pressure was proposed as a trauma criterion. Local extent of injury in the lung is correlated to the peak pressure measured in each finite element, categorized as no injury (< 60 kPa), trace (60-100 kPa), slight (100-140 kPa), moderate (140-240) and severe (> 240 kPa). The calculation of the mean value of the peak lung pressures of all of the finite elements allows for an overall estimate of the injury level, with 35 kPa predicting threshold damage, 129 kPa for one percent lethality, and 186 kPa for fifty percent lethality. The simple blast results also compared well to the

predictions of two previously validated mathematical models. Variation of predicted injury within a given loading severity was 15%, which is comparable to the model by Stuhmiller that had a variation of 20%. The model by Axelsson had very little variation (1.4%), but the differences between levels of severity were quite small, and often difficult to decipher. In addition to predicting consistent levels of injury, the finite element models were able to provide insight into the trauma mechanism, map the extent of injury through the lungs, and validate a local injury criterion.

The models were then applied to predict injury under complex blast loading by subjecting the human finite element torso to a threshold level blast while located at varying distances from a wall or a corner. The results compared well to the validated mathematical models, showing a sharp increase in injury severity as the model approached the reflecting surface. When directly against the wall, the mean of the peak lung pressure values was 57 kPa, and in the corner, the mean value reached 69 kPa. Although these values did not reach the level representing one percent lethality, they do represent a significant increase in injury above threshold as a direct result of the surrounding geometry. Once again, the finite element models correctly showed injury trends and lung injury patterns reported in experiments. The models predicted the level of injury and were able to predict the time varying pattern of injury, which is something existing models cannot do.

Having designed the models from physical principals, and having validated the models against published results, they can now be used in the continued development of protective equipment. Acknowledging that this model was the first iteration, the author believes that improvements in material properties, mesh refinement, and the investigation of other possible parameters for the prediction of injury will lead to substantial advances in the understanding of primary blast injury.

ACKNOWLEDGMENTS

To list all of the individuals who are partly responsible for helping me complete this thesis would add significant heft to this collection of paper. There are, however, certain people who must clearly be thanked.

Starting at the beginning, I definitely would not be where I am, or who I am if it weren't for the unending support and guidance from my parents, Paul & Cynthia Greer and my entire family. Although it may have taken me a while to realize it, I can now see clearly how lucky I am to be part of such a big, caring family.

At Waterloo, Darrel Doman, Christian Kaufmann, Patrick Forbes and many others helped make this a couple of the best years, with a lot of laughs, a lot of life, and a little bit of work. Thank you to my supervisor, Dr. Duane Cronin for his support and guidance, and for having allowed me the academic freedom to explore, and to draw my own box in the sand. Research of this scope would not have been possible without my co-supervisor, Dr. Kevin Williams and the support of Defense Research and Development Canada – Valcartier. And finally, I owe a great deal of thanks to Chris Salisbury, who provided so much technical assistance and the occasional shot of motivation whenever things looked gloomy.

The last person I'd like to thank is my wife, Karen, who has always been there to encourage me, and to keep me on the right track. I truly could not have done it without you. Thank you.

TABLE OF CONTENTS

LIST OF FIGURES

LIST OF TABLES

Chapter 1 Introduction

1.1 Motivation

In times of both peace and war, there are appreciable reports in the news of civilians and military personnel dying of blast related injuries. Unfortunately, due to the chaotic nature of the environment surrounding most of these blasts, accurate statistics are difficult to find, and of limited accuracy. Blast injuries can result from industrial accidents, war-time activities, terrorist assaults, or even the repeated exposure to high powered industrial equipment or weapons. One important subset of blast related trauma, and the focus of this research, is primary blast injury: those injuries which occur as a direct result of the interaction and transmission of pressure waves through the body, primarily affecting air-filled organs, such as the lungs.

There is currently a lack of fundamental understanding regarding the actual tissue damage mechanisms that lead to primary blast injury, even in simple blast environments. This understanding is considered essential to develop the next generation of personal protective equipment, vehicles and structures to protect against primary blast injury. Currently, the design of protective equipment must rely heavily on experimental validation using animal studies. Aside from the ethical questions of such studies, there is also a significant cost involved, and the results are typically difficult to interpret as they relate to humans. Complex blasts resulting from some explosives or exposure within confined areas create an additional challenge, and the effects on injury outcome are not well understood.

Some simple models currently in use have been correlated to extensive blast studies, and are able to reasonably predict primary blast injury when provided with measured pressure-time curves. Unfortunately, these models tend to have narrow regions of applicability, providing little explanation of primary blast injury or insight into the related

injury mechanisms. Even the models that have been validated for complex blast cannot be used currently in the development of personal protective equipment due to the nature of the experimental setup required to measure the desired inputs.

The primary goal of this research was to develop a numerical model capable of predicting primary blast injuries in simple and complex environments, while being flexible enough to be used as an engineering tool for the development of protective equipment. This model also provides insight into the mechanisms of trauma, reducing our dependency on animal testing.

1.2 Background

Although reports of soldiers dying without external signs of injury – now understood to result from blast waves interacting with the body - started to be investigated during the Spanish civil war (1936-1939), much of the focused research on primary blast injury began during World Wars I and II. As other forms of protection improved, and as flack vests became commonplace, the prevalence of lung trauma as the primary mode of injury increased [Bellamy, 1991]. In addition to the casualties of war, terrorism in the past quarter century has produced vast numbers of victims, many of whom have been subject to significant blast pressures from large explosive devices – making blast injury a worldwide, and population wide concern.

The research into, and the importance of primary blast injury has increased for a host of reasons, including the ongoing threat of nuclear weapons [Elsayed, 1997]. Blast injury becomes paramount for crews of modern armoured vehicles in which the threat of fragments and fire has been reduced [Bellamy, 1991]. Thermobaric weapons are now being used that have been designed to use the blast energy to injure, as opposed to using fragments. Larger and more powerful weapons have become a threat to the user as repeated exposure to lower-pressure waves is causing blast-related injuries [Bellamy, 1991]. Another significant concern making blast injuries relevant in the current climate is

the enhancing effect that the urban environment has on pressure wave driven injuries through reflection and superposition of blast waves in confined areas.

Significant blast injury research began in the 1950's, related to significant long-duration blast loading from nuclear weapons. The initial experimental and theoretical work of Clemedson [Clemedson, 1956] pointed out many findings and assumptions that still form the basis of our understanding: blast injury is a pressure wave dominated effect; gas-containing organs are the most vulnerable; pulmonary edema and arterial air emboli are the main causes of death; pressure, duration and wave form shape are related to the injury outcome. Based on this work, Bowen et al. developed a substantial blast injury pathology database from experimental blast studies. From this database, Bowen and his colleagues created the Bowen curves [Bowen, 1968], a simple empirical model using the peak pressure and duration of the blast wave to predict injury outcome. While this work is invaluable and remains relevant, it is limited since it is a load-based injury criterion, defined for specific conditions. The relevance and applicability of the Bowen curves in complex blast environments is also not well understood.

Based on extremely simplified mathematical and fluid-mechanics models of the human torso, Axelsson et al [Axelsson, 1994] and Stuhmiller et al [Stuhmiller, 1996] managed to correlate physical responses of the models to the threat level of the input pressure-time curve. Axelsson tied the lethality of the wave to the peak inward chest wall velocity of the model, while Stuhmiller quantified the lethality by defining the normalized work, a measure of energy absorbed by the lung. While both of these models tend to correlate with simple and complex blast data, they are still a step removed from the actual injury, and provide limited insight into the mechanisms of injury. Of significant importance, these approaches are limited in terms of protection development since they are based on blast pressure measurements.

1.3 Research Objective and Scope

The primary goal for this research was the development of a finite element model capable of predicting primary blast injury and assisting in the development of personal protective equipment. While a human model is required, a sheep model was also created for direct comparison to the animal test data available in the literature, and to compare results of sheep studies and scaling to humans. Material models and properties were gathered primarily from the literature and from studies conducted at the University of Waterloo, except in the case of lung tissue, where a specialized model was created to account for its unique properties, and the specific requirements of this model.

A flexible and representative air blast model was then developed to accurately simulate both simple and complex blast environments. With the models embedded into the air blast model, the fluid-structure coupling was validated with experimental blast studies carried out at DRDC Valcartier. Once the modeling approach was validated, the actual models were validated under simple blast loading against the Bowen curve predictions of injury level, and an appropriate injury criterion was defined. The models were then compared to the Axelsson and Stuhmiller models, in both simple and complex blast. These comparisons prove the applicability of the model, and provide insight into the foundations of primary blast injury. At the conclusion of this study, the model will be ready to be used for the design and optimization of personal protective equipment and the ongoing study of primary blast injury. It must also be noted that a recent publication [Bass, 2006] has offered further modifications to the Bowen curves, reinforcing that the understanding of primary blast injury is ever evolving, and that it is hoped that the model will continue to evolve as more information comes to light.

Chapter 2 Literature Review

The primary goal of this research was the development and validation of a numerical model for the prediction of primary blast injury to the lung, which requires a detailed understanding of blast loading and related physics. Blast injuries in general are explained in terms of their causes, and their effects on different parts of the body, focusing on the respiratory system. Experimental data are presented, detailing how the information was collected, and highlighting the most relevant findings. In order to assess the results of the numerical modeling completed for this research, other forms of injury prediction and significant numerical modeling projects are explored, including research lead by Bowen, Stuhmiller and Axelsson.

2.1 Blast Loading

Blast loading may occur from a variety of different sources, with the common aspect being a high transient pressure. In a civilian environment, controlled detonations are necessary in numerous industries such as mining, the construction of canals, or the destruction of buildings. Blast waves that are of interest to the military include: the repeated, low pressure pulse from the firing of large caliber weapons; high pressure, short duration explosive blasts; and medium pressure, long duration blast waves from nuclear weapons. However, not all explosives create shock waves. Explosives can be categorized as high explosives or low explosives, depending on their reactions to certain conditions. High explosives, such as nitroglycerine, TNT, C-4, Semtex and dynamite are defined as those that can readily detonate without being confined, thus leading to a supersonic over-pressurization shock wave. It is this shock wave, or discontinuity in the pressure field as it interacts with the human body that leads to blast injuries. Low explosives, or burning mixtures, are those that will burn relatively slowly and will only explode when sufficiently confined. A typical low explosive, gun powder, will burn if ignited by a heat source, but will detonate when subjected to an impulsive force, such as from a hammer or

detonator, while confining the explosive. It is this detonation that creates the shock wave, and extremely rapid release of energy [Meyers, 1994; Johansson, 1970; Kinney, 1962].

In addition to the standard high- and low-explosives, there exists a class of exotic munitions that are characterized by a rather different pressure profile. Volumetric-type blasts refer to thermobaric munitions, fuel-air explosives or enhanced blast munitions designed to cause damage by means of blast overpressure, rather than fragmentation.

For the purposes of this research, the source of the blast is of little interest, but the characterization of the blast wave and pressure field is of great importance. Blast overpressure (BOP) is defined as the pressure, in excess of ambient atmospheric pressure, that directly follows a shock wave. Blast is sometimes referred to as acoustical energy impulse noise due to its physical similarity to sound waves of extremely large amplitude. In terms of overpressure, typical sound levels in the human audible range are 20 micropascals (μPa) to the threshold of pain at around 20-150 Pa (depending on frequency), whereas blasts from explosions can produce pressures in the range of 10 to 1000 kilopascals, depending on the explosive and environmental factors [Januszkiewicz, 1997; NPL, UK, 2005].

Upon detonation, a high explosive undergoes a chemical reaction and is transformed into a region of extremely high pressure, high temperature gas that rapidly expands into a volume at least 10^5 times greater than the original substance [Bellamy, 1991]. Blast overpressures in air decrease approximately as the inverse cube of distance from the explosion [Mellor, 1992]. Perhaps the most significant difference between sound waves and blast waves is the sharp instantaneous rise in ambient atmospheric pressure at the leading edge of the wave. The state of a gas or liquid can be characterized by temperature, pressure and density, which are related to one another through an equation of state (EOS). The most commonly known EOS is the ideal gas equation, which can be used for gases at low pressures and high temperatures, where the molecules are relatively far apart and have negligible effects on one another. However, this simple equation is not sufficient to describe the state within a shock wave due to the high pressure and relative

proximity of the molecules, or to describe the shock properties of tissues as the molecules exert significant forces on one another. For a more complete description of the pressure-volume relationship, the Gruneisen equation of state calculates pressure based on volume change using material-specific data from a curve defining the velocity of a shock wave relative to the particle velocity (U_s-U_p curve). The Gruneisen EOS uses the speed of sound in the uncompressed material, the density change, and various other material dependant constants. The Gruneisen EOS is explained in more detail in Section 3.4.2.

If a small region of moderately elevated pressure is released in an enclosed area, the higher pressure is dissipated throughout the environment by pressure waves traveling outward until an equilibrium pressure is achieved at the new slightly elevated ambient pressure. The speed at which the pressure waves travel outwards is the local speed of sound, or the wave speed of an infinitesimal disturbance. The speed of sound in air and water at atmospheric conditions are approximately 340 m/s and 1500 m/s, respectively. If the pressure difference is sufficiently high, the force of the expanding gas may accelerate the nearby molecules to a velocity exceeding the original speed of sound. If the outward traveling pressure waves cannot dissipate the high pressure quickly enough, there is a build up of pressure at the wave front. This discontinuity in pressure, density and temperature is known as a shock wave. The speed of sound in a medium increases with pressure, so the high-pressure wave is then capable of traveling at a speed greater than the sound speed of the ambient medium. The final speed of the shock wave is determined by the pressure differential between the high pressure region, and the undisturbed region [Bellamy, 1991; Meyers, 1994].

2.1.1 Simple and Complex Blast Waves

Blast waves can be generally classified as simple or complex. The detonation of a typical high explosive in an open space produces a simple, or so-called Friedlander wave, the name coming from the simple equation used to describe the pressure history (see below). A simple blast wave is characterized by an instantaneous increase in pressure to a peak value (P^+) followed by an exponential decay to sub-atmospheric conditions (P^-) and then

a slow return to atmospheric pressure (P_{atm}), as shown in Figure 2.1. The length of time from the initial peak until the pressure drops to atmospheric is termed the positive phase duration (T^+), followed by the negative phase duration (T^-) that lasts until the pressure returns to the ambient level. To deal with real, non-ideal waves (not perfectly smooth, small reflections, etc.) some experimental studies define the end of the negative phase duration as the time at which the difference between the overpressure and the initial ambient pressure is less than 10% of the peak pressure [Elsayed, 1997]. The pressure profile is dependant on the type of explosive, charge size and shape, density of travel medium (air, water) and wave reflections due to the ground, walls, etc. In order to put such blast waves in perspective, the positive phase duration for conventional explosives is generally a few milliseconds, but for large nuclear blasts it can last up to several seconds [Januszkiewicz, 1997]. Weapon noise usually reaches a maximum overpressure of less than one atmosphere with durations of less than five milliseconds and negligible blast winds. Nuclear detonations, however, can produce overpressures of several tens of atmospheres accompanied by blast winds of several hundred miles per hour [Bellamy, 1991]. If these blast winds are channeled by corridors or alleys, the speeds can be magnified substantially.

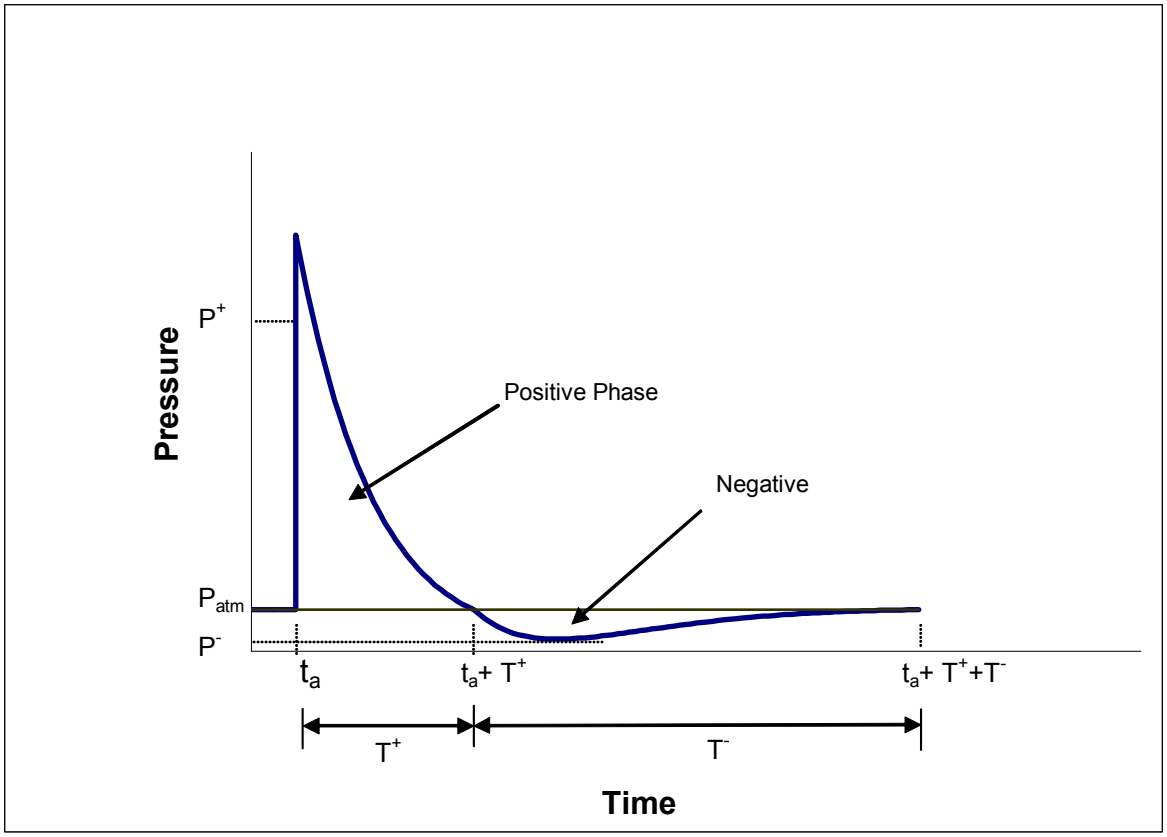

Figure 2.1: Simple blast wave showing peak overpressure and the durations of the positive and negative phases.

A mathematical representation of the positive phase of a simple blast wave is described by the modified Friedlander curve:

$$p(t) = p_o + P^+\left(1-\frac{t}{T^+}\right)e^{-\frac{bt}{T^+}} \tag{2.1}$$

Here the pressure is a function of the peak pressure, P^+, the positive phase duration, T^+, and an empirically fit parameter, b. The time, t, is measured from the time of arrival, t_a. The negative phase is described by the following equation:

$$p(t) = p_o - P^-\left(\frac{t}{T^-}\right)\left(1-\frac{t}{T^-}\right)e^{-4\frac{t}{T^-}} \tag{2.2}$$

Similarly, the negative phase is described by the underpressure (vacuum), P^-, and the negative phase duration, T^-. The values for the peak pressures and phase durations are derived from experimental measurements. The decay constant is typically related to the

type of explosion, the environment, and the proximity to the blast [Salisbury, 2004; Josephson, 1988].

A complex blast wave is typically the result of wave reflections and refractions resulting from interactions with the local environment (e.g. a wall or enclosure) or created by enhanced blast munitions. The former is generally characterized by a wave that arrives in a stepped fashion, with repeated rises and drops in pressure, while the latter is characterized by a sustained duration at high pressure [Mayorga, 1997; Bellamy, 1991]. Complex blast waves are often characterized by the impulse of the positive phase duration, mathematically described as the integral of pressure multiplied by time, $\int p \cdot dt$. Pressure time histories are shown in Figure 2.2 below, with (a) an idealized simple blast wave, (b) a recorded simple blast wave with some deviation from the ideal condition, and (c) a complex wave recorded near a shoulder fired weapon fired from inside a bunker. Figure 2.2 (d) shows a complex blast wave recorded inside a defeated armoured vehicle.

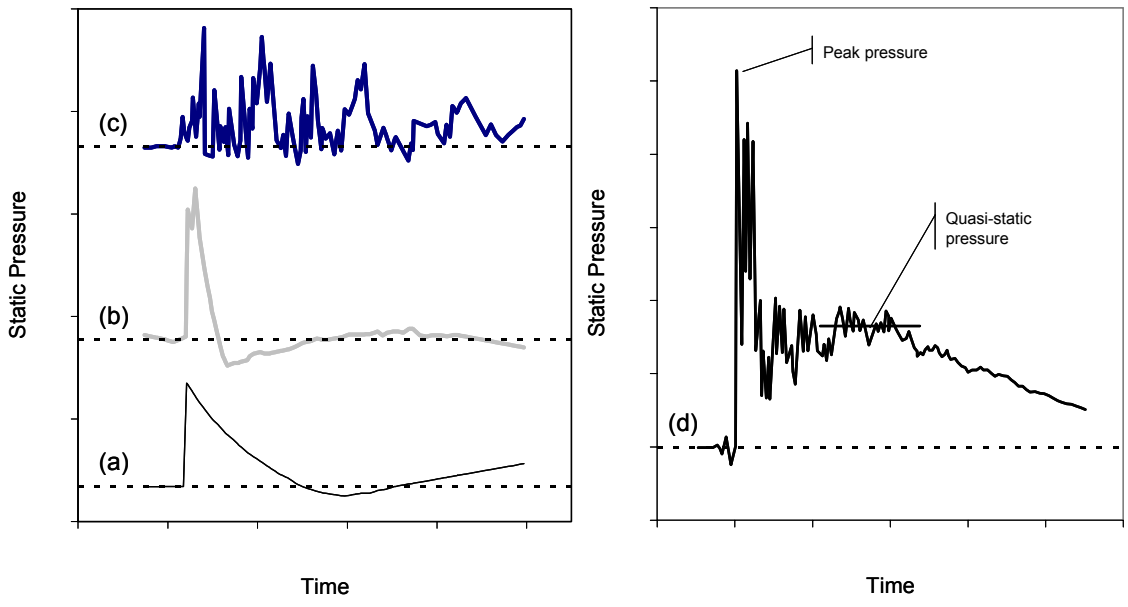

Figure 2.2: Pressure-time histories of various blast signatures: (a) idealized Friedlander (simple) wave, (b) recorded simple blast wave, (c) complex wave from a weapon fired from an enclosure (d) complex blast wave recorded inside a defeated armoured vehicle. Dashed line indicates ambient pressure [Mayorga, 1997; Bellamy, 1991].

It must also be noted that the measure of pressure shown in Figure 2.2 is the static pressure, also known as the side-on pressure. This is typically measured using a lollipop gauge, a device with a knife edge aligned parallel to the direction of the blast flow so that there is minimal disturbance of the flow (described in more detail in Section 4.7.1: Experimental Test Setup). The static pressure is the pressure that a particle traveling with the flow would sense. Dynamic pressure is caused by the movement of air displaced by the explosive products, and is also known as blast wind. The blast wave caused by a high explosive detonation must be distinguished from blast wind which can be produced by both HE and low explosives [CDC, 2005]. Total pressure is the summation of the static and dynamic pressures, and can be measured by placing a specially designed sensor, such as a pitot tube, perpendicular to the blast flow. When a fluid flow is forced to stop at a stagnation point (the gauge or a bluff body), the kinetic energy converts to pressure resulting in the total pressure (static + dynamic). This resultant build up of pressure in front of a wall or the body can significantly affect trauma outcome, which is why a thorough understanding of pressure waves is required in order to predict injury.

Reflected pressure is defined as the maximum pressure measured at a wall, or rigid interface placed normal to the blast flow. Figure 2.3 shows the effect of increasing peak static pressure of a blast wave on the pressure and velocity parameters in the flow. Dynamic and reflected pressure builds quickly as the higher pressure blast wave displaces great amount of air. The figure on the right shows how the shock velocity increases with increasing pressure, allowing for a large pressure differential to drive a shock wave at a speed far in excess of the sound speed at ambient pressure.

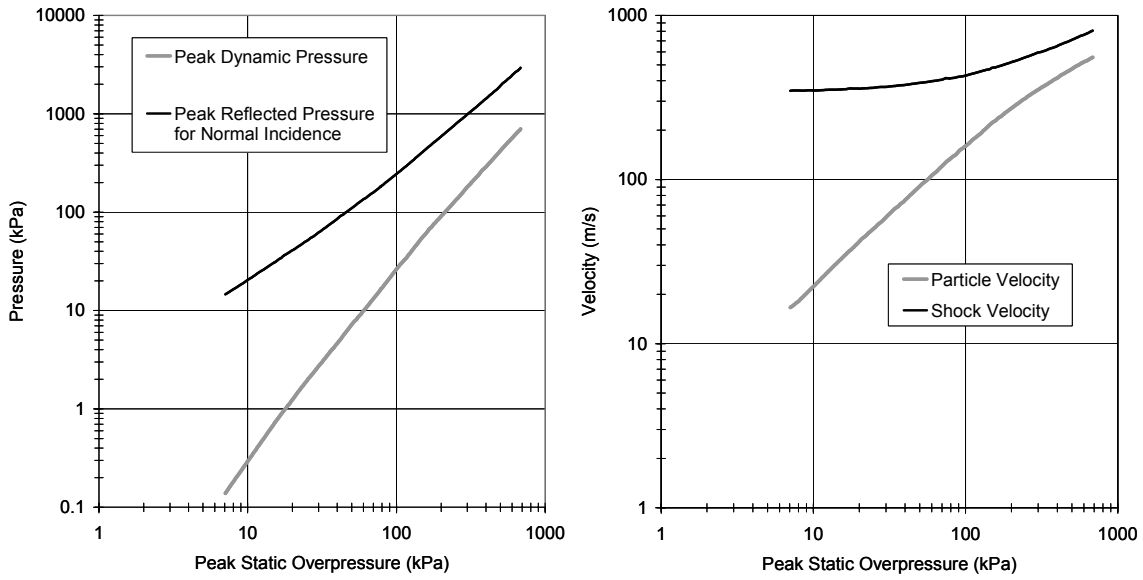

Figure 2.3: Shock wave pressure and velocity parameters as a function of the peak static overpressure [Bellamy, 1991].

While these sensors work well with stable, lower speed flows, there are some issues with measuring the rapidly changing pressure waves and pressure waves that exceed the local speed of sound. One issue that can complicate pressure measurements is the disruptive nature of the device in the flow field. If the flow around the sensor exceeds the speed of sound, a shock wave can form around the sensor. If the sensor is disturbing the flow in an unknown way, or even in a known, but flow velocity-varying way, it is difficult to interpret exactly what the sensor is measuring. To obtain the most accurate results, calibration of the sensors to the experiment is required.

2.2 Blast Injury

Blast injuries can be described as any injuries sustained as a direct or indirect result of a rapid rise in ambient pressure, including the mechanical tissue damage and the clinical syndromes that result from that damage [CDC, 2005; Bellamy, 1991]. Blast injuries are typically classified as primary, secondary, tertiary and quaternary. Primary blast injury (PBI) is regarded as the injury sustained directly due to the rapid variations in ambient pressure, and generally affects the air-containing organs of the body first. These injuries

are typically related to the tearing or failure of very sensitive biological materials. In order to effectively protect against such injury, the clinical syndromes and the function of critical organs must be understood. PBI can also occur in underwater environments, but this thesis will focus on air blast injuries. Secondary blast injuries arise from the impact of debris and fragments propelled by the pressure wave. Tertiary injuries include traumatic amputation and any injuries sustained due to whole body displacement, such as tumbling or striking a stationary object [Januszkiewicz, 1997; Josephson, 1988]. Quaternary injuries are defined as all other explosion-related injuries, illnesses, or diseases not due to primary, secondary or tertiary mechanisms, such as burns, inhalation of toxic gases, etc. [CDC, 2005].

2.3 Primary Blast Injury

Until the Second World War, there was very little known about PBI for various reasons: diagnosis was difficult due to the internal nature of the trauma, individuals with PBI often have other, more visible, life threatening injuries and the occurrence of PBI was rare in relation to injuries from shrapnel or small arms fire. Such injuries were previously referred to as: air concussion, shell shock, shell concussion, blast chest or vent du boulet [Clemedson, 1956]. With advancements in protective equipment such as cloth ballistic vests (CBV) and helmets, the prevalence of primary blast injuries as the dominant injury mechanism has increased as victims who would otherwise have died from fragment wounds would now survive. Another factor increasing the interest in protection from PBI is the trend towards more powerful munitions and enhanced blast munitions, which are designed to injure by means of their blast effects rather than by fragmentation [Wightman, 2001; Bellamy, 1991].

Extensive animal blast experimentation has focused on the respiratory system within the thorax as the most critical region in the body, with resulting pulmonary edema and air emboli as the most likely cause of death [Stuhmiller, 1998]. Air-containing organs within the human body are the regions most vulnerable to blast overpressure, and include the auditory system, the respiratory system and the gastrointestinal (GI) tract [Clemedson,

1956; Bowen, 1968a]. Although the threshold for injury to the auditory system is lowest, trauma to the pulmonary system is more likely to be life threatening [Elsayed, 1997; Mayorga, 1997; Wightman, 2001; Bellamy, 1991] and hence, is the primary focus of the current research. Recent research has led to speculation that lung and GI injuries may appear at approximately the same time, depending on the loading environment, but that significant injuries to either region can be life threatening [Stuhmiller, 1997].

The ear is the most frequently damaged organ from blast overpressure because the auditory system has the lowest threshold for injury [Ripple, 1997]. However, even severe auditory injuries are non-lethal and as a result will not be the focus of the current research. Tympanic membrane perforation is the most common injury to the middle ear, and can result in hearing loss, earache, vertigo, and bleeding from the external canal [CDC, 2005]. Estimated required pressure levels for injury to the ear range drastically depending on orientation and the rate of pressure rise, providing such varied results as: 8-56 kPa [Wightman, 2001]; 50 kPa for long duration [Garth, 1997]; and 57-345 kPa [Mayorga, 1997]. Richmond [1991] suggests a human threshold range of 20-35 kPa, and that fifty percent of the population would show significant injury at 100 kPa.

With the development of better aural protection and more energetic weapon systems (and associated intense noise), the potential for injury to nonauditory structures has become an occupational medicine concern. Some studies have shown that lesions in the GI tract (esophagus, stomach, small intestine, large intestine, rectum and anus) occur at similar pressure levels to lung injuries when exposed to complex blast waves [Clifford, 1984; Richmond, 1993]. As a gas-containing organ, the damage mechanisms are similar to those of the lung (as will be discussed), but the resulting clinical syndromes are unique. Symptoms will normally include abdominal pain, nausea and vomiting [CDC, 2005].

Lower-level blasts can cause small hemorrhages on the surface of the tissue, while more severe blast loading can cause perforation of the entire organ, spilling blood and ingesta being into the peritoneal cavity. Higher concentrations of contusions and perforations are typical in tissues surrounding gas pockets [Stuhmiller, 1998]; this may be due to the

trapped pockets of air violently re-expanding after the pressure wave has passed [Mellor, 1992].

At higher levels of blast overpressure, solid organs can be affected as a direct result of the blast wave, particularly the liver and spleen. Contusions, lacerations and in extreme cases even rupture of these organs has been recorded. This type of injury is seldom considered in PBI, however, since these injuries will generally only appear in the most extreme cases, and would be part of much more severe, multi-system trauma.

Headache, fatigue, poor concentration, depression and insomnia have been recorded in victims of blast. Such symptoms can be caused by concussions, or mild traumatic brain injury without a direct blow to the head [CDC, 2005]. Blast waves have been found to cause contusions with or without skull fractures, and coup contrecoup injuries may result in subdural hematoma, cerebral hemorrhage, or edema [Mayorga, 1997].

2.4 Anatomy and Function of the Respiratory System

The main components of the thoracic cavity can be seen below, in Figure 2.4. The thoracic cavity is bounded and protected by the ribs, sternum and cerebral column. The ribs are flexibly connected to the sternum and cerebral column, and are separated by intercostal tissue and muscles.

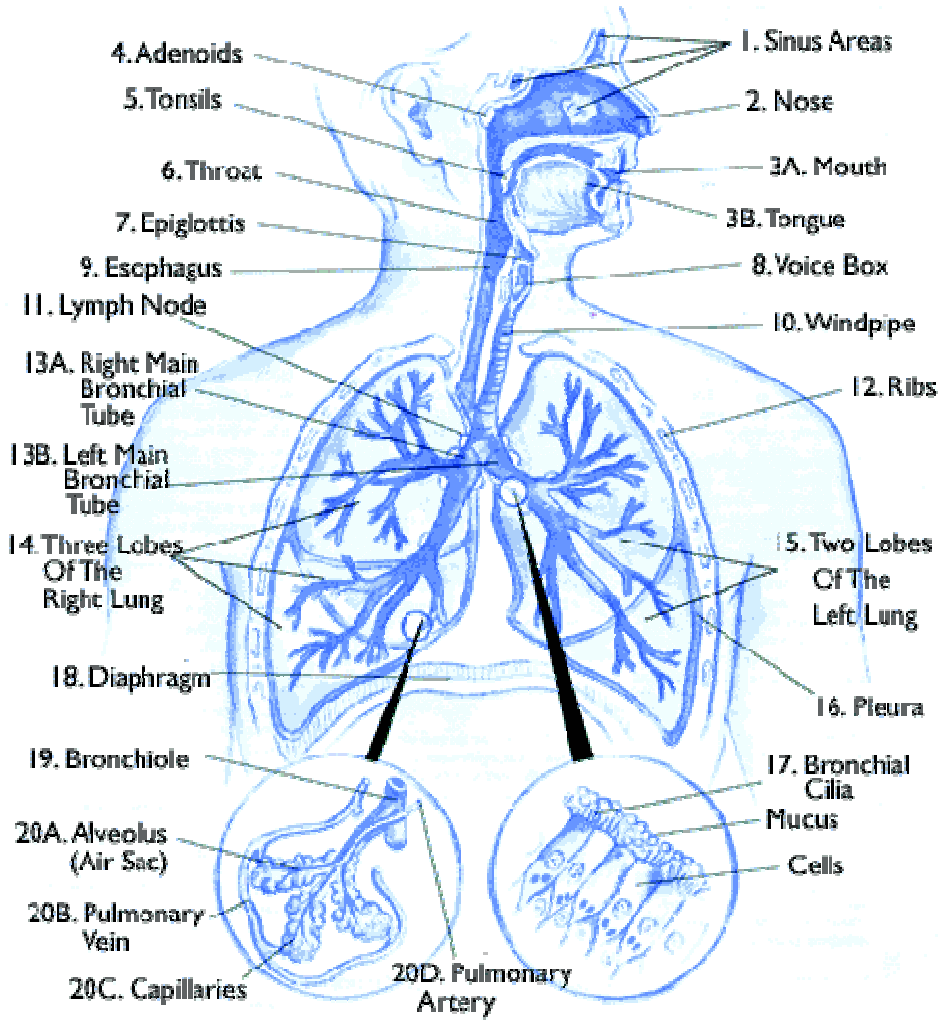

Figure 2.4: The respiratory system [American Lung Association, 2004].

Not shown in Figure 2.4 is the heart, which lies slightly left of centre, and is partially surrounded by the lungs. The space for the heart can be seen toward the bottom of the left lung in Figure 2.4, as it is slightly pushed aside.

2.4.1 Function

Air, taken to the lungs through the mouth and nose, is permitted by the epiglottis to enter the trachea (windpipe). The trachea then splits into two main bronchial tubes, and further divides to direct air into the individual lobes of the lungs. After many further divisions, the tiny bronchioles end in air sacs, called alveoli. The alveoli contain many small blood

vessels (capillaries) that allow blood to exchange oxygen and waste (carbon dioxide) with the alveolar gas.

The lungs are surrounded by a thin membrane, the visceral pleura, while the parietal pleura lines the thoracic cavity. The pleurae are lubricated by pleural fluid, allowing the lungs to slide easily within the thoracic cavity during respiration. The diaphragm is located below the lungs and separates the chest cavity from the abdominal cavity. The diaphragm is a strong wall of muscles that, when activated downward, increases the volume of the thoracic cavity which decreases the pressure in the pleural space, thereby enlarging the lungs and causing air to be drawn inward.

The respiratory system includes the main airway passages such as the trachea and bronchi, the lung tissue (parenchyma) and alveoli. There are approximately 300 million alveoli in a pair of human lungs, each alveolus having an average diameter of 0.2 millimeters [Guyton, 1996]. The average thickness of the pulmonary membrane, the membrane used for respiratory diffusion, is 0.6 micrometers and the average diameter of pulmonary capillaries is only about 5 micrometers. In one set of lungs, there are approximately 70 square meters of respiratory membrane available for the diffusion of oxygen and carbon dioxide. The total volume of air that a typical lung can hold varies between four and six liters, but normal aspiration usually only involves the exchange of half a liter of air. Only about ten percent of the lung is composed of solid tissue, while the remainder is air and blood [Guyton, 1996].

The primary purpose of the respiratory system is to provide oxygen to the body while removing carbon dioxide. This is accomplished by continually introducing new atmospheric air to the lungs, where the gases can be exchanged across a very thin membrane, primarily within the alveoli. Figure 2.4 and Figure 2.5 show a general view of the lung and respiratory system while Figure 2.6 shows a closer view of the alveolar structure. The membrane surrounding – and thus creating – the alveolus is called the alveolar epithelium and is lined with fluid and a surfactant layer, and is backed by an epithelial basement membrane. For the oxygen to travel from the alveolus to the blood

flow, it first must pass through the epithelium and epithelial basement membrane, followed by the interstitial fluid in the interstitial space. The final two layers to be penetrated are the capillary basement membrane and the capillary endothelium. Additional fluid in the interstitial space impedes the flow of oxygen into, and the flow of carbon dioxide out of the blood [Guyton, 1996].

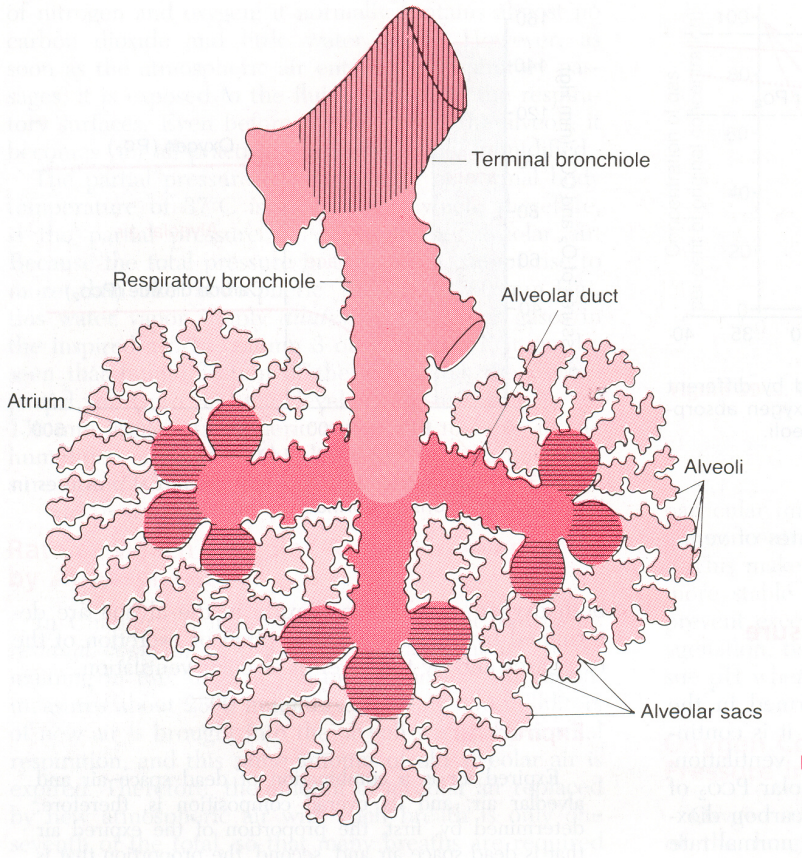

Figure 2.5: A simplified schematic of the lung showing bronchiole and alveolar sacs [Guyton, 1996].

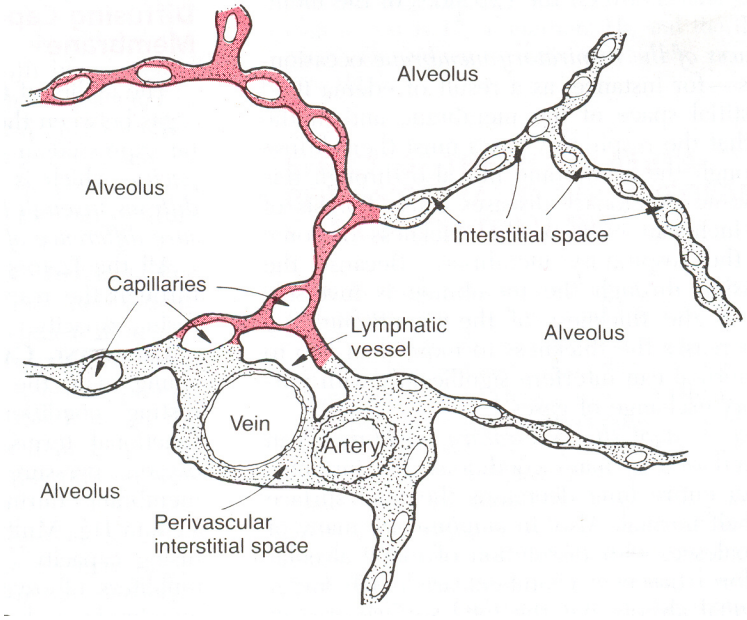

Figure 2.6: Microscopic schematic of alveolar structure and interstitial space [Guyton, 1996].

In order to inhale, the pressure in the alveoli, small air sacs where the majority of the gaseous exchange takes place, must be lower than atmospheric pressure. By raising the ribs and lowering the diaphragm the thoracic cavity volume is increased, thereby creating a negative pressure in the alveoli and drawing air in. The opposite is done for exhalation.

As an elastic structure, the lung would collapse similar to a balloon if not acted upon by external forces. However, the exterior surface of the lung is not attached to the chest wall; it merely floats in a small amount of lubricating pleural fluid within the thoracic cavity. The lymphatic system continually sucks excess fluid out of the pleural space, thereby maintaining a slight negative pressure between the visceral surface of the lung pleura and the parietal pleural surface of the thoracic cavity. A negative pressure of approximately 0.5 kPa is required to hold the lungs open at rest, while a pressure of –0.75 kPa is required for inhalation. Transpulmonary pressure is the difference in pressure between the alveolar space and the outer surface of the lung, and is caused by the internal collapsing forces of the lung. One third of the collapsing force is attributed to the elastic nature of the lung tissue, composed primarily of elastin and collagen fibers, while the remainder of the collapsing force is due to surface tension within the alveoli. The surface tension is controlled by the constant production of surfactant, which lines the alveolar

surfaces and reduces the tendency of the alveoli to collapse. Although the trachea and bronchi have some cartilage to prevent collapse, the bronchi and alveoli are made primarily of smooth muscle, and are prevented from collapsing by the transpulmonary pressure.

2.5 Respiratory Trauma

Victims in close proximity to a blast will tend to have multi-system life-threatening injuries, making diagnosis of PBI somewhat challenging. At low levels of blast, unprotected victims typically have injuries to the auditory system, such as ruptured tympanic membranes, ossicular disruption, or the presence of foreign bodies. The upper respiratory tract (URT), composed of the naso-oropharynx, larynx and trachea will begin to show lesions and edema, which become more severe with increasing blast severity [Mayorga, 1997]. At more lethal levels of blast, pulmonary contusions become evident with large areas of hemorrhaging and interstitial edema. Flooding of the alveoli greatly reduces the gas exchange capacity of the lung, and can lead to suffocation [Elsayed, 1997]. With the break down in the air-blood barrier, air emboli that originate in the lungs can travel to other vital organs causing sudden death [Mayorga, 1997]. The gastrointestinal tract begins to show lesions, which, if severe enough to cause lacerations, can lead to hemoperitoneum and peritonitis [Mayorga, 1997; Junkui, 1996].

An extremely serious group of conditions is hemothorax, pneumothorax and hemopneumothorax, in which both blood (hemo) and air (pneumo) escape into the thoracic cavity. Exposure to significant blast loading can cause pleural rupture and tearing of the lung that creates a passageway between the lung and pleural space. Because the lung is an elastic material under tension, the vacuum in the pleural space is required to keep it inflated. Major rupture of the pleura can decrease the intrathoracic pressure and lead to lung collapse [Januszkiewicz, 1997; Mayorga, 1997]. Below is an overview of the types of injury seen at increasing distances from a blast.

Table 2.1: Expected injuries to unprotected victims at relative distances from a high-explosive detonation in open air [Bellamy, 1991].

Location	*Close Proximity*	⇨	⇨	⇨	⇨	⇨	⇨	*Distant*
Total body disruption								
Burns and inhalation injuries								
Toxic Inhalations								
Traumatic Amputations								
PBI of the lung and bowel								
Tertiary blast injuries								
PBI of the ear								
Secondary Blast Injuries								

There are several outwardly recognizable symptoms that are common results of PBI related respiratory ailments. Depending on the extent of injury, individuals with lung PBI can have a combination of symptoms, including the temporary absence or cessation of breathing (apnea), slow heart rate (bradycardia) and abnormally low blood pressure (hypotension) [CDC, 2005]. At lower levels of injury, experiments with sheep have also noted an increased respiratory rate, decreased tidal volume (volume of air exchanged with each breath), and decreased functional reserve capacity (the volume of air left in the lungs after exhalation) [Mayorga, 1997]. Simply stated, shortness of breath and laboured breathing are to be expected when pulmonary damage has occurred. The expectoration of blood or blood-streaked sputum from the larynx, trachea, bronchi or lungs has been seen in more severe cases [Januszkiewicz, 1997; Clemedson, 1956; Mayorga, 1997]. A short time after the insult, a bluish discoloration of the skin and mucous membranes can be seen resulting from inadequate oxygenation of the blood [Januszkiewicz, 1997; Clemedson, 1956].

Pulmonary trauma can also cause symptoms that appear outwardly not related to the respiratory system. Such symptoms include stroke, acute abdomen, blindness, deafness or spinal cord injury, and are caused by arterial air emboli [CDC, 2005].

2.5.1 Biological Causes of Symptoms

The symptoms listed above are generally the results of tearing or failure of sensitive biological materials, and are sometimes referred to as pulmonary barotraumas [CDC, 2005]. An early sign of PBI to the upper respiratory tract is visible damage to the membranes in the airway [Mayorga, 1997]. The threshold of pulmonary injury is defined as the occurrence of scattered petechiae and/or ecchymoses on the surface of the lung. Petechiae, or small surface bruises, are the result of broken blood vessels, and if more severe, are referred to as ecchymoses. Such injuries typically appear on the pleural surface of the lung adjacent to the diaphragm and the heart, as well as on the posterior surface of the lung.

Higher blast doses can cause significant hemorrhaging and tissue disruption in one or multiple lobes. Lung injury is likely to occur in the lower lobes and adjacent to the spinal column [Januszkiewicz, 1997; CDC, 2005; Dodd, 1990; Mayorga, 1997; Junkui, 1996]. Ecchymoses in parallel bands were originally thought to occur behind the ribs, but were later found to correspond to the intercostal spaces, the vertical space separating each rib from the next. This finding suggests that the lungs are partially shielded by the ribs, which is contrary to what is seen in impact injuries, such as car crashes [Januszkiewicz, 1997; Wightman, 2001]. Pulmonary hemorrhaging is the result of the fracture of blood vessels and subsequent filling of the alveolar spaces with blood. It has also been suggested that well before fracture of the blood vessels, overstretching of the endothelium and epithelium could cause changes in the permeability of the membranes to solutes, leading to reduced performance [Fung, 1988]. Diffuse hemorrhaging will tend to make the entire lung look dark and solid [Januszkiewicz, 1997; Junkui, 1996]. Alveolar hemorrhage induced by BOP exposure can cause alveolar flooding that greatly reduces the gas exchange capacity of the lung [Januszkiewicz, 1997; Elsayed, 1997; Mayorga, 1997].

The lungs are particularly vulnerable to PBI because of their structure and location. In order to enhance the gaseous exchange within the lung parenchyma, the walls of the capillaries and alveoli are typically only one cell thick. The low thickness and

corresponding low strength in the walls within the parenchyma provides little defense against the effects of strong pressure waves. When subjected to a blast wave, the rib cage, sternum and intercostal muscles are rapidly pushed into the thoracic cavity, thereby creating compressive pressure waves in addition to the directly transmitted pressure waves. The lungs are further compressed when the abdominal wall is deformed which, in turn, pushes the diaphragm violently into the lungs. The pressure waves then intensify upon reflection against the relatively hard surfaces of the heart and vertebral column. Damaged lungs often show hemorrhagic zones adjacent to firm or hard structures, such as the heart, ribs and vertebral column. After the initial compressive wave passes through the torso and into the lungs, a complex system of reflected waves occurs along with low frequency oscillation of the chest caused by the elastic strength of the rib cage and the high internal pressure due to the inertial compression [Phillips, 1988]. Such an explanation is echoed by experimental findings in animal tests showing hemorrhaging in the vicinity of the tip of the lobes, the heart, and the spinal cord [Stuhmiller, 1997].

Similar to pulmonary hemorrhage of blood, interstitial fluid can flood the alveolar space and is known as pulmonary edema. As a result of the gross deformation and the pressure waves traveling through the lungs, local stretching of the lung tissue occurs at the scale of the alveolar sacs. The additional space between the cells after stretching (possibly proportional to the maximum principal strain) could be the cause of pulmonary edema, but both edema and hemorrhage of the lungs can also be caused by increased interstitial pressure or the failure of the alveolar epithelial layer [Fung, 1988]. The interstitial pressure can be increased by a pressure wave, or the addition of blood from ruptured capillaries. Once flooded into the alveolar space, interstitial edema may disturb the pulmonary gas exchange to an extent which is lethal. In severe cases, pulmonary contusions and lacerations of larger parts of the lung are not uncommon [Clemedson, 1956; Januszkiewicz, 1997; Elsayed, 1997]. Pathologically, these conditions are sometimes described as Acute Respiratory Distress Syndrome (ARDS), a life-threatening condition in which inflammation of the lungs and accumulation of fluid in the air sacs (alveoli) lead to low blood oxygen levels [Ho, 2002].

Stresses and pressure differentials within the lung can lead to a tear between the alveoli and the wall of a blood vessel within the adjacent lung tissue. When these tears are coincident, they are referred to as alveolovenous fistulae and can permit direct exchange between the air space and the circulatory system. If alveolar gas is permitted to enter the blood circulation in the lung, it can embolise and obstruct the flow of blood in critical pathways. The occlusion of an air embolism in the coronary blood vessels can cause cardiac arrest, and an embolism in the cerebral vessels can cause a stroke. In other pathways, emboli can cause blindness, cardiovascular collapse, acute abdomen, deafness or spinal cord injury [Januszkiewicz, 1997; CDC, 2005; Ho, 2002].

The formation of air emboli in the coronary and cerebral arteries has been identified as the most probable mechanism of immediate death from PBI, and the cause of most deaths that occur within an hour of the blast incident [Stuhmiller, 1998; Januszkiewicz, 1997; CDC, 2005; Mayorga, 1997; Bellamy, 1991]. Due to the difficulty of locating an embolism during an autopsy, it is possible that older studies have overstated the relevance of edema, and understated the importance of embolism formation. It has been noted that the likelihood of air embolism formation is proportional to the amount of edema formation in the lung such that both may be good measures of the level of damage [Mayorga, 1997; Stuhmiller, 1998]. Edema is also desirable as a measure of injury since it can be correlated with lung weight. Lung weight is typically 0.6-1.2% of the total body weight. Values outside of this range typically correspond to hemorrhage and edema. The degree of contamination of the lung with edema fluid and blood is typically determined by the ratio of lung weight to body weight (LWR) and this approach is commonly used in blast injury assessment with animal models. A quotient of injury can be defined as the ratio of LWR for the blast tested animals to the LWR for the control animals. Much of the experimental data on blast injury is quoted in this fashion – one of the challenges with this data, however, is that it obscures many of the details of the injury.

Difficulties may also be encountered when there is insufficient ventilation in the lungs. In this case, a certain amount of the blood flowing through the pulmonary capillaries will not be fully oxygenated and is referred to as shunted blood. If the lungs are not able to

absorb sufficient oxygen, the blood oxygen levels will continue to drop. Low blood oxygen level, or hypoxia, generally causes depressed mental activity, reduced work capacity of the muscles and can culminate in coma. Acute hypoxia can occasionally cause headache, nausea or even euphoria, and severe cases result in death of the cells [Guyton, 1996].

2.5.2 Mechanisms and Criteria of Respiratory Trauma

Blast injuries are characterized by anatomical and physiological changes caused by the direct or reflective over-pressurization force impacting and passing through the body [CDC, 2005]. The blast wave has been called "the invisible sword that can kill without blood" and "a shot without a bullet, a slash without a sword" [Bellamy, 1991], and it is this aspect that makes comprehension of the related fundamental mechanisms of injury challenging.

When a blast wave reaches the body, it induces a stress wave in the torso leading to internal damage. The blast effect does not enter the lungs via the trachea, but rather as a direct stress wave transmission through the torso [Clemedson, 1956; Bellamy, 1991].
German testing on dogs showed that the effect of airflow into or out of the trachea had no effect on blast lung injuries when subjected to blast loading while located within and beyond the lethal limit for unprotected dogs. The researchers also found that lung injury did not occur if the thorax of the dog was protected but the upper airway was not, and therefore the impact and coupling of the blast waves to the chest must be the primary cause of pulmonary trauma [Stuhmiller, 1998]. Recent experimental testing has focused on understanding the transmission of blast waves in the thorax as well as the effect of different materials covering the thorax in order to modify the blast waves entering the body.

The peak velocity of the body wall has been related to the magnitude of the stress wave generated. Reflections from the opposite edges of the lungs lead to reinforcement with peaks of pressure in the lung that may exceed those seen at the leading lung surface

[Cooper, 1989]. It has been suggested that three types of waves are present in such scenarios: stress waves, shock waves and shear waves. Stress waves are longitudinal pressure waves similar to sound waves, traveling through the body at speeds similar to sound waves, but with much greater amplitude. Shear waves are transverse waves of long duration and lower velocity, and are responsible for producing the gross distortions of tissues and organs [Mellor, 1992]. A shock wave may be present if the advancing chest wall accelerates particles to a velocity greater than the speed of sound in that medium. This is generally not a concern for muscle, fat or bone, where sound speeds are in the range of 1500-3500 m/s, but for lung with a sound speed in the range of 25-45 m/s, this is a distinct possibility [Fung, 1985; Yen, 1986]. These shock waves and high amplitude stress waves can cause lung damage far from the site of initial load – explaining the diffuse, and opposite side injury often seen in blast studies [Mayorga, 1997] Petechiae and ecchymosis are typically located inferiorly adjacent to the diaphragm, medially next to the heart, and laterally and posteriorly against the rib cage [Mayorga, 1997].

In the past, some researchers believed that pulmonary contusion in blast was a result of the compression between the rib cage and thoracic spine. However, assuming that lung overpressure causes injury, because the gross deformation of the rib cage seen on high speed film does not coincide with the maximum overpressure measured in the lung during blast loading, it is unlikely to be responsible for true blast lung [Mellor, 1992]. Studies suggest that stress waves are the main contributor to blast lung injury. A complex wave environment is created in the lungs due to reflection and focusing of the waves off the mediastinum and other dense biological materials. Shear waves may also be responsible for shearing lung tissue from the more rigid bronchioles. These phenomena could explain why damage is typically found in the hilar and peripheral regions of the lung parenchyma, and not just at the blast exposed surface. In more severe loading conditions, mass distortion and compression could also account for some tissue damage, such as pleural lacerations and tears between the alveoli and walls of intralobular venules [Januszkiewicz, 1997; Mellor, 1992; Wightman, 2001]. At various loading rates, chest compression and chest velocity have been associated with severity of injury [Clemedson, 1968; Viano, 1989; Axelsson, 1994], as has the amount of work done on the lung by a

blast wave [Stuhmiller, 1996; Mayorga, 1997]; these injury criteria are discussed in more detail in Section 2.7: Experimental Testing and Injury Prediction.

In terms of injury outcomes, there are certain similarities between blast loading and high speed blunt impact. It is believed that non-penetrating impacts of sufficient velocity must produce stress waves because injury is routinely found far from the impact site. Researchers have shown that minor displacements of the body wall are capable of causing significant injury if the resulting body wall velocity is sufficiently high [Cooper, 1989]. Higher speed impacts (similar to blast) create high frequency compression waves, whereas slower impact predominantly create low frequency shear waves. Localized, very high velocity non-penetrating impacts to the lateral chest of animals cause contusion in the medial border of the lung, a perfect location for the reflection and reinforcement of stress waves. Injury at hilar and peribronchial sites following blast exposure are also likely the result of stress concentrations at these structures [Cooper, 1989].

The local physical mechanisms that have been proposed to describe the cause of typical primary blast injuries include: (1) spallation, (2) implosion, (3) inertia, and (4) pressure differentials [Januszkiewicz, 1997; Cooper, 1989; Bellamy, 1991].

Spallation can be observed when a compressive wave traveling through an elastic medium reaches a free surface, or passes from a high-density material to a low-density material. Elastic wave theory demonstrates that when a compressive wave meets a free surface it will be reflected back into the solid as a tensile wave of the same magnitude. For example, a compressive wave traveling in the lung parenchyma will meet a free surface at the interface between the alveolar wall and the alveolar space; the resulting tensile wave could damage the epithelial surface due to excessive tension, leading to edema formation. A similar phenomenon is seen as water droplets sprayed into the air following an underwater explosion [Januszkiewicz, 1997; Clemedson, 1956; Cooper, 1989].

Implosion is referred to as the extreme compression of a gas bubble, which, upon decompression creates small, locally destructive shock waves. The kinetic energy in the surrounding high density material compresses the air much more than the pressure of the shock wave would normally have done. It is possible that the small air pockets within the alveoli are highly compressed during the compressive wave transmission, and once the compression wave has passed, they could violently expand to a volume well above their equilibrium state causing overstretching of alveolar walls [Januszkiewicz, 1997; Clemedson, 1956]

Vast differences in the mass densities of various structures in the body can lead to significantly different accelerations and displacements subsequent to a sharp-fronted stress wave. When two attached bodies are subjected to different accelerations, damaging shear stresses can be produced. An example of such a situation is the delicate portions of a leaf being blown away by the wind while the more dense and rigid veins remain intact. Pathological studies reveal hemorrhaging at the interface between the bronchovasular structures (similar to the veins in the leaf) and the more sensitive lung parenchyma [Bellamy, 1991].

Pressure differentials have been proposed as a general explanation for tissue injury and the forcing of fluids from one region to another. A large pressure differential between the alveolar space and the capillary can cause blood or other fluids to be forced through membranes and in more severe cases may result in failure of the barrier. The pressure differentials could also cause dissimilar displacements resulting in shearing of connected tissue [Cooper, 1986; Januszkiewicz, 1997; Cooper, 1989].

A pressure differential in space is directly related to the time rate of change of pressure. Experimentation has shown that the rate of change of pressure, dp/dt has a profound effect on the type and degree of trauma. Slow, stepped pressure increases tend to allow the body to equilibrate to a certain extent, thereby reducing the lethality of a given peak overpressure [Tamagawa, 1996; Stuhmiller, 1998]. French-German studies have found that animals can tolerate very high overpressures if there is no shock front – that is, if the

peak pressure is reached relatively slowly. Stuhmiller et al. (1996) also found that rise time has a profound effect on the lethality of the wave, and it has been suggested that the rapid pressure increase can cause pressure differences across the alveolar wall, leading to overstretching and fracture.

2.6 Experimental Data

The previously mentioned injury mechanisms of spallation, implosion, pressure differentials and inertia appear to be reasonable, but none have actually been directly observed due to the difficulty of experimentation at such a small scale. The purpose of modeling is to use fundamental science to further the understanding of blast injury and to develop a method for the prediction thereof [Bellamy, 1991].

Development and validation of FE models requires experimental data. Once the model has been validated, more complex scenarios can be simulated with reasonable confidence. Various authors over the past half-century have carried out experimental blast testing using mice, sheep, pigs and even low-level blast testing with human volunteers. A summary of this data and the resulting conclusions and theories pertinent to the validation of the numerical model are presented in the following sections.

2.6.1 Factors Affecting PBI

The level and type of trauma inflicted on a body or organ by a blast overpressure is related to many factors including: blast characteristics, body orientation, equipment worn and the number of exposures to blast loading [Januszkiewicz, 1997; Dodd, 1990; Clemedson, 1956; Elsayed, 1997].

Auditory, respiratory and digestive system blast injury has been correlated to many parameters including: peak overpressure of the incident blast wave, positive pulse duration, positive impulse (the time integral of pressure), rate of pressure increase and the frequency content of the input. The orientation of the human body relative to the blast wave and any reflecting surfaces also has a profound effect on the level of injury because

geometry of the person and environment strongly influence the blast field and pressure impacting the various areas of the body. Blasts in enclosed areas (bunker, building, large vehicles) are associated with greater morbidity and mortality due to reflections and superposition of waves, regardless of whether the explosion was inside or outside of the enclosure. Studies have shown that the smaller the volume/area ratio of the space, the worse the trauma. In addition to the enclosure, proximity to walls and corners will increase the risk of PBI [CDC, 2005; Wightman, 2001]. When the blast wave impacts a barrier, the gas is further compressed and ultimately begins to travel back toward the incident wave, creating a region of intensely pressurized air.

The impulse (and hence duration) of the blast wave has been shown to relate to injury. Defining P_{50} as the peak pressure required for fifty percent mortality, German researchers found the P_{50} for dogs decreased by a factor of three when the duration of the blast wave's positive phase duration was increased from 1.8 to 12.0 milliseconds [Bellamy, 1991]. Underwater tests were also used to demonstrate the importance of impulse. When an explosion occurs underwater, a compressive wave travels outward. Upon reaching the surface, the wave is reflected as a tensile wave, and effectively cuts off the compressive wave as it returns downward. This situation results in pressure waves near the surface being cut off quite quickly (low impulse) while those at greater depths have longer durations (high impulse). Studies have shown that sections of the body at greater depths show much greater injury, which also explains the predominance of GI injuries over lung injuries in victims submerged vertically in water. Underwater blasts are also more lethal due to the higher density of water, the higher speed of the wave front and the improved coupling of the stress wave to the body [Clemedson, 1956; Elsayed, 1997; Bellamy, 1991].

However, a large impulse delivered over an extremely long duration can cause no damage if the peak pressure is not sufficiently high to damage the structure. Animal blast studies have shown that at longer durations, the peak pressure required for a given lethality becomes nearly constant, and hence impulse alone cannot be used to determine the injury. At short durations, there is an interaction between peak pressure and duration,

but for durations longer than 20-30 ms (nuclear or very large conventional explosives) the injurious effect may vary solely with the peak overpressure [Bellamy, 1991]. It must be noted, however, that the terms short duration and long duration are also dependant on the species or tissue in question. If the tissue has a low natural period (high natural frequency) then the biomechanical effect will be that of a shock wave of longer duration. If the natural period is greater, the wave is effectively shorter. Otherwise stated, if the duration of the blast wave is shorter than the natural period of the system, the impulse becomes the major factor in injury prediction. If the duration of the blast wave is longer than the natural period, the peak pressure alone is the injurious factor [Bellamy, 1991]. This is also of interest when scaling results from small animals, whose thorax typically have higher natural frequencies, to humans with lower natural frequencies. The natural frequency of a human chest is approximately 40-60 hertz, while that of a dog chest is about 100 hertz [Clemedson, 1956; von Gierke, 1968].

Unfortunately, the dependence on these variables becomes difficult to assess when the blast environment changes from a Friedlander wave, to a more complex form, such as inside a defeated vehicle [Dodd, 1990; Elsayed, 1997]. These findings indicate that impulse, peak pressure, duration, and rate of pressure change must all be considered when predicting injury solely from the measurement of the external air pressure.

It has also been found that repeated blast exposure at relatively low levels of pressure causes injury. This is of particular interest for safe operation of munitions and workplace safety. Experimentation has shown that there is a marked difference between the overpressure required for severe injury due to one blast, as opposed to twenty blast exposures [Stuhmiller, 1998; Dodd, 1990]. A study was conducted using sheep and swine exposed to blasts at one minute intervals in order to examine the effect of multiple blasts on injury. It was found that a given blast that resulted in 1% mortality when delivered only once produced 20% mortality when delivered twice and 100% when delivered three times [Bellamy, 1991]. Figure 2.7 shows the pronounced effect of multiple exposures on the estimated blast tolerance of humans, based on experiments with sheep and swine [Bellamy, 1991]. Threshold injury is defined as the appearance of scattered pleural

petechiae, and severe injury is confluent hemorrhage covering a significant portion of the lung's surface. Another finding visible in Figure 2.7 is the synergistic effect of multiple higher-level blasts. While there is little difference between the single or multiple pressure waves required to cause threshold level injury, there is a marked difference between what is required for severe injury, when exposed once and twenty times. This information becomes pertinent for those firing high-powered munitions. The blast waves produced by large-caliber weapons and high-energy incoming rounds are referred to as impulse noise and, although they don't typically cause immediate, acute injury on their own, repeated exposure can lead to acute injury. Although dependant on positioning and environment, mortar crews typically experience blast waves with high peak pressures and short durations (low impulse), whereas large-caliber artillery crew positions will be subject to lower peak pressure waves with long durations (high impulse) [Januszkiewicz, 1997].

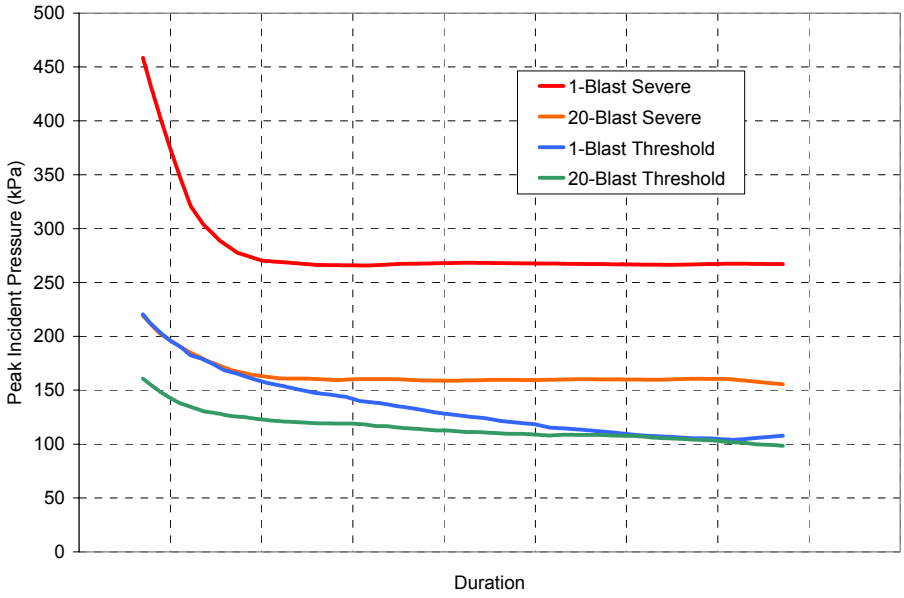

Figure 2.7: Estimated free field overpressure conditions for one and twenty blasts resulting in threshold and severe injury to the lungs [Bellamy, 1991].

In addition to recording the mortality rates and post-mortem examination of injuries within the organs, it is important to be able to compare levels of injury to the level of assault. One technique that has shown considerable success is the measurement of lung weight to body weight ratios. Sheep have shown an injury level-dependent increase in

lung weight to body weight ratio (LWR) [Januszkiewicz, 1997]. The increase in weight reflects hemorrhage and edema fluid accumulation in the alveolar spaces, and was found to increase in proportion to blast peak pressure. Figure 2.8 shows the correlation of LWR to injury and mortality following blast loading [Elsayed, 1997; Bellamy, 1991].

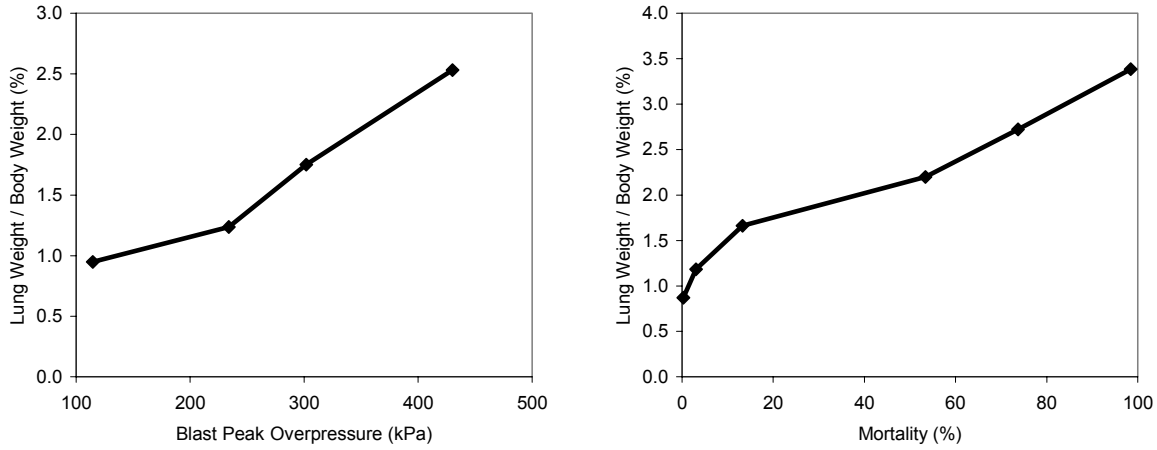

Figure 2.8: Experimental blast results showing correlation between lung weight to body weight ratio (LWR) and peak blast overpressure in rats (left), and LWR to mortality in guinea pigs (right) [Elsayed, 1997].

2.7 Experimental Testing and Injury Prediction

Many experimental and theoretical studies have been carried out during the past fifty years to correlate blast wave characteristics, the physical response of the body, and the resulting trauma. Three of the leading groups in the field, lead by Bowen, Axelsson and Stuhmiller have undertaken numerous experimental tests, and have proposed three different methods of predicting the level of trauma sustained by a human subject to blast overpressure. Although the methods appear to correlate fairly well with the experimental data, there remains a great deal of uncertainty regarding trauma thresholds and the actual cause of the biological tissue damage.

2.7.1 Lovelace Foundation for Medical Education and Research – Bowen Curves

Based in Albuquerque, New Mexico, the Lovelace Foundation for Medical Education and Research has conducted blast related research for many years. Some of the principal investigators involved are Bowen, Fletcher, Richmond, and White, and their contributions resulted in the Bowen Curves for blast injury prediction, and a mathematical model to simulate the response of the thorax.

Bowen Curves for Blast Injury Prediction

Perhaps the most prevalent method for relating injury to simple (Friedlander) blast loading at present is the Bowen curves. Developed by Bowen and a team of researchers using experimental blast testing of animals in the late 1960's, the results have been scaled to be representative of a 70 kg man (approximately 50^{th} percentile male), and can be used to predict such conditions as injury threshold, 50% probability of mortality (LD_{50}), and 99% mortality (LD_{99}) [Bowen, 1968a; Bowen, 1968b; Richmond, 1968].

Test data was compiled from experiments using a variety of blasts to provide different pulse magnitudes and durations, and numerous mammals to evaluate trauma including monkeys, sheep, swine, goats, dogs, cats, steers, rats, hamsters, rabbits and mice. Shock tubes were used to produce longer duration blasts and high-explosive charges for short duration tests. Shock tube experiments were carried out with the left side of the animal placed against a reflecting end-plate, thereby directing the right side of the body toward the blast (Figure 2.9). Maximum overpressures and durations were measured using pressure transducers located near the end-plate without the animal in place. Short duration testing was carried out by restraining the animal in a prone position on a concrete pad with a high explosive located overhead. Overpressures and durations were measured using pressure transducers located at or near the surface of the concrete pad. Very few experiments were carried out with the animal in the free field. The Bowen curves are based on experiments with blast durations ranging from 0.24 to 400 milliseconds.

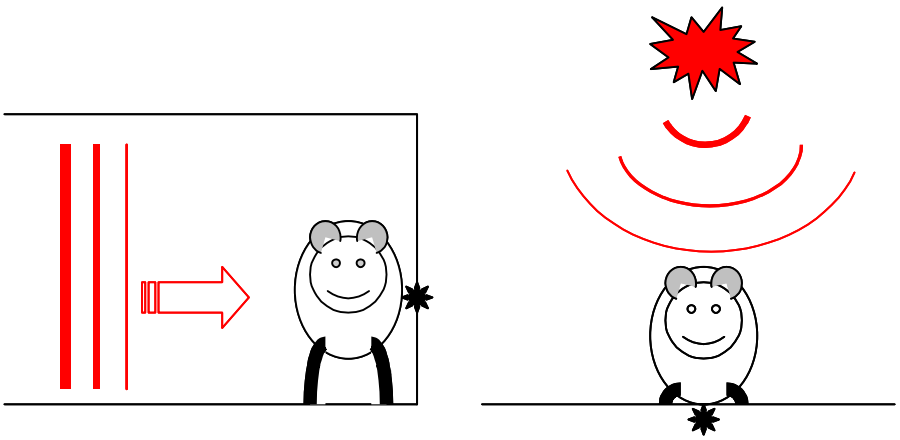

Figure 2.9: Shock tube orientation (left), and high-explosive experimental setup (right). Black star shows location of pressure transducer at the end-plate and on the concrete pad.

The Bowen curves were created after analyzing a wealth of experimental data. Applying dimensional analysis to the data, equations were formulated relating the animal mass, a resultant pressure in the lung, ambient pressure, a characteristic time for the blast wave, as well as weapon yield, height of burst and distance from the blast.

Once the data was sorted, it was found that the results could be split into two general groups depending on the size of the species: (1) small animals, such as mice, rats, guinea pigs, and rabbits, and (2) large animals, such as monkeys, dogs, goats, sheep, and swine. Within each group, the results were comparable once scaled appropriately to the mass of the animal tested. The Bowen curves were scaled to approximate a 70-kilogram man, extrapolating data from testing of the large animal group. It must be noted, however, that limited tests on monkeys indicate primates may have a higher blast tolerance relative to other species tested [Bowen, 1968b]. This was not considered in the development of the curves for human tolerance. Below, Figure 2.10 shows the relative tolerance of man, mouse, rabbit and dog for blast injury [von Gierke, 1968].

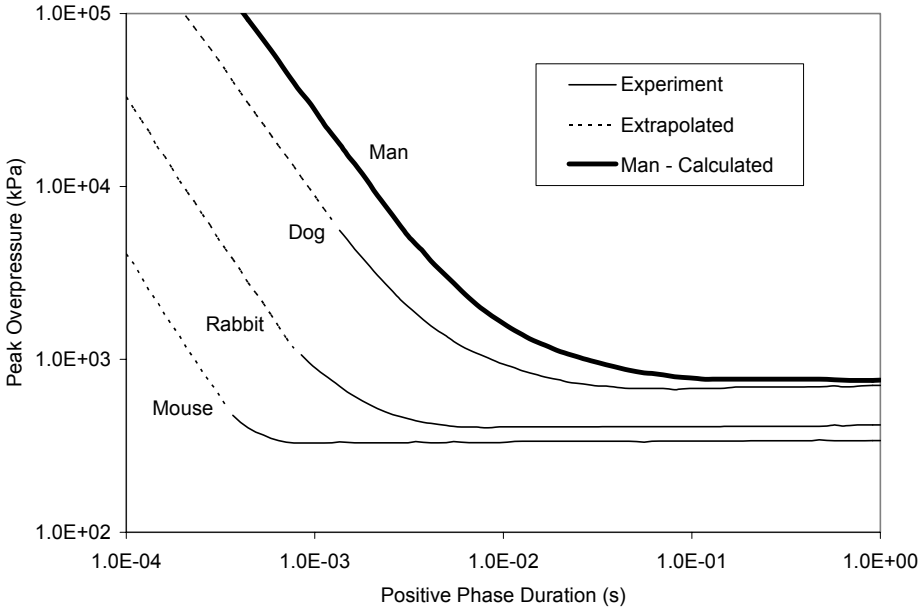

Figure 2.10: Relative tolerance levels resulting in similar injuries for man and various mammals [von Gierke, 1968].

It was first noted by Schardin (1950) that blast injury for mammals is typically related to the impulse of the blast if the duration is "short", and related to the peak pressure if the blast duration is "long." A simple mathematical relation representing such a phenomenon was suggested:

$$P = P^* (1 + aT^{-b}) \tag{2.3}$$

where:

- P is the experimental blast overpressure
- T is the duration of the positive phase
- P^* represents an overpressure criterion for long duration blasts for a given trauma outcome
- a and b relate the impulse to the trauma criterion for short duration

Equation (2.3) ensures that if T is large, P approaches P^*; but if T is small, then the impulse plays a greater role in the determination of P^*, the trauma criterion. The values of a and b are constants determined through experimental testing.

Researchers determined by dimensional analysis that the significance of a particular blast wave duration could be scaled using the ambient pressure, p_0 (psi), and the mass, m (kg), of the experimental mammal:

$$T = t_t \ (70/m)^{1/3} \ (p_0/14.7)^{1/2} \tag{2.4}$$

The experimental duration, t_t, was scaled to a representative duration, T, applicable to a 70 kg mammal, and an ambient pressure of 14.7 psi. A scaling relationship between ambient pressure and maximum overpressure for a given level of injury was also proposed. For the purpose of Bowen's study:

$$P = p_r \ (14.7/p_0) \tag{2.5}$$

where P is the maximum reflected overpressure applicable to an ambient pressure of 14.7 psi and p_r is the maximum reflected overpressure measured at an ambient pressure of p_0. The term reflected overpressure is used indicating that most testing was carried out with the animal against a solid surface, but Bowen et al. then converted the results, and presented them in curves based on the side-on pressure measurements. Free field, side-on pressure measurements are measured perpendicular to the flow direction with the animal absent from the flow.

Relating the equations and subsequent regression analysis of the blast data, values for constants a and b were found, as well as the square wave (or long-duration) overpressure, P_{sw}, resulting in 50 percent mortality for each mammalian species. Mortality data in all cases refers to death in the 24-hour period following the blast experience. It was also possible to create curves relating the equivalent square-wave overpressure to mortality for each species by combining the values for a and b and the test data. The P_{sw} for various mammals can be seen in Table 2.2. The square wave pressure for a human male was chosen as the geometric mean of the large species, 61.5 psi, also shown in Table 2.2. Available evidence suggests that the tolerance of man is likely similar to that of the high tolerance group consisting of the larger animals. Of interest to the current research

project, the tested sheep ranged from a mass of 48.9 to 59.2 kg and were found to have a P_{sw} of 68.5 psi. The relation suggested by Richmond et al. [Richmond, 1991] between the pressure required for 50% mortality and body weight can be seen in Figure 2.11.

Table 2.2: Square wave pressure resulting in fifty percent mortality for various species [Bowen 1968a].

Species	P_{sw} (psi)	P_{sw} (kPa)	Number of animals
Burro	71.9	495.7	6
Monkey	71.1	490.2	25
Sheep	68.5	472.3	173
Swine	62.5	430.9	16
Goat	61.8	426.1	115
Dog	56.6	390.2	204
Cat	53.4	368.2	48
Steer	50.0	344.7	27
Large Species	**61.5***	**424.0***	**614 (Total)**
Rat	36.9	254.4	368
Hamster	34.8	239.9	110
Rabbit	31.7	218.6	204
Mouse	31.5	217.2	504
Guinea Pig	30.8	212.4	297
Small Species	**33.1***	**228.2***	**1483 (Total)**

*Geometric mean of the P_{sw}'s

In order to compare the experimental findings for all species as one set of 50 percent survival data, the experimental test pressures and blast wave durations were scaled to the human mass (70 kg), the human square wave pressure (61.5 psi), and an ambient pressure of 14.7 psi. The scaling equations used were:

Scaled peak overpressure:

$$P = p_r \, (61.5/P_{sw}) \, (14.7/P_0), \text{ psi} \tag{2.6}$$

Scaled duration:

$$T = t_t \, (70/m)^{1/3} \, (P_0/14.7)^{1/2}, \text{ msec} \tag{2.7}$$

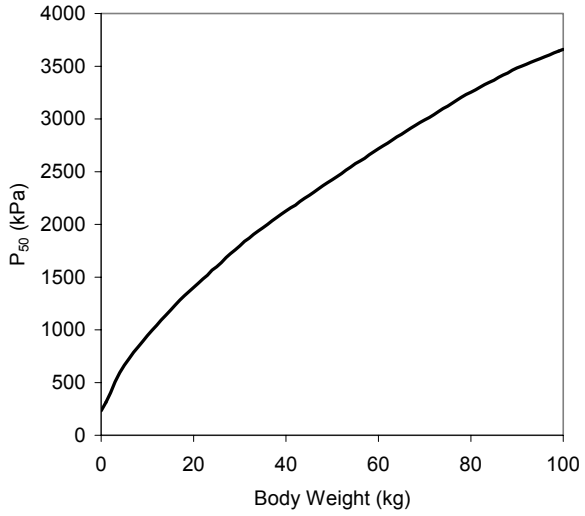

Figure 2.11: Extrapolated data from UK interspecies studies showing the relation between the overpressure required for 50% mortality (P_{50}) and body weight [Richmond, 1991].

The Bowen curves also indicate values for threshold lung damage, which Bowen has considered as one-fifth the 50-percent survival overpressure (LD_{50}). Richmond et al. [Richmond, 1968] generalized the onset of lung injury as one-quarter the dose for LD_{50}, and the beginning of severe lung injury (threshold for lethality) as three-quarters of LD_{50}. As the results later in the research indicate similar findings by Stuhmiller and Axelsson, this author finds the assumption to be valid.

Although the analysis was carried out with data from experiments with animals located against solid, reflecting surfaces, lethality curves have also been created for prediction of trauma in free field situations, with the body parallel, or perpendicular to the blast direction. This is possible by assuming that equivalent trauma will result if the peak reflected pressure and duration when against a reflecting surface are equivalent to the incident (side-on) pressure and duration for a body with the long axis parallel to the direction of the blast. For a body perpendicular to the blast, the incident pressure plus the dynamic pressure is equated to the peak reflected pressure for equivalent trauma. This author, however, does not fully agree with the assumption that free field results will agree completely with those when the subject is situated directly in front of a reflecting wall.

The reason for this is that peak pressure and duration alone cannot fully account for the effects of the blast wave. Parameters such as the shape of the pressure-time curve, the impulse and the rise time to peak pressure must also be involved.

The Bowen curves, originally developed in 1968, can be used to predict the lethality of simple blast waves based on the incident blast overpressure and the positive phase duration of the blast wave. The simplicity of the curves, as well as the wealth of data used to develop them has ensured their continued use as a reference and validation tool. Figure 2.12, Figure 2.13 and Figure 2.14 show the Bowen curves for a human (70 kg man) subject to a blast overpressure while oriented parallel to the blast direction, perpendicular to the blast direction, and near a reflecting surface, respectively. It should be emphasized that this approach has only been validated for simple blast loading. Attempts to apply these curves to complex blast waves rely on the use of peak pressure and pulse duration, but may not be appropriate and have not been validated at this time.

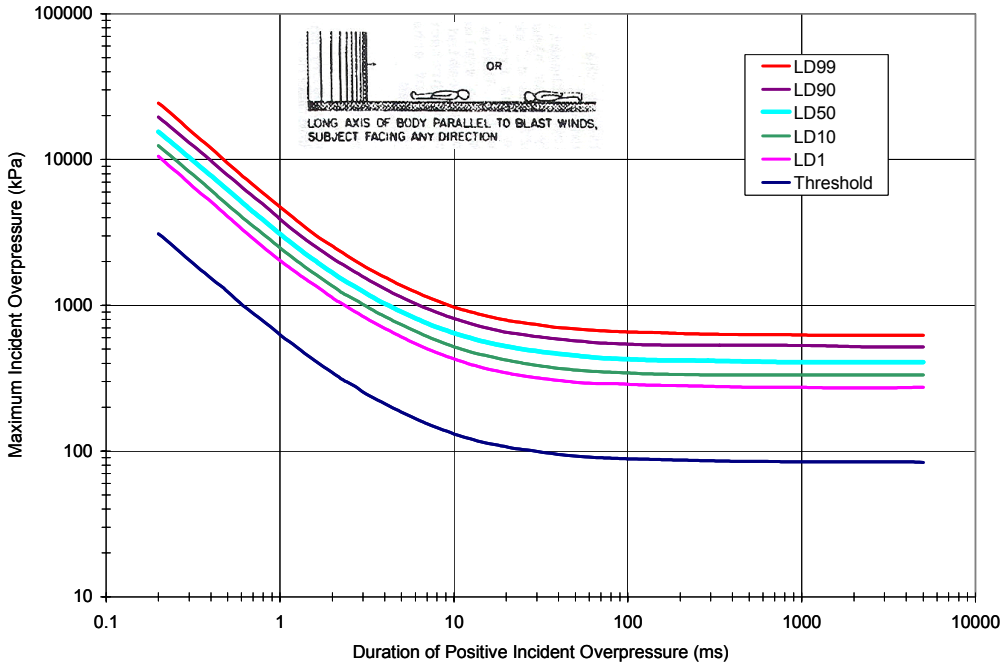

Figure 2.12: Estimated survival curves for a single air blast at sea level is given for a 70 kg human in the free field where the long axis of the body is parallel to the direction of propagation of the blast wave [Bowen, 1968a].

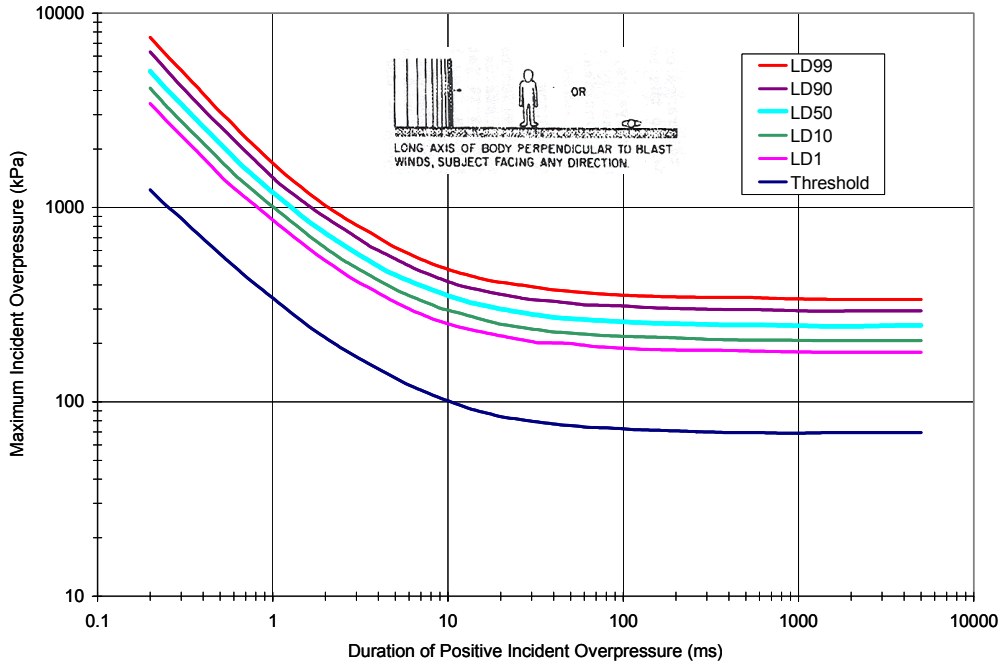

Figure 2.13: Estimated survival curves for a single air blast at sea level is given for a 70 kg human in the free field where the long axis of the body is perpendicular to the direction of propagation of the blast wave [Bowen, 1968a].

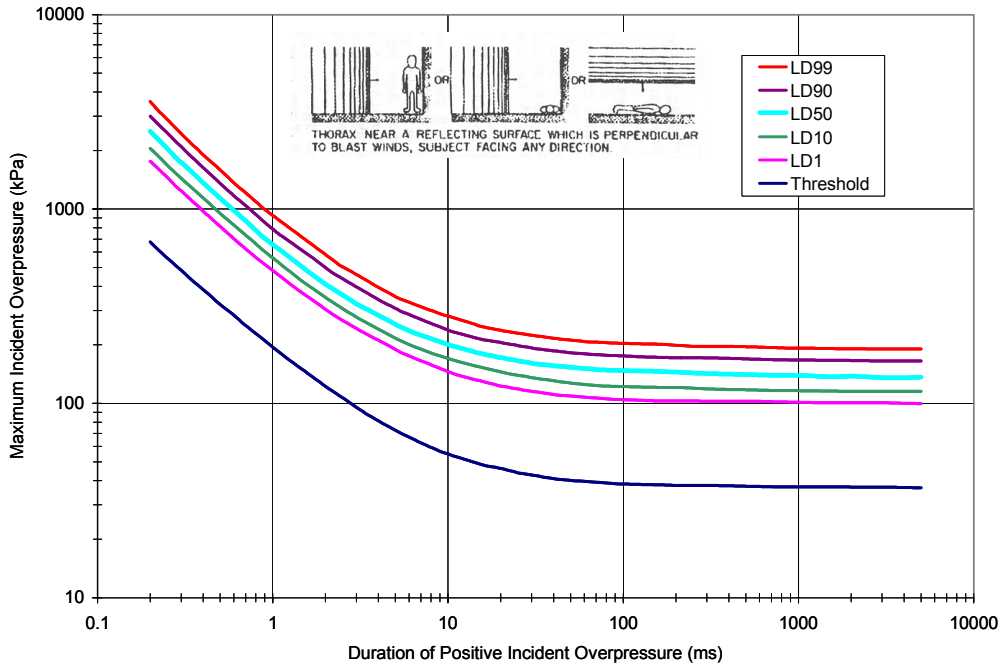

Figure 2.14: Estimated survival curves for a single air blast at sea level is given for a 70 kg human where the thorax is near a reflecting surface oriented normal to the direction of propagation of the blast wave [Bowen, 1968a].

When considering complex blast loading, the orientation of the human body relative to any surrounding reflecting surfaces is of great importance, and further complicates the understanding of this issue. In general, body orientation and position relative to a reflecting wall is related to the effect that geometry has on the peak overpressure felt by the body – the pressure that would be measured by a flush mounted pressure gauge. For example, if a blast wave strikes a flat wall that is perpendicular to the blast wave direction, the magnitude of the reflected wave will be increased due to the reflection of the wave as well as the accumulation of pressure from blast winds – this is the result of dynamic pressure adding to the static pressure as its kinetic energy is turned to pressure. If the body is perpendicular to the blast direction and is in the free field, the effective peak pressure is typically the sum of the peak static overpressure and the dynamic pressure, since the body has considerable reference area to create a stagnation point. A body that is lying down, parallel to the direction of propagation of the blast wave will sustain an overpressure equal simply to the peak static overpressure since there will be very little reference area to cause a stagnation point of significance.

Comparing the required blast for threshold injury in different body orientations gives an idea of the effect that reflective pressure can have on injury. While lying end-on to the blast, a static pressure of 12 psi [83 kPa] is required for threshold injury, while side-on subjects would need 10 psi [69 kPa] (with 2 psi [14 kPa] dynamic pressure built up in front of the chest) and a subject against a reflector would only need 5 psi [34 kPa], which reflects to 12 psi [83 kPa]. This simple comparison shows that for different incident blast waves, the effective blast loading can be the same, depending on orientation and environment [Bellamy, 1991].

Using peak pressure and duration to predict injury in complex blast waves becomes difficult. With reverberations in an enclosure, the duration becomes extremely long, and the models tend to overpredict injury. Attempts to calculate equivalent free field waveforms tend not to be scientifically justifiable, and have proven unreliable [Stuhmiller, 1997]. Another complication arises from the extreme variation in pressure

traces from one location to another that arise due to additions and cancellations of waves from reflections. The pressure traces also change significantly when a body is placed in the flow field, changing significantly the reflections and locations of pressure accumulation.

Also, there remain some issues with the Bowen curves and the derivation thereof. In the transition from "short" to "long" duration blast waves, the experimental setup changes from overhead high-explosives to shock tubes with a reflecting wall. The data in this transition period could be slightly misleading as the shock tube generally produces a higher impulse than high-explosives for a given overpressure and duration. Also, when comparing free field to shock-tube blasts of the same duration, the pressure-time curves and the impulses can vary considerably.

2.7.2 Modified Bowen Curves

It must also be noted that the Bowen curves have recently been modified to reflect corrections to the original findings. The general change was lowering of the required peak pressure for a given lethality in the short duration region. Although these curves have only been recently presented at blast conferences [Bass, 2005], the numerical models developed at the University of Waterloo have been compared to the modified Bowen curves, recognizing that this is an improved representation of tolerance to blast loading. The modified Bowen curves for a human in the free field, standing perpendicular to the direction of propagation of the blast wave is shown in Figure 2.15. The solid lines represent the modified data, and the dashed lines show the original data. At the completion of this research, further modifications to the Bowen curves were presented [Bass, 2006], generally reassessing the injury curves to pressures located between the original predictions, and those made in the 2005 presentation by Bass. As this research continues, it is possible that the model may be reassessed against these recently published figures; unfortunately they were presented during the final stages of this research.

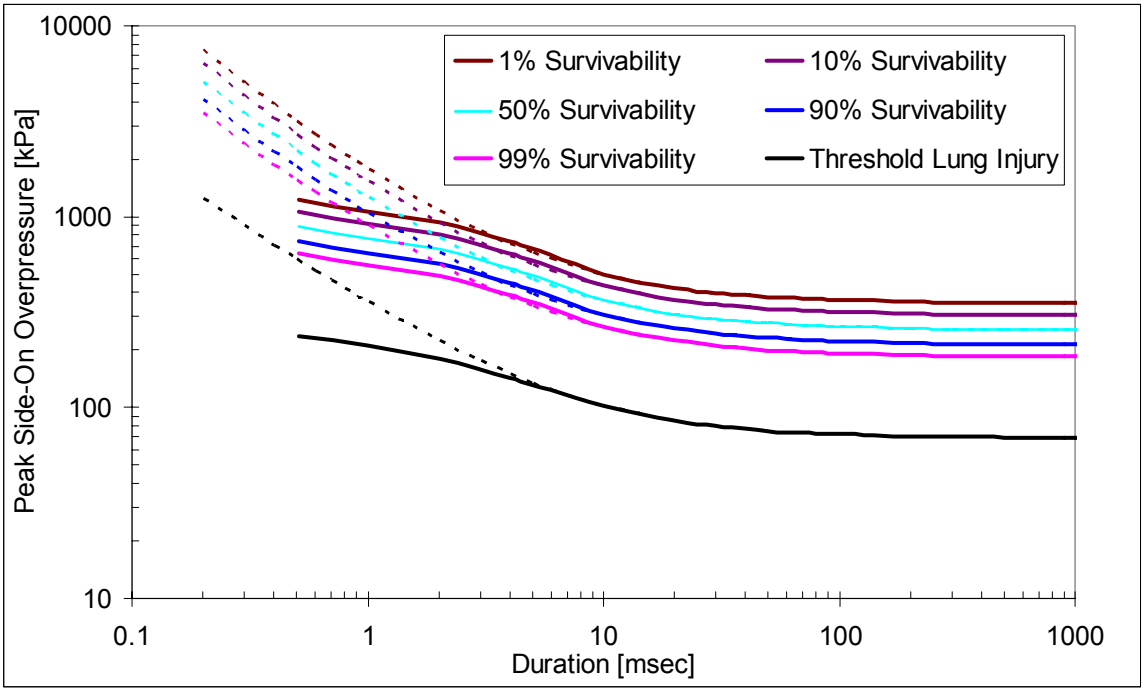

Figure 2.15: Modified Bowen curve for a human in the free field, standing perpendicular to the direction of propagation of the blast wave. Dashed lines show original data [adapted from Bowen, 1968a and Bass, 2005].

2.7.3 Mathematical Model

In search of methods for predicting PBI in simple and complex blast cases, researchers began to investigate fluid-mechanical and biomechanical models that could be built and tested, but also be represented using simple mathematical models. One of the first attempts was a fluid-mechanical model of the thoracoabdominal system, designed by Bowen et al [1965] to predict the response of the thorax to simple blast. The model was composed of:

- Masses to represent the chest wall, heart, mediastinum etc.
- Springs to represent the elastic strength of the rib cage and the pressure built up in the lungs
- Dampers to model friction and viscoelastic properties of the thorax
- Orifices to simulate the airways of mammals.

This model was then modified and re-analyzed by Bowen et al. in 1968 [Bowen, 1968b], and can be seen in Figure 2.16. The model consists of two lung chambers, three masses representing the chest walls and the mediastinal tissue, and the associated springs and dampers. The models varied in terms of the number of springs-masses-dampers, and the model parameters used. Some parameters of the model were estimated based on mechanical properties of animals tested, other values were estimated and then refined to match experimental animal blast results of intrathoracic pressure (ITP), displacement and velocity [Bowen, 1968b].

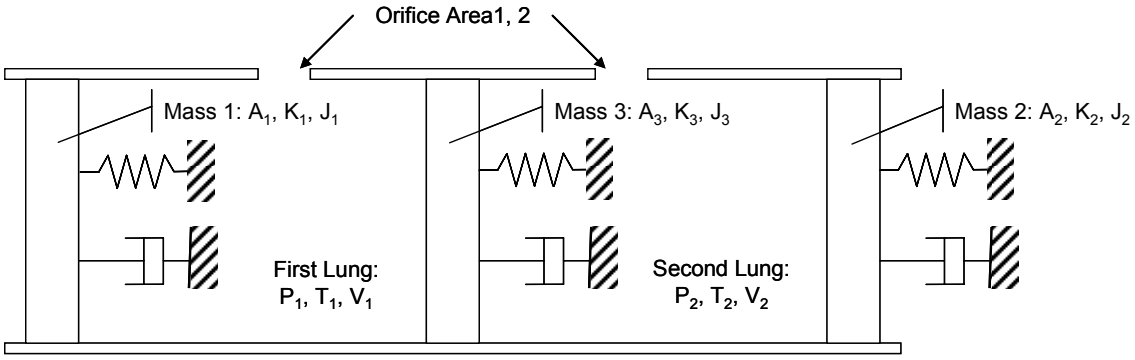

Figure 2.16: Mathematical model of the thorax to simulate fluid-mechanical responses to blast [Bowen, 1968b].

White et al. made further modifications to the model in 1971 [White, 1971] and calibrated the model to predict the esophageal pressure measured in large animal blast testing. Figure 2.17 shows the predicted and experimental intrathoracic pressures due to a fast-rising, long-duration overpressure of approximately 20psi. Note that the internal pressure rises to approximately three times the initial external peak overpressure, followed by damped oscillations.

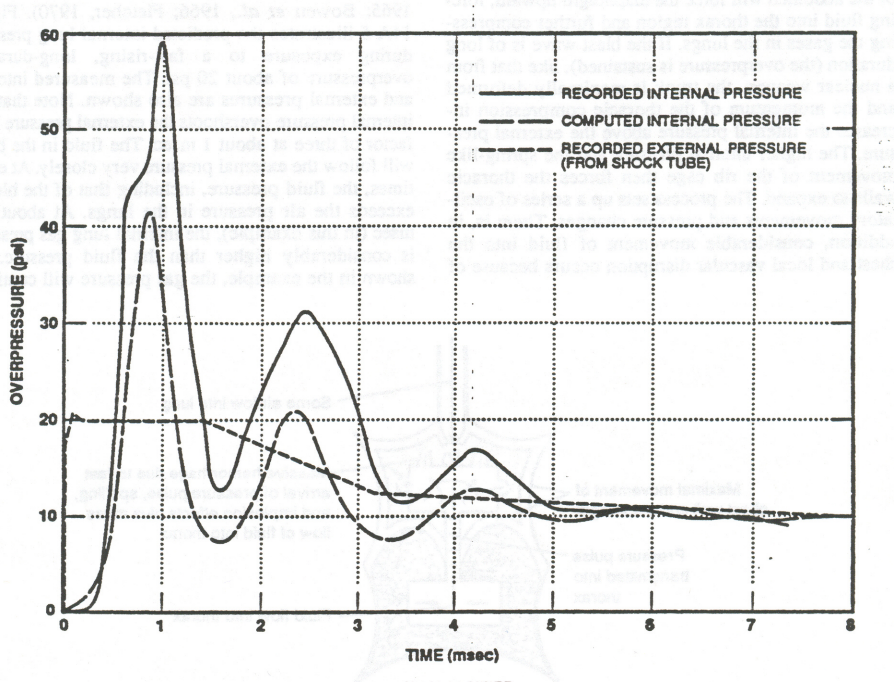

Figure 2.17: Experimental and predicted internal lung pressures and experimentally measured external pressure [White, 1971].

Josephson and Tomlinson [Josephson, 1988] later revisited the model in order to relate the injury caused by complex blast waves to that caused by simple waves. Figure 2.18 shows the predicted internal lung pressure and the experimentally measured pressure in the esophagus of a 40 kg sheep exposed to a low-level complex blast wave. The experiment was carried out by the U.S. Army and the predicted pressure was calculated using the model suggested by Josephson and Tomlinson (1988). This type of pressure signal may be useful in determining the type of oscillations to be expected in a predictive model. Unfortunately the test was carried out in a closed chamber, so there were many reflections, and the blast wave input is not shown with the internal pressure, making it of limited use to the current study. Josephson and Tomlinson had some success matching predicted pressures to various levels of injury. However, in terms of correlating the model to the human thorax, the internal pressures are extremely high, and are not related to those of a human thorax [Josephson, 1988; Stuhmiller, 1997].

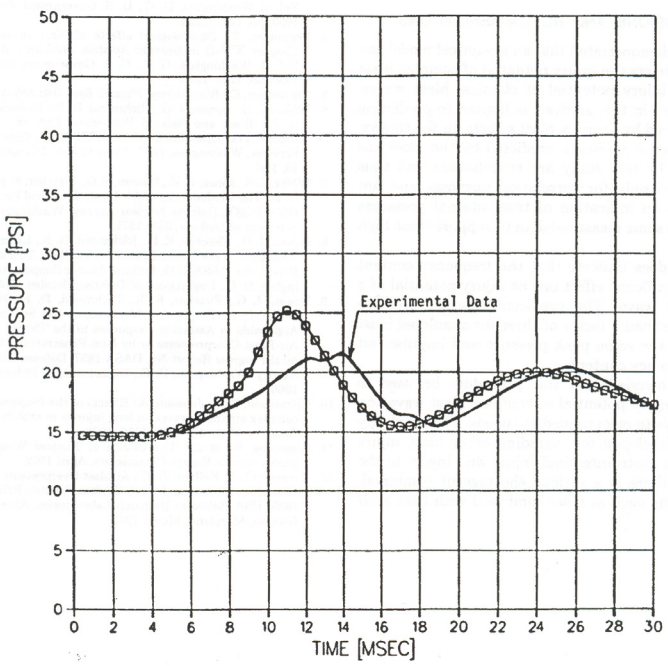

Figure 2.18: Comparison of predicted internal lung pressure with pressure measured in the esophagus of a 40 kg sheep exposed to a complex blast wave [Josephson, 1988].

2.7.4 Chest Wall Velocity Injury Criterion - Axelsson

Significant blast research has also been carried out by scientists at the Swedish Defence Research Establishment (FOA), leading to a novel approach to blast injury prediction based on chest wall velocity. Experiments involving rabbits showed that the severity of injury from blast correlated with the maximal inward chest wall velocity [Jönsson, 1979]. Research using biofidelic models showed similar results, where researchers observed a linear relation between the velocity of the chest wall and the strength of the internal compression wave [Stuhmiller, 1997].

In order to predict non-auditory blast injury from complex waves, Axelsson et al. [Axelsson, 1994] correlated the peak velocity from a mathematical model, shown in Figure 2.19 to their own experimental data, and data from the Bowen [Bowen, 1968a] iso-injury curves. The one-dimensional spring-mass-damper system was scaled to represent the thorax of a 70 kg mammalian. The parameters used in the model and the

predicted values, however, have limited physical meaning because of the extreme degree of simplification from a living thorax to the single chamber spring/mass/damper model.

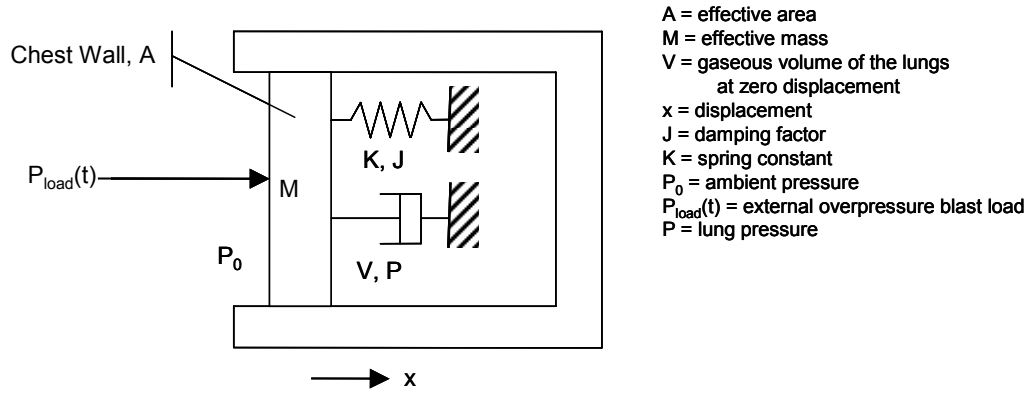

Figure 2.19: Single chamber mathematical model of the thorax [Axelsson, 1994].

Given an applied pressure history recorded by a blast test device (BTD), the model predicts a chest wall response (displacement, velocity and acceleration) and intrathoracic pressures (ITP) for simple and complex blast loads. The BTD, a schematic of which is shown in Figure 2.20, consists of a 12 inch diameter cylinder, 30 inches long, with four pressure sensors located around the circumference at the midpoint [Yu, 1990].

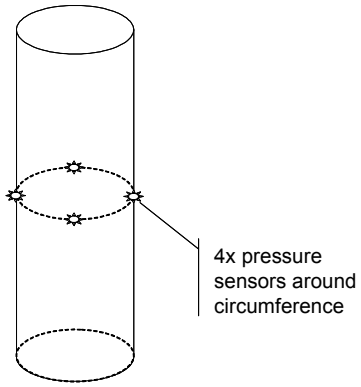

Figure 2.20: Blast test device showing locations of four flush-mounted pressure sensors.

The model can be mathematically represented as:

$$M\frac{d^2x}{dt^2}+J\frac{dx}{dt}+Kx=A\left[p(t)+P_0-\left(\frac{V}{V-Ax}\right)^g P_0\right] \tag{2.8}$$

Blast testing was carried out using sheep in various enclosed areas to validate the mathematical model for complex loading. Sheep were chosen as the test specimen because the weight of the human and sheep thoraces are very similar; all data was subsequently scaled to a 70 kg man. Blast testing was carried out in order to assess the trauma sustained by the sheep as well as to collect representative pressure histories to be used as input for the mathematical model. A cylindrical test device instrumented with four pressure sensors was used to capture the three-dimensional, complex loading. This pressure-time data was then used with the mathematical model to predict the response of the chest wall.

Shortly after blast testing, the sheep were assessed by inspection of their internal organs and given an injury score classifying the level of injury sustained by the lung, pharynx/larynx, trachea, gastrointestinal tract, and inter-abdominal organs. Injuries were rated as being negative, trace, slight, moderate or extensive and a value representing the level of trauma was obtained using the adjusted severity of injury index (ASII) seen in Table 2.3.

The results of peak inward chest wall velocity and peak intrathoracic pressure as calculated by the mathematical model were compared with the experimental trauma values. The correlation was then compared to Bowen's iso-injury curves and it was found that the predicted peak ITP values did not correlate well to injury. For a given trauma level, the predicted peak intrathoracic pressure varied by almost a factor of 10, and there was significant overlap of different trauma levels at specific pressures. Therefore, given an ITP, one must also know the loading overpressure and duration to make a reasonable assessment of the possible trauma outcome. The magnitude of the calculated ITP also appears to be extremely high when compared to experimental measurements in the esophagus or bronchioles of test animals.

The chest wall velocity, however, was found to correlate well with the level of trauma sustained, and compared well with the Bowen curves for threshold lung damage (TLD),

1, and 50 percent lethality. Axelsson et al. predict TLD at 3 – 4.5 m/s inward chest velocity, LD_1 at 8 – 12 m/s and LD_{50} at 12 – 17 m/s.

Associating the Adjusted Severity of Injury Index (ASII) with data from Yelverton [Yelverton, 1994], inward chest wall velocities from the model can be directly used to predict injury levels, as shown in Table 2.3. Use of the mathematical model in combination with the experimental testing on sheep also allowed for a simple mathematical correlation between the ASII and the inward chest wall velocity, although this model provides very little detail or insight:

$$ASII = (0.124 + 0.117\ V)^{2.63} \tag{2.9}$$

Table 2.3: Injury as a function of peak inward chest wall velocity [Axelsson, 1994].

Injury Level	ASII	Chest wall velocity (m/s)
No injury	0.0 – 0.2	0.0 – 3.6
Trace to slight	0.2 – 1.0	3.6 – 7.5
Slight to moderate	0.3 – 1.9	4.3 – 9.8
Moderate to extensive	1.0 – 7.1	7.5 – 16.9
>50% lethality	> 3.6	> 12.8

Although the peak inward chest wall velocity appears to be an indicator of trauma, closer inspection of the data in the Axelsson report shows that, depending on the blast duration or peak pressure, the same chest wall velocity can predict LD_1 and LD_{50} values – thereby requiring knowledge of the characteristics of the blast and the predicted wall velocity. There are instances where, for a given chest wall velocity, the damage could result in 1 or 50% mortality, depending on the loading conditions. Also, it remains uncertain whether the predicted velocity is an accurate estimation of the true chest wall velocity in mammals.

Alternatively, when the peak ITP is used as a guide, significant variation based on loading overpressure can provide misleading results. Finally, even if the models can be

tuned to accurately represent the dynamics of the thorax, they offer no mechanistic explanation of the injury process. Such difficulties highlight the need for a more comprehensive approach to predicting human trauma based on the characteristics of the blast wave loading.

2.7.5 Injury 8.1 - Stuhmiller

Taking an approach similar to that of Axelsson, Stuhmiller et al., in association with the U.S. Army and Jaycor (now known as Titan Corp.) formulated a mathematical expression based on a one dimensional model of the human thorax. In place of the spring-mass-damper system, a pleural dynamics model was created composed of the lung volume and the chest wall represented as a piston, as shown in Figure 2.21. The model considers the forces on the chest wall arising from the external blast load, the internal pressure resulting from the bulk compression of the lung volume, and the compression wave directly in front of the piston generated by the inward motion. This model assumes that the blast loading and the inertia of the chest wall are the dominant factors, while the elastic effect of the rib cage and the viscoelastic damping properties of the tissues have limited influence on the overall dynamic behaviour. The major underlying assumption remains that respiratory PBI is caused by the compressive wave that travels through the lung.

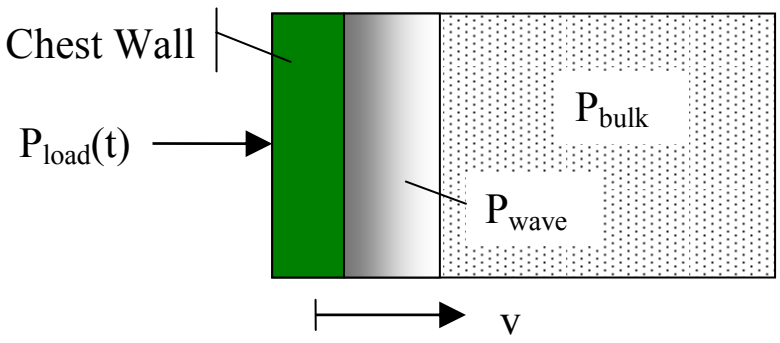

Figure 2.21: Stuhmiller's pleural dynamics model [Stuhmiller, 1996]

Treating the lung as a compressible material, Stuhmiller et al. relate the pressure wave in a gas to the motion of a piston with the equation:

$$p(t) = p_0\left(1+\frac{1}{2}(\gamma-1)\frac{v}{c_0}\right)^{\frac{2\gamma}{\gamma-1}} \tag{2.10}$$

where p_0, ρ_0 and c_0 are the pressure, density, and speed of sound in the undisturbed lung, respectively; v is the velocity of the piston, and γ is the ratio of specific heats. Linearization of the previous equation is carried out based on the assumption that the piston velocity is small compared with the speed of sound. Also, the effects of internal reflections of the wave on the motion of the thorax are ignored for simplicity. Considering Newton's law and the applied forces, we obtain the equation of motion as:

$$m\frac{dv}{dt} = P_{load}(t) - p_0\left(1+\frac{1}{2}(\gamma-1)\frac{v}{c_0}\right)^{\frac{2\gamma}{\gamma-1}} - \frac{p_0 L}{L-x} \tag{2.11}$$

Where v is the velocity of the piston, x is the displacement, m is the mass/chest wall area, and L is the ratio of the volume of the lung/chest wall area. Given the pressure as a function of time, the resulting velocity of the chest wall can be calculated. Assuming the velocity and displacement are small, the equation can be linearized to:

$$m\frac{dv}{dt} = P_{load}(t) - \rho c_0 v - p_0\frac{x}{L} \tag{2.12}$$

It is hypothesized that the lung injury comes as a result of the strains which are related to the average energy dissipated in the lung tissue, a form of work. Normalized work is defined by Stuhmiller as the total work done to produce the wave, divided by the volume of the lung and the ambient pressure. Using the velocity calculated above, the normalized work can be found from this equation:

$$W^* = \frac{W}{p_0 V} = \frac{1}{p_0 L}\int_0^\infty \rho_0 c_0 v^2 dt \tag{2.13}$$

Dimensionless variables X and T are defined based on a time scale τ, where:

$$P_{load}(t) = Pf\left(\frac{t}{\tau}\right) \tag{2.14}$$

$$T = \frac{t}{\tau} \tag{2.15}$$

$$x(t) = \frac{P\tau^2}{m} X(T) \tag{2.16}$$

The dynamics equation then becomes:

$$\frac{d^2X}{dT^2} + 2\left(\frac{\tau}{t_d}\right)\frac{dX}{dT} + \left(\frac{\tau}{t_c}\right)^2 X = f(T) \tag{2.17}$$

Where:

$$t_d = \frac{2m}{\rho c} \tag{2.18}$$

$$t_c = \sqrt{\frac{mL}{p_0}} \tag{2.19}$$

Through non-dimensional analysis and appropriate scaling laws, it is found that the dynamics are independent of the body mass, provided the time scales are scaled by the cube root of the body mass. This also means that the normalized work will be invariant with body mass.

With the dynamics equations derived, the sole required input is now the pressure-time history. Because the pressure pulse is quite different on all sides of the body depending on orientation, a blast test device (BTD) much the same as that of Axelsson, was developed to record multiple pressure signals [Yu, 1990]. Tests are first performed with the BTD to record the pressure traces, followed by a test where the BTD is replaced by a test animal. The work generated from each signal is then calculated and summed as the total work.

The mathematical results were then compared to the extent of injury reported following experimental animal testing. Lung injuries were classed based on the area of injury as: trace (appearance of small petechiae), slight (up to 10%), moderate (10-50%), and severe (above 50%). The increase in lung weight was also used as a marker of injury for some correlations.

A log normal correlation between incidence of injury and normalized work was found, and can be seen in Figure 2.22. The probability of a given level of injury has a bell-

shaped distribution, and the probability of injury above a given level has a log-normal distribution. The relation between average area of lung injury and normalized work can be seen in Figure 2.23, while normalized work versus lung weight in percent of body weight can be seen in Figure 2.24. The experimental data points, although not completely clear, are left in place to show the degree of scatter observed.

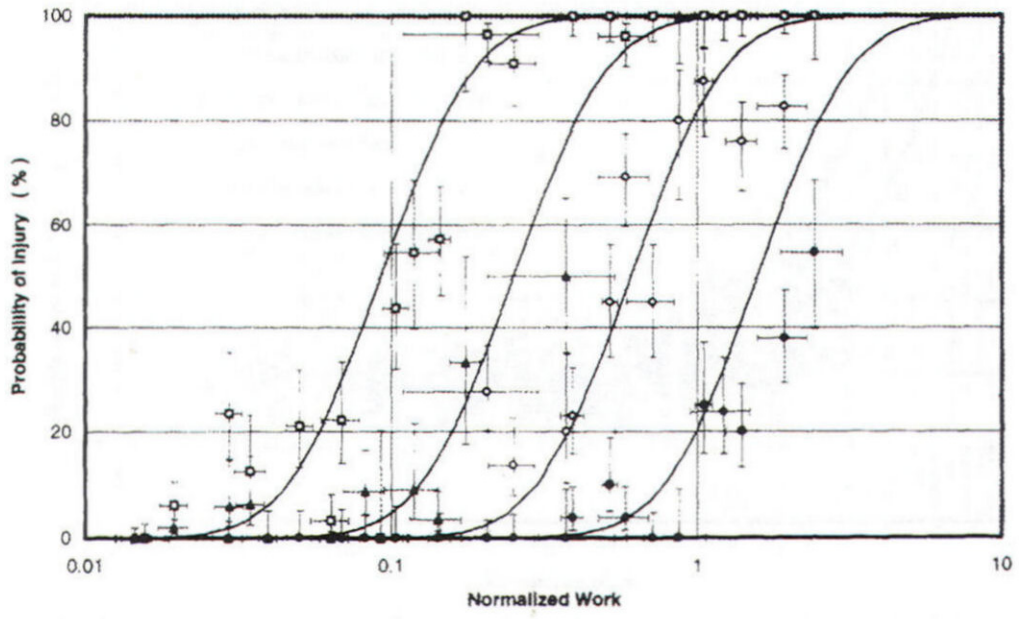

Figure 2.22: Actual experimental data and correlation of incidence of injury with normalized work. Experimental results were sorted as: (□) trace or greater, (▲) slight or greater, (○) moderate or greater, and (●) severe [Stuhmiller, 1996].

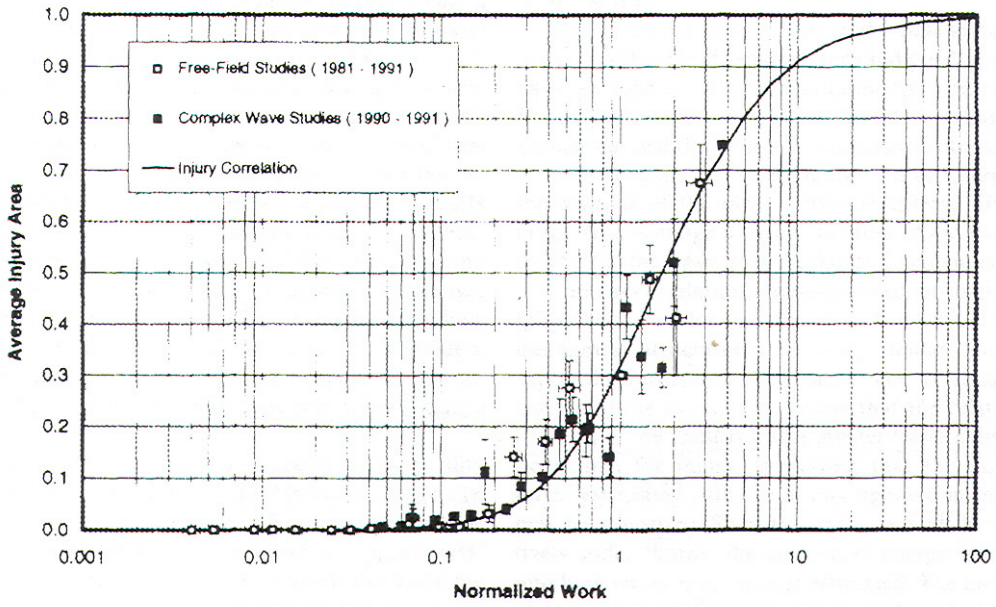

Figure 2.23: Proportion of the area of injured lung against the normalized work. Error bars indicate one standard deviation in either direction after having averaged the values from numerous experimental animal tests [Stuhmiller, 1996].

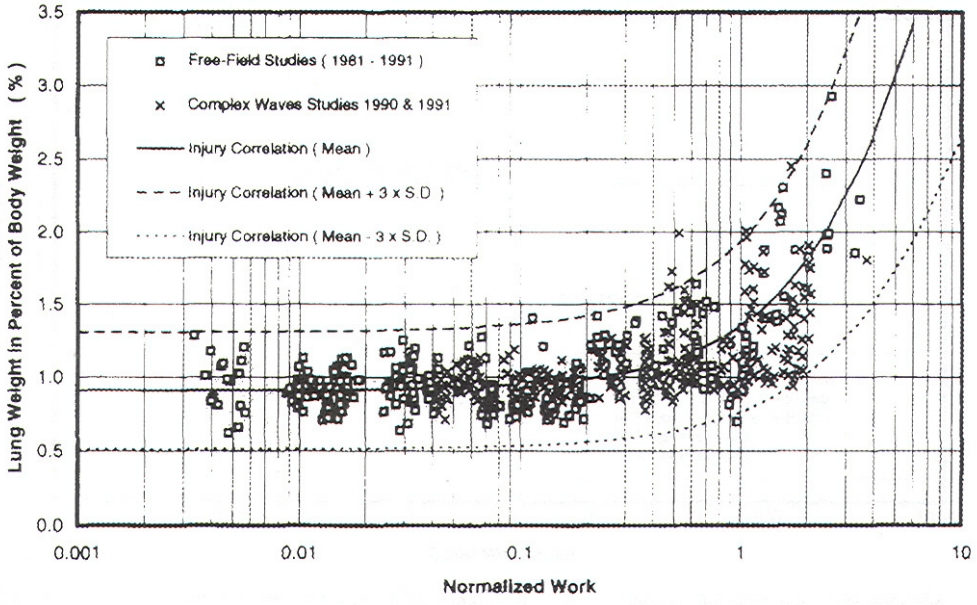

Figure 2.24: Correlation of the lung weight as a percentage of the body weight with normalized work. The variability of the results has to do with the natural variability seen in the control population [Stuhmiller, 1996].

Although the details of internal wave propagation, interaction with internal organs and the viscoelastic forces of the thorax have been neglected, the model correlates well to the lung damage recorded in experimental studies. Also, due to the relatively small displacements of the chest seen in blast loading, neglecting the elastic forces of the rib cage may not be a significant source of error. Another advantage to this system that lends its use to complex blast loading is that the normalized work for slow rising peaks and for stepped peaks drops off significantly with increasing rise time. This finding is significant given that experimental studies have shown that mammals can tolerate higher peak pressures when the duration of the pressure rise is increased, or if the pressure increases in steps.

The results from the Stuhmiller model compare favourably with the experimental results from White et al. (1971) in the free field, as well as near a reflecting surface. Furthermore, in order to justify the case for mass scaling, the normalized work associated with 50% lethality for various species was plotted against body weight. As was seen by Bowen et al., the small and large animal groups centred around two distinct, but constant values. For normalized work, this was calculated as 0.85 for small mammals and 2.08 for large mammals, including sheep, as can be seen in Figure 2.25. Error bars represent uncertainty in the pressure data used to correlate to injury.

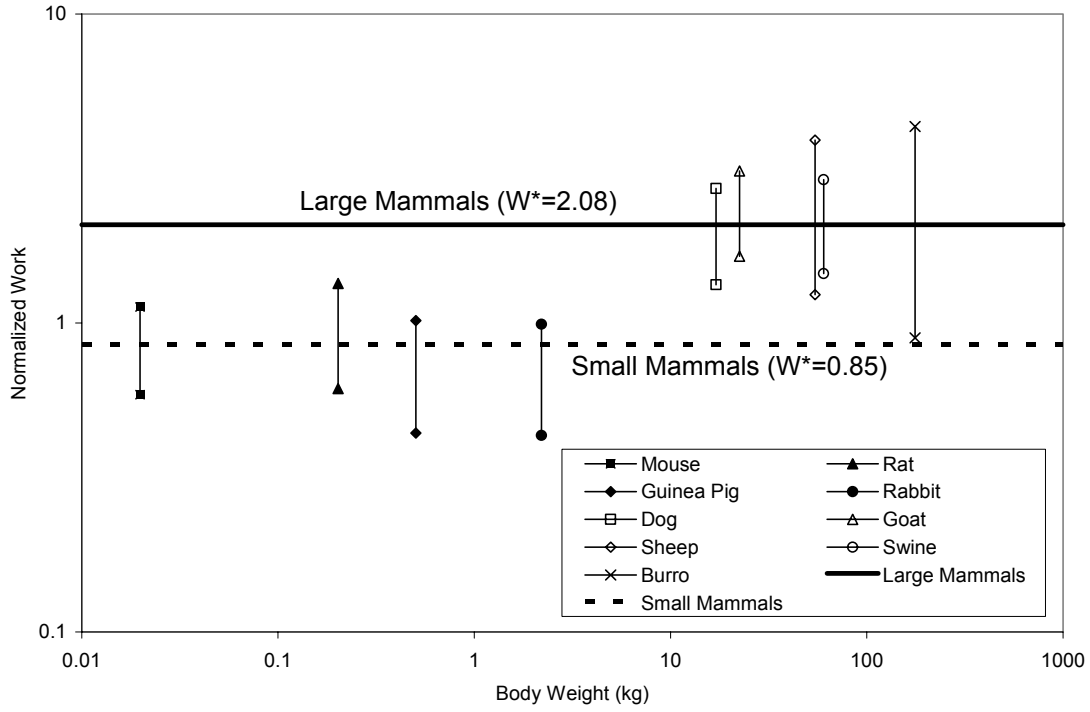

Figure 2.25: Normalized work required for 50% mortality as a function of body weight for various species [Stuhmiller, 1996].

The equations and findings from the above mentioned research was used to create the *INJURY 8.1 Blast Prediction Software*. This software, released by Military Operational Medicine Research Program (MOMRP, www.momrp.org) can predict the level of PBI to humans or sheep of any weight, given the appropriate pressure-time curves. Although this method appears to correlate well to experimental findings, the software lacks the ability to explain the origins of injury, the locations of injury, and cannot be used to compare or develop new personal protection systems since injury is based on pressure measurements of the BTD.

2.8 Numerical Modeling to Predict Blast Injury

For years, the automotive industry has developed complex impact simulation numerical models of vehicles, humans and dummies that would appear to assist in the prediction of blast injury. Unfortunately, significantly different rates of loading, injury mechanisms

and model requirements make the automotive models inappropriate for use in blast studies. Based on similar principles, however, researchers have applied numerical modeling tools to the prediction of blast injury with some success.

2.8.1 Jaycor and U.S. Army

Working as the principal invesigator for Jaycor (now Titan Corp.) on a project from the U.S. Army Medical Reseearch and Development Command at Fort Detrick, Maryland, Stuhmiller developed a very coarse 2-dimensional slice model of a sheep thorax, and later an even coarser 3-dimensional model. They note specifically that the mesh density was too coarse to predict the behaviour of more rapid phenomena, such as accurate wave propagation behaviour. The load is simply applied to the tissue elements on the blast side using a blast pressure-time history. Ribs and intercostal tissue originally alternated around the thorax predicting unnaturally large distortions and pressure results completely unlike experimental measurements. In order to approximate the wave propagation and the long term deformation, intermediate values between bone and tissue were used.

Parametric testing showed that the viscoelastic properties for the biologic materials involved had no significant influence on the pressures measured in the lung. The elastic properties of the ribs and heart were found to make little difference, so long as they were chosen within a few orders of magnitude of the correct physiologic values. The mass density of the ribs, muscle and heart did not have significant influence so long as they remained within tens of percent of the correct values. The mass density and bulk modulus of the lung, as well as the effective shear modulus of the muscle layer were found to be the most sensitive parameters, and caution must therefore be taken in their selection.

Results from the finite element model showed higher pressures behind the ribs on the assaulted side, and were explained as relating to the ‘rib markings’ theory. However, that theory was later proven to be quite the opposite of what really occurs, where the ribs actually shield the lungs during blast loading [Yen, 1985]. They do, however, note that higher pressures are seen in the lung regions that are located against the ribs on the far

side of the thorax, where the pressure waves reflect off the ribs and back into the lung, corresponding to damage seen in experimental testing [Chuong, 1985]. Figure 2.26 shows the experimentally measured esophageal pressure in a sheep exposed to a single blast (left) and two consecutive blasts (right) as well as the ITP predicted by the finite element model.

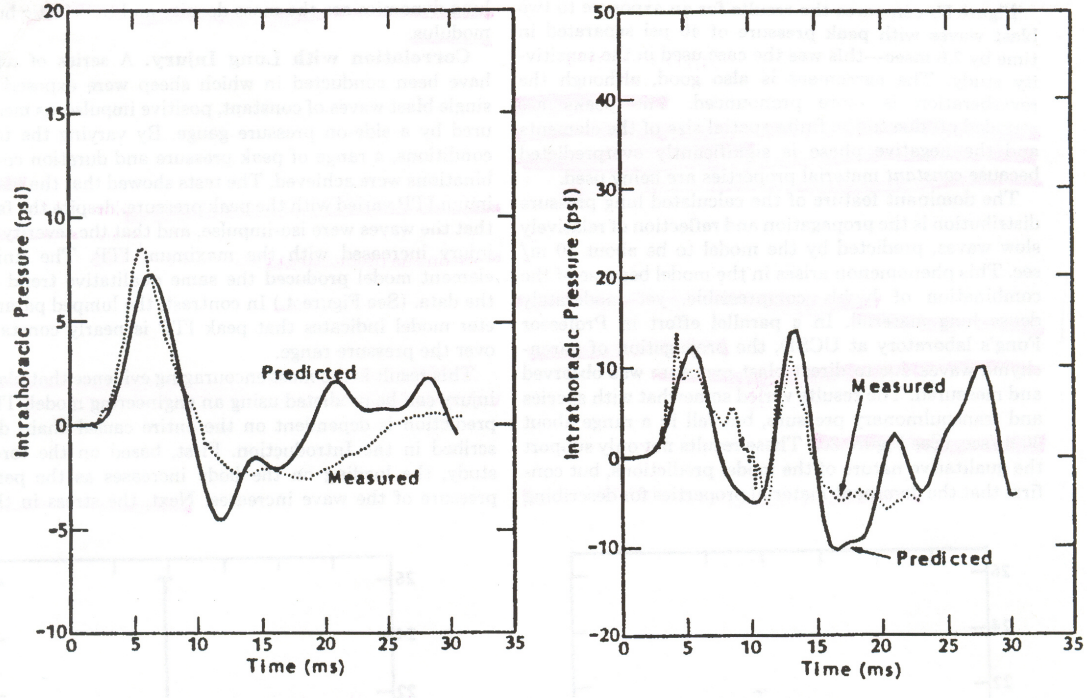

Figure 2.26: Left- Intrathoracic pressure of a sheep exposed to a single blast from a 16 lb TNT charge. Right - Intrathoracic pressure of a sheep exposed to two 40 psi blast waves separated by 7.6 milliseconds [Stuhmiller, 1988].

The researchers state that their lung pressure-history results are within the uncertainty of the blast conditions, instrument response, and particular animal anatomy. However, having created a mechanical model of the thorax, researchers at Jaycor found that pressure measurements varied between the large airways and the parenchyma. This brings into question the value of pressure measurements within the esophagus, and whether they relate in any meaningful way to the pressure variations within the lung parenchyma.

One significant finding was that the strength of the internal compression wave varied linearly with the velocity of the chest wall. This may help explain why Axelsson's macroscopic prediction of chest wall velocity related well to the sustained lung injury [Stuhmiller, 1996].

A significant change from previous findings, Stuhmiller et al. found that the maximum intrathoracic pressure (ITP) varied with peak applied overpressure despite the blast waves being of constant impulse. Their prediction of increasing injury with increasing pressure, but constant impulse does not appear to correspond to the experimental findings of Bowen et al. [Stuhmiller, 1997; Bowen, 1968a]. Fortunately, a lung wave velocity of approximately 30 m/s was measured, and is in agreement with their experimental data [Chuong, 1985; Stuhmiller, 1988]. Overall however, due to the non-coupled nature of the model, the reliance on experimental ITP measurements for correlation, and the extremely coarse mesh design, the applicability of the model to advancing the fundamental understanding of PBI is limited.

Chapter 3 Human and Sheep Thorax Model Development

The goal of this research was to develop a simple but predictive model of the human torso with the capability of predicting primary blast trauma from varied inputs, and assisting in the development of personal blast protection systems. This goal was refined to focus on loading and trauma to the lungs specifically, since this is considered to be the most lethal injury in terms of PBI. A simplified two-dimensional geometry capable of modeling the wave behaviour in the thorax was chosen as PBI is considered to be a wave dominated injury.

The necessary components of a suitable thorax model include: geometry and meshing, material models and properties, and finally contacts and coupling to integrate the thorax with the blast model. In addition to the human torso, a two-dimensional sheep thorax model was created for comparison to the available experimental blast data from animal testing. The sheep was chosen because of the extensive experimental test data available for this animal, and because it is a species with thoracic dimensions and physiology similar to humans. Sheep have proven to be a reasonable human surrogate model for characterizing occurrence, location and severity of pulmonary PBI [Dodd, 1990]. Sheep are also one of the larger species used by Bowen et al. to create the lethality curves, permitting more direct correlation between the finite element analysis and the actual trauma measured during the experimental blast testing.

Throughout the torso model development, the guiding principles included: maintaining accuracy and relative simplicity, limiting computational cost, and ensuring that the models were adaptable to varying loading conditions.

3.1 Quasi Two-Dimensional Thorax Model

Primary blast injury is a pressure wave dominated injury mechanism; for this reason, a predictive finite element model must be capable of accurate wave propagation and reasonable shock resolution in order to provide a realistic prediction of injury at a local level. Mesh density analyses have shown that a very fine mesh, on the order of 2.5 – 5mm element sizes, is required for reliable results – this is further discussed in Section 3.2. Due to computational limitations, a 3-dimensional model of the entire human body at this resolution would not be feasible, and could not be used as an engineering tool.

Although recent studies have highlighted the importance of GI injuries, pulmonary trauma is regarded as a critical form of primary blast injury, making it reasonable to focus on the lungs and the surrounding organs. In order to gain a better understanding of the stress wave interaction within the thorax, a quasi two-dimensional model has been proposed. This model corresponds to a horizontal cross-section through the human torso at mid-sternum level. The two-dimensional simplification is based on two assumptions: (1) since the model corresponds to a location roughly at the midpoint of the thorax, the majority of the air flow at that level travels around the body in a horizontal manner; and (2) the initial wave propagation that causes most of the injury through the thorax is primarily in the horizontal plane when struck by a planar wave. Although some of the longer term wave reflections will deviate from that plane, reasonable predictions and a great amount of insight can be gleaned from the wave behaviour in a 2-dimensional model. For these reasons, and the fact that a 3-dimensional model would have limited practicality, a 2-d simplified model was determined to be of great value, with limited compromise.

3.2 Geometry and Anatomy of the Human Thorax Model

Geometric information from the Visible Human Project (VHP) [NLM, 2004] was used as a guide for creating a pseudo two-dimensional, finite element model of the human thorax.

The VHP is available through the National Library of Medicine in the United States, and the images can be viewed using various applications available on the internet. The VHP began by acquiring the body of a deceased man who was slightly above 50th percentile in size, at 71 inches and 199 pounds [Spitzer, 1996]. The data set consists of 1871 cross-sectional images through the body at 1mm slice increments along the longitudinal axis. The high-resolution pixilated data can be used to view horizontal or vertical slices at any position within the human body. The digital, colour photograph of the chosen slice, located between the 5th and 6th thoracic vertebrae can be seen in Figure 3.1. The chest depth is approximately 230mm and the rib breadth, at 310mm, is slightly above the fiftieth percentile male value of 298.5mm [Robbins, 1983], but is considered reasonable bearing in mind the vast geometric variability of the population.

The mid-sternum location, seen in Figure 3.1 and Figure 3.2, was also chosen because it is a region of significant lung cross-sectional area, allowing for an appreciable view of wave propagation, reflection and focusing. A necessary simplification for this model was the assumption that the ribs are aligned with the horizontal plane. In reality, a horizontal plane would be crossed by three or four ribs/costal cartilages, as seen in Figure 3.1. If a 2-dimensional rib cage were built according to true anatomy, there would be alternating regions of ribs and soft tissue around the periphery, providing unrealistic deformation resulting from an incorrect representation of the stiffness of the rib cage. The solution was to create a half rib layer on top of a half intercostal tissue layer. The half layers, shown in Figure 3.3, were justified by acknowledging the vertical, repeating symmetry of the rib cage. This simplification resulted in a thorax with appropriate wave propagation characteristics and stiffness of the rib cage and intercostal tissue.

Figure 3.1: Cross section of human thorax [NLM, 2004]

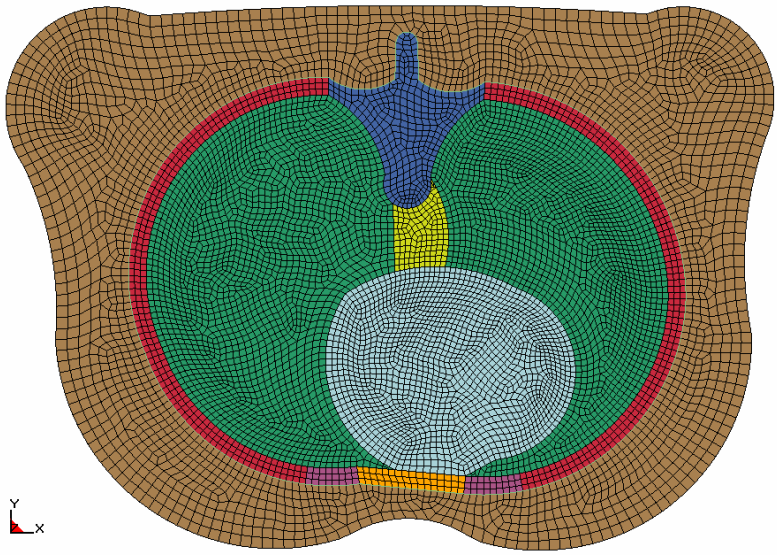

Figure 3.2: Finite element model of human thorax

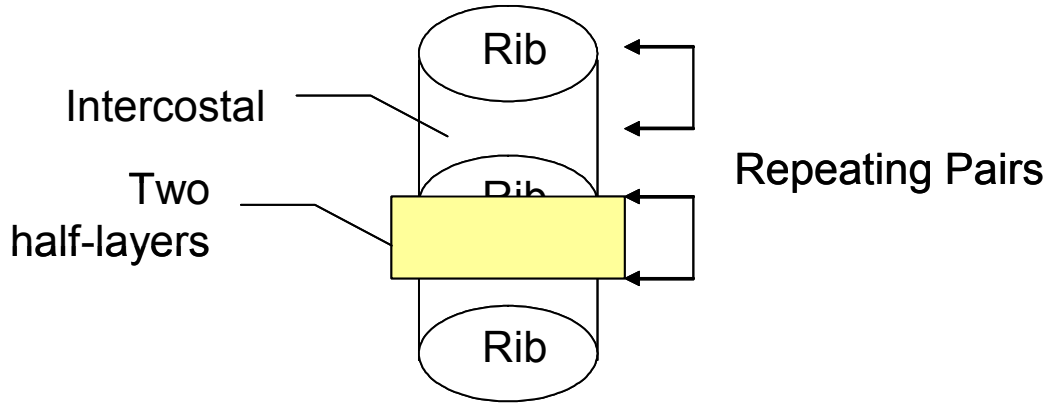

Figure 3.3: Repeating pairs of rib and intercostal tissue shown along with the chosen half-layers forming the quasi 2D model.

To create the model geometry, digitizing software (Engauge Digitizer, Version 2.12) was used to enlarge the image in Figure 3.1 to a life-sized image. Cartesian x and y coordinates were recorded for numerous points on the digitized image and were used to recreate the basic geometry in a commercial modeling and meshing program (MSC/Patran 2005, MSC). A semi-automatic meshing algorithm was used to mesh a single layer of 2-D shell elements, shown in Figure 3.2, which could then be extruded to create four layers of solid elements. Mesh parameters such as size limits, edge ratios and densities were specified, but due to the complex geometry, actual meshing was performed by the software. To simulate the effect of a repeating structure of ribs and intercostal tissue, the rib volume in the upper two layers of the thorax represent a half rib, while the lower two layers represent a half intercostal space. The vertical, repeating symmetry condition was enforced using appropriate displacement boundary conditions. The total thorax model thickness was 1.4cm to approximate the thickness of a half rib and half intercostal tissue pair.

3.3 Geometry and Anatomy of the Sheep Thorax Model

The sheep thorax model was created in the same manner as the human model, but geometric data was found using pictures from "An atlas of x-ray tomographical anatomy

of the sheep," by Davies et al. [Davies, 1987]. An x-ray computer assisted tomographic (CT) machine was used to develop a series of black and white scans through the body of a two-year old, 56.5-kilogram ewe. Fortunately, the mass of this ewe falls comfortably in the range of sheep tested by Bowen, 48.9 to 59.2 kg. The ewe was anaesthetized and placed in a semi-circular trough. Deformation of the thorax due to body weight was minimal and was restricted to the ventral region of the abdomen.

The visibility (amount of light) in the scans is based on the attenuation coefficient, which is related to the atomic number and electron density of the materials relative to the surroundings. The fat, muscle, heart, bones and lungs can be readily identified, and the pictures in this reference are accompanied by labeled drawings. The 48th scan, taken at the level of the 5th and 6th thoracic vertebrae, was used to create the finite element model because it was most anatomically similar to the modeled human torso. Scan 48 is shown in Figure 3.4 with the associated labeled drawing.

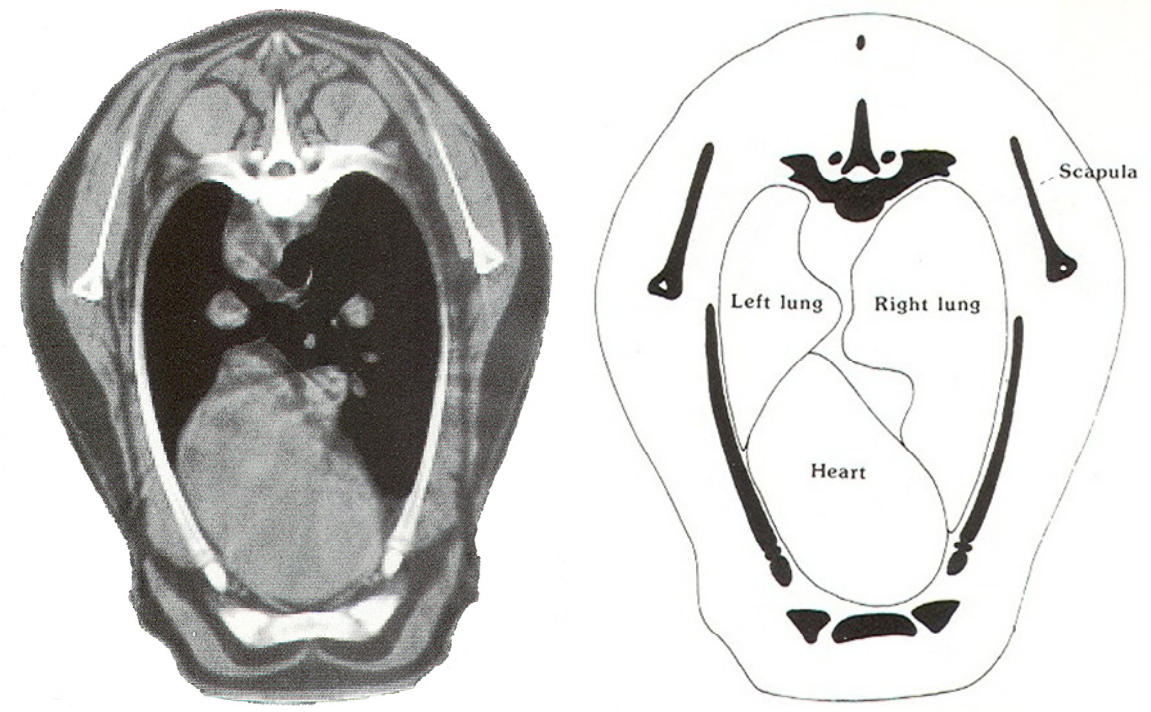

Figure 3.4: X-ray tomographic image (left) and drawing (right) of the thorax of a 56.5 kg ewe, at the 5th-6th thoracic vertebrae [Davies, 1987].

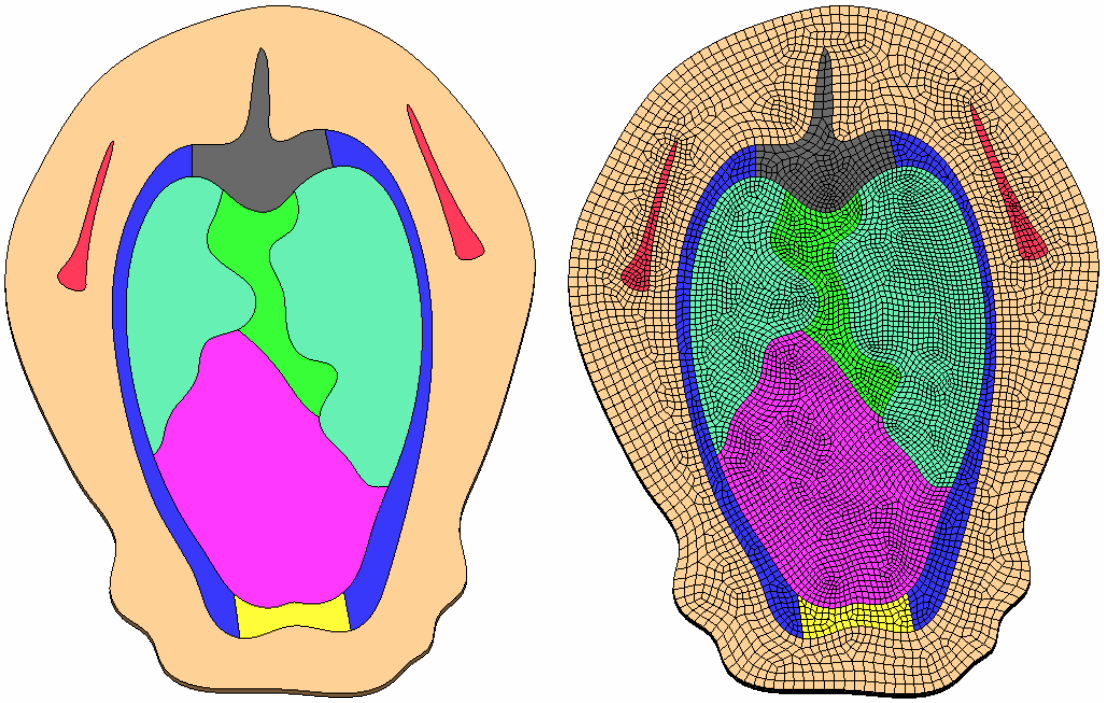

Figure 3.5: Finite element model of sheep thorax showing part outlines (left) and element mesh (right).

The sheep thorax section used for this development measured approximately 261-mm in width (left-right) and 343-mm in depth (ventral-dorsal), making it deeper, but not as wide as the human torso. Each model is composed of several materials and parts representing soft tissue, ribs, intercostal tissue, costal cartilage, sternum, vertebrae, heart, mediastinum and lungs. Comparing the models, one can see that the general anatomical features are quite similar, with the addition of two scapulae, or shoulder blades, in the upper portion of the sheep thorax.

A mesh density analysis showed that elements of air with edge lengths of approximately 4mm were sufficient to represent the pressure loads in the vicinity of the thorax model. In order to improve coupling, the elements on the periphery of the thorax were made to be of the same dimension as the air elements in that region. Elements in the lung were made smaller since the low wave speed in lung would result in large timesteps. Small timesteps are needed to resolve shock wave phenomenon. Because the stress wave is still fairly sharp fronted in the lung, the peak pressure is of very short duration, and hence, is located

only in a small region. If the elements are larger, the peak pressure will be smeared over a greater area, and will no longer be representative of the true peak pressure. Mesh density analyses of the lungs showed that elements of approximately 1.0mm were ideal for a very high degree of accuracy, but elements of that size would cause run times up to a month long. A compromise was reach ed with 2.0 to 2.5mm lung elements, allowing reasonable computation times, and peak pressures approximately 15% below the highest resolution mesh, but with the same trends and pressure profiles. The human torso is composed of 42,165 nodes and 34,328 elements, while the sheep thorax contains 36,740 nodes and 29,856 elements. The vast majority of the elements are 8-noded hexahedrons (bricks) using a constant stress solid element formulation. The remaining elements are 4-noded fully integrated shell elements used only for geometry and contact purposes, described in section 4.5 ALE/Lagrange Coupling.

Numerous blast experiments have been carried out on animals, but unfortunately the orientation of the animal to the blast is often different. Many studies suggest that this does not play a role in trauma, but there was no conclusive data available. In order to study the effect of orientation on trauma, the sheep and human models were exposed to blast waves from the side as well as from the front (sternum). Preliminary analysis (not presented here) of ventrally loaded sheep models showed significantly lower blast pressures on the ventral surface of the sheep and significantly lower pressures in the lungs, as compared to laterally loaded sheep models and ventrally loaded human models. Analysis showed that the worst case scenario for the sheep is to be loaded from the side, likely due to the higher presented area causing much higher air pressures to build up in front of the thorax. Because of this clear variation due to orientation, it was decided that the shock tube test conditions cited by Bowen for sheep should be used as a standard for this research, as they would be represent the experimental data [Bowen, 1968a]. All sheep models in this report are oriented such that the right side of the sheep is positioned facing the blast wave, while the human models are oriented with the sternum facing the oncoming wave.

3.4 Material Models and Properties

Although geometric features are important, appropriate material properties and wave propagation characteristics must also be implemented in numerical models. To simulate the characteristics of the thorax, it was necessary to specify appropriate material properties and constitutive models for all of the biological materials used. The FE model of the human can be seen in Figure 3.6 showing all material parts, except for the exterior soft tissue which has been removed for visibility. There have been several iterations, improvements and simplifications made throughout the course of the study, and the final properties are presented.

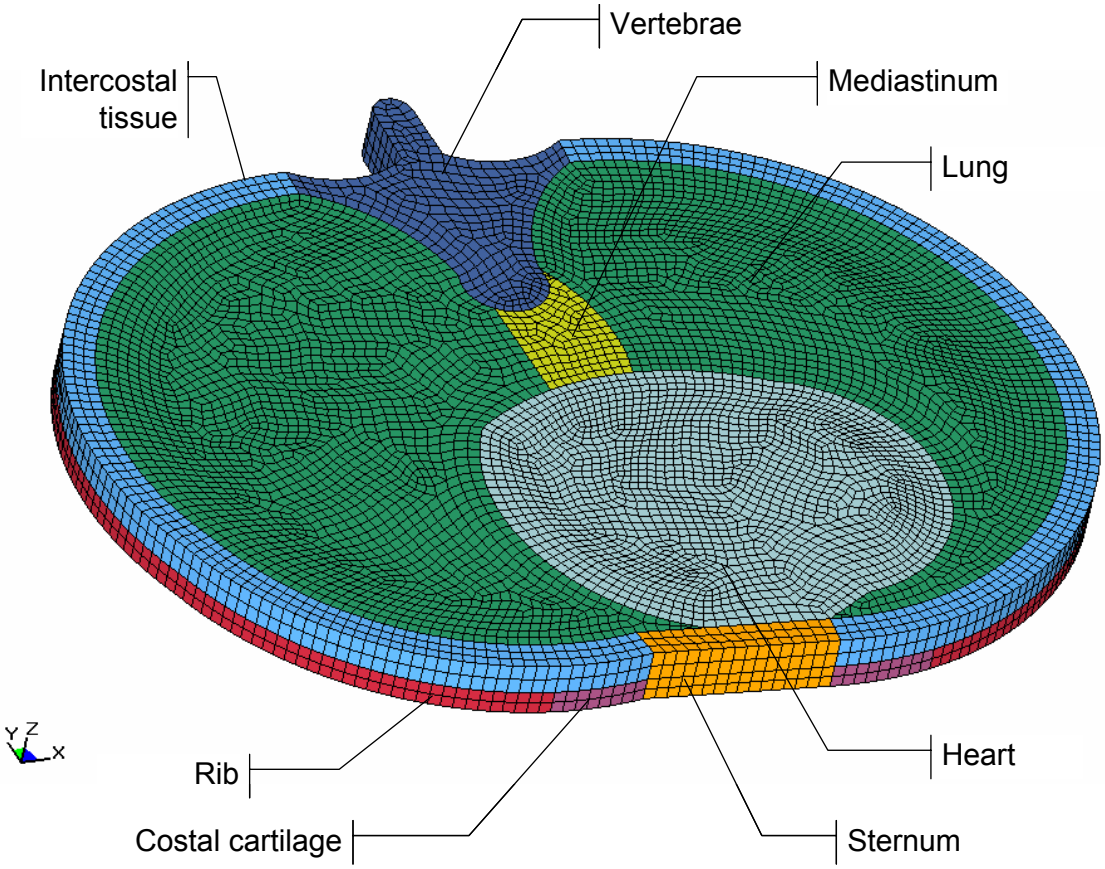

Figure 3.6: FE model of human with exterior soft tissue removed to show parts and element mesh.

In the field of trauma modeling, high-rate biomaterial characterization is likely the greatest challenge facing researchers at the present time. Many automotive companies have carried out testing on human cadavers and biomaterials, but the information obtained is generally for medium rate impact, and the dynamic behaviour of the materials

can seldom be extrapolated to the shock loading regime because of strain-rate dependencies, and wave propagation characteristics.

Y.C. Fung and other researchers have proposed constitutive models to predict the viscoelastic behaviour of lung and other tissues, but once again, they are generally only valid at low rates of strain [Vawter, 1979]. When blast loading of materials is considered, a stress-strain relation is not always sufficient as the effects of stress wave transmission become important, and at very high stresses the hydrostatic material behaviour becomes the dominant factor, as described by Cronin et al. (2000a). In order to accurately predict deformation and stress wave transmission, an appropriate equation of state may be required in combination with a deviatoric constitutive model.

3.4.1 Bone and Costal Cartilage

Macroscopically, and of interest in predicting response to loading, whole bone in the rib structure is composed primarily of two types of bone tissue with very different mechanical properties. Cortical bone makes up the stiff, brittle exterior shell of the bones, while the soft, porous material inside is cancellous bone. The porous cancellous bone is filled with blood, arteries and marrow, where the marrow is composed primarily of fat and water. Attempting to individually model the two types of bone in each of the bone parts (ribs, sternum, vertebrae etc.) would require extremely small elements, forcing the entire model to become overly costly in terms of computation time. To incorporate the properties of cortical and cancellous bone into a unique material model for each of the bone parts, average material values were calculated using a weighted average based on the volume ratios of the two types of bone. This procedure is commonly used in FE models, and the values are typically referred to as *smeared properties*; this is reasonable for the thorax model as the net bending stiffness will be acceptable and the wave speeds for both types of bone are similar. Once the mechanical properties of cancellous and cortical bone are found, and the volume ratios of each type of bone are determined for each of the bone parts, then the smeared mechanical properties can be calculated.

The original bone material properties used in the model were adopted from studies conducted at the University of Waterloo where a simplified lower leg model was used to predict damage from a landmine blast [Cronin, 2000b; Motuz, 2001b]. In order to simulate the deformation and wave propagation in bone, an elastic-plastic-hydrodynamic material model was originally used in conjunction with the Gruneisen equation of state (explained further in Section 3.4.4). The relevant material constants can be seen in Table 3.1.

Table 3.1: Original material properties for cortical bone (Cronin, 2000a).

Mat'l	Density (kg/m^3)	Shear Modulus (Pa)	Yield Stress (Pa)	Plastic Hardening Modulus	Failure Strain	Speed of Sound (m/s)	U_s-U_p Slope: S_1, S_2, S_3
Bone	1762	2.187 E+9	290.0 E+6	1.0 E+6	0.3	2360	1.4, 0, 0

Previous research undertaken at the University of Waterloo focused on bone material models capable of predicting stress wave transmission and failure. However, since broken ribs or scapulae are seldom the result of pure PBI incidents between threshold and LD_{50} levels, failure is not considered in the constitutive models for bone. This is justified by the relatively high blast force that would be required to break ribs, which is above the typical range of interest for PBI. As such it was decided that the original elastic-plastic-hydrodynamic material model for bone included an unnecessary amount of detail and complexity, and therefore unnecessary computational cost.

The original model also permitted the use of an equation of state to account for hydrostatic stresses and the accompanying change in wave speed. However, analyzing the pressure-volume curve and the shock velocity – particle velocity (U_s-U_p) curve, it is clear that the area of interest is limited to the region of linear behaviour; this observation leads to the conclusion that a constant bulk modulus provides a very reasonable approximation for the bone material properties. Given the density, Young's modulus and Poisson's ratio for whole bone (the combination of cortical and cancellous), an elastic material model is therefore capable of predicting the stress wave transmission and elastic

behaviour of various types of hard tissues, including ribs, vertebrae, sternum and costal cartilage.

The three required values for the elastic material model in LS-DYNA are density, elastic modulus and Poisson's ratio. After comparing data from numerous authors, it became evident that there were differences between the material properties for humans, and those for cows, pigs or sheep; hence the human and sheep models utilize slightly different material properties, but the same material models and constraints. The elastic modulus and density of bovine bones were consistently above those for human, pigs and sheep, and have thus not been used as a basis for the models. Mechanical properties from the human femur have also been avoided where possible, as they appear to be superior to other, non-load bearing bones. Pig data is commonly available, and has been treated as equivalent to sheep for the purpose of constructing a sheep model. A collection of values for the elastic modulus and Poisson's ratio from various animals, bones and sources can be seen in Table 3.2 to Table 3.5.

The density of cortical bone ranges from 1700 to over 2000 kg/m^3 [Abé, 1996; Cowin, 2001] with an average value of approximately 1900 kg/m^3. Cortical samples from bovine and human femurs are typically at the upper bound, possibly due to the constant load bearing required of these long bones.

The elastic modulus, density and Poisson's ratio for human cortical bone were calculated as simple averages from numerous bones, test setups and sources, as can be seen below in Table 3.2 and Table 3.5. The same procedure was possible for the elastic modulus of cortical bone for sheep, but reliable data was not found for the density or the Poisson's ratio. By comparing the mechanical properties of specific bones in pigs, sheep and humans, it was found that the density and the strength of the sheep and pig bones were typically on the order of 85 to 90% the value of the human equivalent [Yamada, 1970; Abé, 1996]. For this reason, when density and strength values were not found for the sheep, a value of 90% of that of the human model was used. This procedure was employed for the density of cortical bone in sheep. It is assumed that the Poisson's ratio

from sheep to human should not vary significantly, and as such the sheep materials were assigned the same Poisson's ratios as those of the respective human materials.

The elastic modulus for human cancellous bone was calculated as a simple average (Table 3.3). The modulus for cancellous bone for the sheep model was assigned a value of 90% that of the human. The Poisson's ratio for human cancellous bone was calculated from Viano's [1986] tests on whole, human bone. The same value was assigned to the sheep model.

Density values for cancellous bone are typically quoted as "dry" or "apparent," which do not represent *in vivo* conditions. Apparent density is defined as the mass of bone tissue divided by the bulk volume of the test specimen, including mineralized bone and bone marrow spaces [Mow, 1991]. In order to find a representative density for the cancellous region, including bone, blood, arteries and marrow, the density and volume fraction of the constituents must be found. Abé and Hayashi [Abé, 1996] quote the apparent and true densities for a sample of human cancellous bone as 360.7 and 2032 kg/m^3, respectively, indicating that the actual cancellous bone material occupies approximately 17.75% of the volume. Using a blood/marrow density of 1040 kg/m^3 [Goss, 1978], the *in vivo* density for the cancellous region with bone and blood/marrow is approximately 1216 kg/m^3. A value of 0.9 times this cancellous bone region density was used for the sheep model.

Table 3.2: Experimental data for elastic modulus of human cortical and whole bone and calculated elastic modulus for cortical bone in human model.

Specimen	Detail	Modulus of Elasticity (GPa)	Reference
Humerus, cortical	Tensile	17.2	Yamada, 1970
Radius, cortical	Tensile	18.5	Yamada, 1970
Ulna, cortical	Tensile	18.4	Yamada, 1970
Humerus, whole	Bending	10.0	Yamada, 1970
Radius, whole	Bending	15.9	Yamada, 1970
Ulna, whole	Bending	15.4	Yamada, 1970
Tibia, cortical	Bending	17.5	Abé et al. 1996
Cortical	Longitudinal	17.4	Cowin, 2001
Cortical	Transverse	9.6	Cowin, 2001
Cortical	Bending	14.8	Cowin, 2001
Cortical	Tensile, long.	17.0	Mow and Hayes, 1991
Cortical	Tensile, trans.	11.5	Mow and Hayes, 1991
Human Cortical	Average	15.26	--

Table 3.3: Experimental data for elastic modulus of human cancellous bone and calculated elastic modulus for cancellous bone in human model.

Specimen	Detail	Modulus of Elasticity (GPa)	Reference
Femur, cancellous	Proximal-distal	0.435	Abé et al. 1996
Femur, cancellous	Medial-lateral	0.340	Abé et al. 1996
Femur, cancellous	Anterior-posterior	0.364	Abé et al. 1996
Tibia, trabecular	--	0.702	Abé et al. 1996
Vertebra, trabecular	--	1.340	Rho et al. 1997
Vetebra, trabecular	--	0.570	Abé et al. 1996
Vertebra, trabecular	--	0.660	Ladd et al. 1998 / Abé et al. 1996
Tibia, trabecular	--	0.445	Cowin, 2001
Femur, trabecular	--	0.389-0.441	Cowin, 2001
Human Cancellous	Average	0.568	--

Table 3.4: Experimental data for elastic modulus of cortical bone in the pig [Yamada, 1970] and calculated elastic modulus for cortical bone in sheep model

Specimen	Detail	Modulus of Elasticity (GPa)
Femur	Tensile	14.6
Tibia	Tensile	16.9
Humerus	Tensile	14.3
Radius	Tensile	15.5
Femur	Compressive	4.8
Tibia	Compressive	5.0
Humerus	Compressive	4.9
Radius	Compressive	5.2
Calculated Value for FE Sheep Cortical	Average	10.14

Table 3.5: Experimental data for Poisson's ratio of bone and calculated Poisson's ratio for cortical bone in human model

Specimen information	Poisson's Ratio	Reference
Human, cortical, femur	0.20-0.39	Abé et al. 1996
Human, cortical, femur	0.36	Abé et al. 1996
Human, whole, femur (mechanical test)	0.58, 0.31, 0.46	Viano, 1986
Human, whole, femur (ultrasound test)	0.40, 0.23, 0.37	Viano, 1986
Calculated Human Cortical Average	0.367	--

With material properties for cortical and cancellous bone established, the ratios of the two bone types must be used in order to calculate the whole bone properties for the different bones. The amount of cortical bone ranges from approximately 62% in the vertebra to 92% in the ulna and it is generally assumed that cortical bone makes up approximately 80% of the shaft in long bones [Yamada, 1970; Cowin, 2001]. The ribs are composed of approximately 50% cortical bone, as described by Roberts and Chen [Roberts, 1970] and Yoganandan and Pintar [Yoganandan, 1998]. Gray [1989] describes the structure of the sternum as being "composed of highly vascular cancellous tissue, covered by a thin layer of [cortical] bone." A value of 20% cortical bone has been assumed for the sternum in this model. Properties are summarized in Table 3.6.

Costal cartilage between the sternum and the ribs, as seen in Figure 3.6, is referred to generally as articular cartilage, and can be found in many of the joints in the body. Human articular cartilage is reported by Mow and Hayes [Mow, 1991] to have an elastic modulus ranging from 1 to 10 MPa with an approximate average of 4.5 MPa. The experimental results from various researchers vary drastically, with no clear consensus on a value among the FE modeling community. Yamada [1970] reports a human articular cartilage modulus of 49 MPa (an order of magnitude greater than stated by Mow), while the modulus for pigs was slightly higher at approximately 67 MPa. Various finite element models have been created of the human thorax, primarily for the automotive industry, and the costal cartilage mechanical properties vary substantially from one model to the next. Roberts and Chen [Roberts, 1970] use a value of 276 MPa, but they specifically state that they are not suggesting this to be a typical value. Deng [1999] defines a Young's

modulus of 1200 MPa by stating that the value has been "augmented to account for material transition of bone-cartilage-bone" Such methods have apparently been used by various researchers in order to validate the performance of their thoracic models, without relying on experimentally derived material properties. For this research, the experimental values from Yamada were used. These moduli, although lower than those used in most other models, were the only reliable, experimentally referenced values available. A Poisson's ratio of 0.4 was used, as given by Viano [1986]. A density of 1281 kg/m^3 was calculated as the average between rib and water, which can be considered reasonable as Yamada states that water is the main constituent of articular cartilage.

After reviewing a substantial amount of experimental data from various researchers, the chosen values are summarized in Table 3.6 and Table 3.7. The density, Young's modulus and Poisson's ratio have been calculated as an average of representative values from numerous sources whenever possible, and, as previously discussed, the whole bone values are a volume weighted average of the cortical and cancellous bone properties.

The material acoustic wave speeds in the proceeding tables were calculated using the equation for bulk wave speed [Meyers, 1994], shown here:

$$c = \sqrt{\frac{E(1-\nu)}{(1+\nu)(1-2\nu)\rho}} \tag{3.1}$$

where E is Young's modulus and ν is Poisson's ratio. The calculated values for bone appear to be representative of experimental data, as shown here:
Human cortical bone: 1870-3500 m/s [Goss, 1978]
Human bone: 3500-4300 m/s [Dowsett, 1998]
Pig cortical bone: 2941 m/s [Goss, 1978]
Bovine cortical bone 3270 [Abé, 1996]

Table 3.6: Material model parameters of bone and costal cartilage for human model

Human	Density (kg/m^3)	Young's Modulus (GPa)	Poisson's Ratio	Calculated Sound Speed (m/s)
Cortical	1907	15.26	0.367	3730
Cancellous	1216	0.57	0.392	971
Ribs	1561	7.92	0.379	3073
Sternum	1354	3.51	0.387	2248
Vertebrae	1644	9.68	0.376	3282
Costal Cartilage	1281	0.049	0.400	286

Table 3.7: Material model parameters of bone and costal cartilage for sheep model

Sheep	Density (kg/m^3)	Young's Modulus (GPa)	Poisson's Ratio	Sound Speed (m/s)
Cortical	1716	10.14	0.367	3205
Cancellous	1094	0.51	0.392	971
Ribs / Scapula	1405	5.33	0.379	2657
Sternum	1219	2.44	0.387	1976
Vertebrae	1480	6.48	0.376	2832
Costal Cartilage	1203	0.067	0.400	344

3.4.2 Muscle and Fat

The human body is composed primarily of water, with muscles being approximately 73% water in composition. A natural first step in terms of an equation of state would be to utilize the equation of state for water, with a modified viscosity to more accurately reflect the nature of the muscle tissue. Clemedson [1956] and other authors have noted that due to the high water content of most animal tissues, the low modulus of rigidity and the high bulk modulus, a fluid of high viscosity could reasonably approximate stress wave propagation behaviour in tissue.

For the heart and soft tissue materials in the thorax, a viscous fluid model with an equation of state was originally applied, based on the assumption that accurate wave propagation behaviour required an EOS. Unfortunately, a material model with deviatoric strength (other than viscosity) used in combination with an EOS was not available in LS-DYNA. Although the wave propagation is well represented, the disadvantage of lacking deviatoric strength was clearly seen during longer duration simulations, as the soft tissues showed excessive, unrealistic deformation.

Using the Mie-Gruneisen equation of state, the accompanying shock equations and the available shock properties, it was found that the pressure-density ratios of water, blood, muscle and fat remained linear in the region of interest, and were almost identical to one another. As such, it was determined that using a constant bulk modulus (that of water) would accurately represent the volumetric and wave propagation characteristics, thereby eliminating the need for an EOS.

Relying primarily on a compilation of vast amounts of experimental data from various researchers, it was found that typical sound speeds for fat and muscle were in the range of 1440-1500 and 1540-1580 m/s, respectively [Goss, 1978]. The average density for fat and muscle were found to be approximately 930 and 1070 kg/m^3, respectively. In contrast to the mechanical properties of bone, there was little variation between human and animal data.

The acoustic impedance of materials determines the amplitude of the reflected and transmitted waves at an interface. If typical acoustic impedances ($z = 1.7x10^6$ kg/m^2s for muscle; $z = 1.4x10^6$ kg/m^2s for fat) are used, it is found that only 10% of a wave traveling from fat into muscle would be reflected while 90% of it would be transmitted. With such similar properties, and such complex geometry separating fat and muscle in the thorax, it is reasonable to treat the two soft tissues as one continuous material, with properties derived from the average of its two constituents. The sound speed and bulk modulus were taken directly from water, reflecting the high water content of muscle and fat. Material properties for soft tissue can be seen in Table 3.8.

Table 3.8: Material model parameters for soft tissue (fat and muscle)

Material	ρ (kg/m3)	Sound Speed (m/s)	Bulk Modulus (N/m^2)
Soft Tissue	1000	1500	$2.2x10^9$

Without the need for an EOS, it was decided that better model behaviour could be achieved using a material model capable of strain rate sensitive deviatoric behaviour. Such an approach was taken using published experimental data from Van Sligtenhorst et al. [Van Sligtenhorst, 2003] and McElhaney [McElhaney, 1966].

A strain-rate sensitive, rubber-like material model was used, defined by a series of uniaxial load curves at discrete strain rates [DuBois, 2003]. A linear bulk modulus provides bulk material behaviour, while compressive and tensile stress-strain curves with their associated strain rates define the deviatoric behaviour. Following the numerical work of Van Sligtenhorst et al., the bulk modulus of water was used, and a density of 1050 kg/m^3.

Lacking high-rate experimental tensile data, quasi-static tensile data from Yamada [1970] was used for tensile stress calculations (Figure 3.7). Because much of the high-rate deformation occurs early in the interaction between the blast and the thorax, in a compressive manner, and tension is seen primarily in the later, damped response, the lack of high-rate tensile data is not assumed to be of great influence. The addition of tensile deviatoric properties, however, is seen as a vast improvement over the previous null material as it prevents the unrestrained long-term, large deformation flow that is not representative of actual test data.

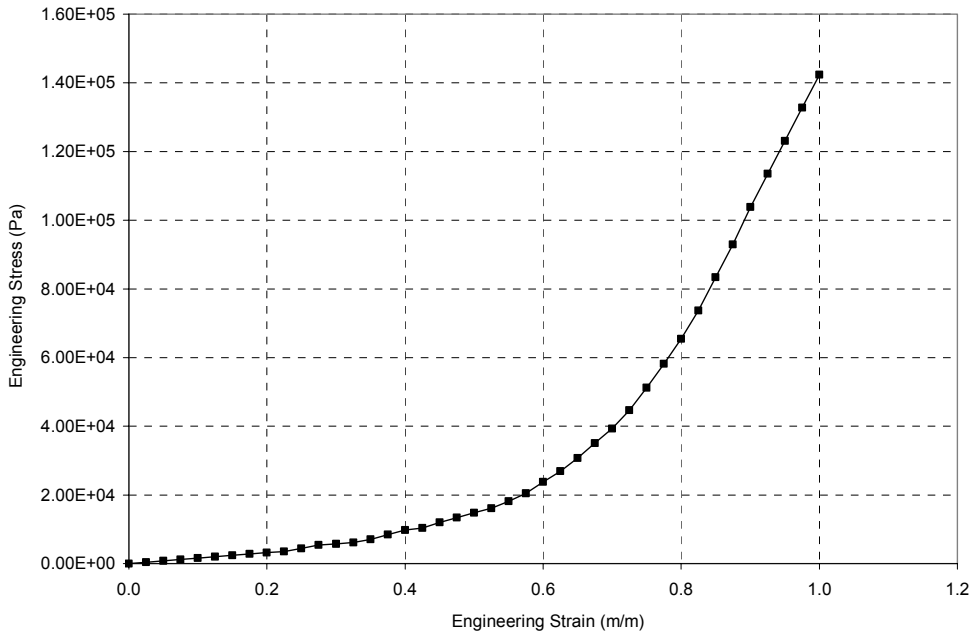

Figure 3.7: Tensile stress-strain curve from Yamada [1970] for muscle tissue

The compressive stress-strain curves were adopted primarily from Van Sligtenhorst et al. [2003], but a curve from McElhaney [1966] at the $100s^{-1}$ strain rate is used in order to better bridge the gap in the data, as can be seen in Figure 3.8. The gap in strain rates is due to the change in apparatus used by Van Sligtenhorst et al.: quasi-static data was found using an Instron machine, while the high-rate data was recorded using a polymeric Split Hopkinson Pressure Bar (SHPB).

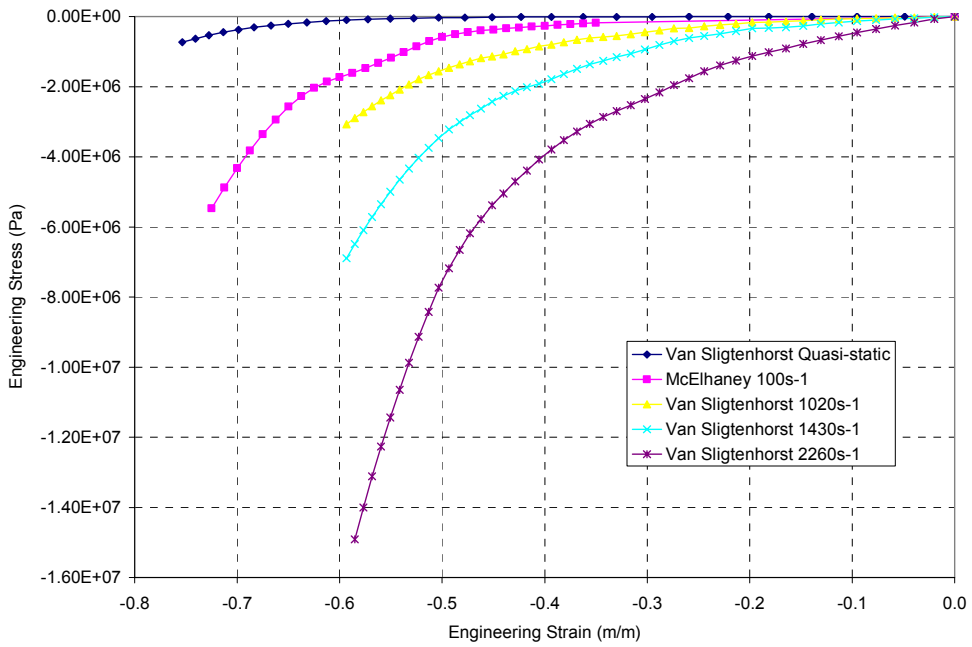

Figure 3.8: Compressive muscle tissue data from Van Sligtenhorst [2003] and McElhaney [1966], with strain rates ranging from quasi-static to 2260 s^{-1}.

Numerical studies were undertaken to ensure that the wave propagation behaviour of the simplified rubber material matched that of the null material with the EOS. The wave propagation speed remained approximately 1500 m/s, which is to be expected given that the bulk modulus of water was used and the relatively modest pressures that are seen in blast. The simplified rubber model showed less extreme long term deformation and a damped response, corresponding to characteristics seen in animal blast studies.

3.4.3 Heart

Just as with soft tissue, the argument can be made for changing the heart tissue to a strain rate sensitive, hyper-viscoelastic material model using high-rate experimental data. There is, however, no specific high-rate data available for the heart. Although the heart itself is a muscle, its nature and function make it rather unique. Resting heart muscle is stiffer than resting skeletal muscle (Fung, 1993), and it is filled with a significant amount of blood. Table 3.9 shows typical properties for the heart and blood.

Table 3.9: Published material data for heart tissue and blood.

Material	ρ (kg/m3)	C (m/s)	Reference
Blood	1040	1560	Goss et al., 1978
Heart	1030-1100	1540-1580	Goss et al., 1978

Given that the bulk modulus for both blood and muscle can be reasonably approximated by that of water, the two constituents of the heart can be assigned the same bulk properties. In terms of deviatoric strength, lacking more detailed data for the heart, it is assumed that the strength lost by having cavities in the heart is balanced by the heart muscle being stiffer than skeletal muscle. As such, the same rate sensitive material properties of the soft tissues are used to represent the heart. This is an approximation, but this model is seen as a significant improvement over the behaviour provided by the viscous fluid material.

3.4.4 Lung

The most unique and challenging biomaterial to model in the thorax is the lung due to its multi-material, multi-scale structure, natural damping behaviour and low wave speed. The lung tissue makes up only approximately 10% of the volume of the lungs, or perhaps as much as 30% when blood is included, while the remainder is filled with air; one can therefore understand the low density of lung compared to other organs. Subject to blast loading, the lung behaves similar to closed cell foam because much of the air does not have time to escape from the alveoli, thereby trapping a significant portion of the air in the lungs.

While the speed of sound in air and water are 340 and 1500 meters per second respectively, the speed of a stress wave propagating through an inflated lung is only 30-40 meters per second [Fung, 1985; Yen, 1986]. The fact that the stress wave propagation speed in lung is significantly lower than both of its primary contributors may at first appear counter-intuitive. However, because this particular material has the high density of tissue and the low bulk modulus of air, a low wave speed can be expected. Knowing

that the speed of sound in an elastic medium is the square root of the modulus divided by the density of the material, a theoretical wave speed can be calculated. Using the theory of mixtures for calculating both the density and modulus of the lungs, theoretical sound speeds correlate well with experimental values [Grimal, 2002; Yen, 1986].

While the pressure-volume relation of the other soft tissues in the thorax remained linear in the region of interest, the lung material behaviour is extremely non-linear, and requires an EOS. As such, a viscous fluid model with a Gruneisen equation of state has been used to model the bulk response and the wave propagation behaviour of the lung. This, unfortunately, precludes the use of deviatoric strength properties because LS-DYNA does not provide a material model that accommodates both deviatoric strength and an EOS. Since PBI is a wave dominated effect, accurate wave propagation was considered more crucial than long-term large deformation behaviour. A material model capable of incorporating both aspects of the physical phenomena would be ideal, and could be done in the future using a user-defined material model.

The Gruneisen equation of state calculates pressure based on volume change using input data from the U_s-U_p curve that defines the velocity of a shock wave relative to the particle velocity. The Gruneisen equation of state for compressed materials is defined as [Halquist, 2003; Meyers, 1994]:

$$p = \frac{\rho_0 C^2 \mu \left[1 + \left(1 - \frac{\gamma_0}{2} \right) \mu - \frac{a}{2} \mu^2 \right]}{\left[1 - (S_1 - 1)\mu - S_2 \frac{\mu^2}{\mu + 1} - S_3 \frac{\mu^3}{(\mu + 1)^2} \right]^2} + (\gamma_0 + a\mu) E \tag{3.2}$$

And for expanded materials as:

$$p = \rho_0 C^2 \mu + (\gamma_0 + a\mu) E \tag{3.3}$$

Where C corresponds to the speed of sound in the uncompressed material, while the subsequent constants, S_1, S_2 and S_3 are the coefficients of the slope of the U_s-U_p curve; γ_0 is the Gruneisen gamma; a is the first order volume correction to γ_0; E is the initial energy (set at zero); and the density change is defined as:

$$\mu = \frac{\rho}{\rho_0} - 1 \tag{3.4}$$

As stated above, the speed of sound in undisturbed lung tissue is approximately 30-40 m/s, but higher sound speeds have been recorded, possibly due to testing at higher than in vivo lung densities (near collapsed lung), increased fluid in the lungs or different measurement techniques.

Typical values for lung density range from 200-400 kg/m^3 [Goss, 1978; Grimal, 2002; Yen, 1986; Fung, 1985], depending significantly on the applied transpulmonary pressure. Bowen et al. [1968a] define the average density of the lung, $\overline{\rho}$, as

$$\overline{\rho} = \frac{M}{(\overline{V} + v)} \tag{3.5}$$

where M is the mass of the lungs, $\overline{V}$ is the average gaseous volume of lungs (functional residual capacity plus one half of the tidal volume) and v is the volume of lung tissue. The approximately 200 kg/m^3 density for human lungs defined by Bowen (and also by Chuong, 1985) is at the lower bound of published values, but was chosen due to the scientific weight of Bowen's published works as well as the rigid definition of how the lung density value was derived.

The available experimental data on lung tissue properties is somewhat limited in terms of stress wave transmission. However, the slope of the U_s-U_p curve may be obtained from theoretical calculations based on porosity and constituent material properties. The effect of the U_s-U_p slope can more readily be understood using a pressure-density graph; these two quantities are related through the Mie-Gruneisen equation of state and its accompanying shock relations.

In the quest for a suitable material model for bird impact analysis, Wilbeck [Wilbeck, 1978] studied the shock behaviour for water with various porosities. Using experimentally validated Gruneisen parameters for both water and air, an equation was

derived by which the two could be combined, and a pressure-density or U_s-U_p curve created. Using this method, Willbeck created curves for porosities up to 40%.

For a given change of pressure, the change in density of the lung is the summation of the changes in density of both air and tissue [Willbeck, 1978]. The material constants and EOS for air, water and lung are shown in Table 3.10 and Table 3.11; *z* is the volume fraction of air in the lung and is used to calculate the lung density by assuming the remainder of the lung is filled with water (representing blood/tissue) with a density of 998 kg/m^3 [Willbeck, 1978]. The bulk lung material behaviour can be modeled numerically using a Mie-Gruneisen EOS, requiring the sound speed in the material, C_0, and k, the slope of the shock velocity – particle velocity (U_s-U_p) curve [Halquist, 2003; Meyers, 1994]. When the equations of state for air and water are placed in the form of density ratios as a function of pressure, the changes in density can then be summed, based on the proportion of each material, as can be seen by the lung EOS in Table 3.11.

Table 3.10: Material constanst for air and water [Willbeck, 1978; Deal, 1957]

Material	ρ_1 (kg/m^3)	C_0 (m/s)	k
Air	1.25	340.9	1.03
Water	998.23	1482.9	2.00

Table 3.11: Equations of state for air, water, and the combination simulating lung [Willbeck, 1978; Deal, 1957].

Air	$\frac{\rho_1}{\rho_2} = (1-q)$ where $q = q_1 - q_2$ and $q_1 = \frac{2\overline{P}k + \frac{\rho_1 C_0^{\,2}}{P_1}}{2\overline{P}k^2}$; $q_2 = \frac{\left[\left(2\overline{P}k + \frac{\rho_1 C_0^{\,2}}{P_1}\right)^2 - 4\overline{P}^2 k^2\right]^{1/2}}{2\overline{P}k^2}$
Water	$\frac{\rho_1}{\rho_2} = \left(\frac{P_2 - P_1}{A} + 1\right)^{\frac{-1}{B}}$ where $A = \frac{\rho_1 C_0^{\,2}}{4k-1}$ and $B = 4k-1$
Lung	$\frac{\rho_1}{\rho_2} = (1-z)\left(\frac{P_2 - P_1}{A} + 1\right)^{\frac{-1}{B}} + z(1-q)$

The above equation of state for lung has been used to calculate pressure-density curves and U_s-U_p curves for lung with varying porosities, shown in Figure 3.9 and Figure 3.10, respectively. When porosity is set to 1 or 0, the equations correctly predict the undisturbed sound speed of air and water at 340.9 and 1483 m/s, respectively. At porosities between pure air and pure water, the sound speed drops drastically, as has been shown in experimental studies of bubbly water [Thuraisingham, 1998; Wilson, 2005].

Matching the calculated lung pressure-density curves with curves created from the Mie-Gruneisen EOS parameters, it was possible to find accurate values for C_0 and k for various porosities, shown in Table 3.12.

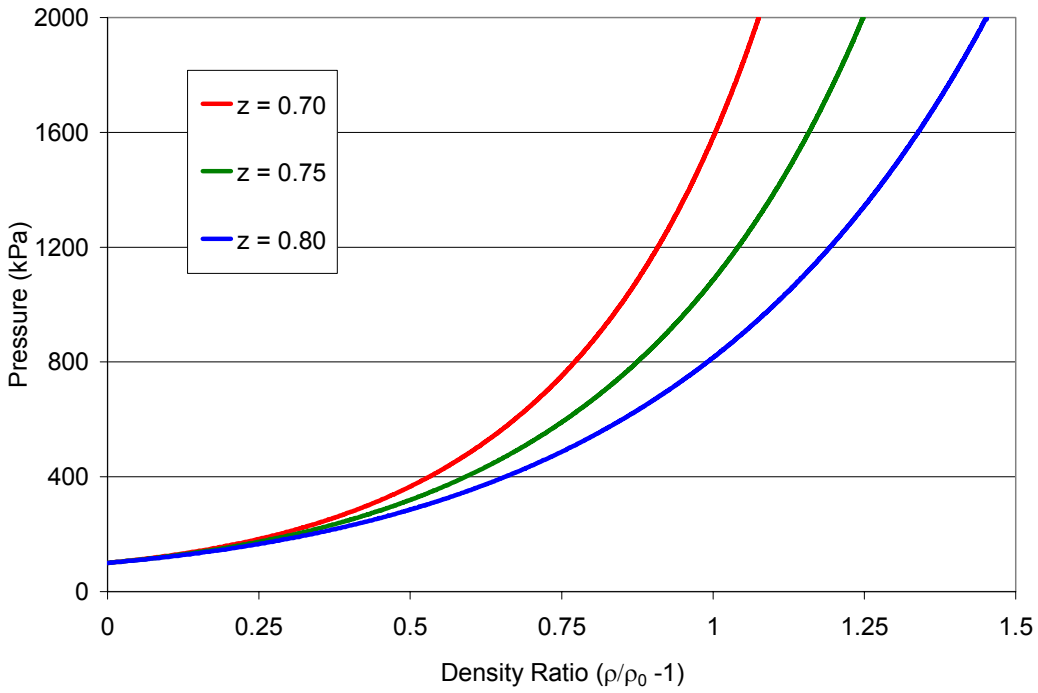

Figure 3.9: Relationships between pressure and density ratio for lung with varying porosities.

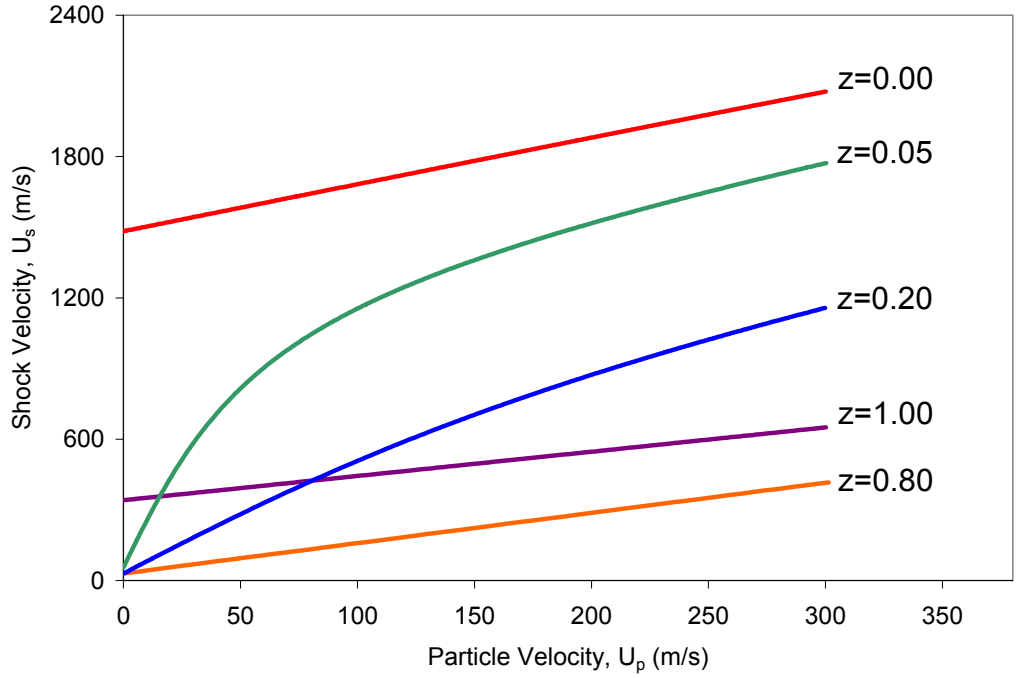

Figure 3.10: Relationships between shock velocity and particle velocity for lung with varying porosities.

Table 3.12: Calculated material values for lung with varying porosities.

Porosity, z	0.70	0.75	0.80
Speed of Sound, C_0 (m/s)	26.3	27.8	30.1
Slope of U_s-U_p, k	1.480	1.380	1.295

The calculated speed of sound for lung tissue matches well to experimental data for human lungs noted earlier in this section. Figure 3.11, below, shows the variation of wave speed in animal lungs with transpulmonary pressure [Stuhmiller, 1988]. Transpulmonary pressure is defined as the difference between the alveolar pressure and the pressure in the pleural space, and hence cannot be compared directly to the effects of lung material compression due to a pressure wave. However, by comparing the wave speeds in undisturbed lungs, it can be seen that the C_0 calculated by the above equations is in agreement with the experimental data.

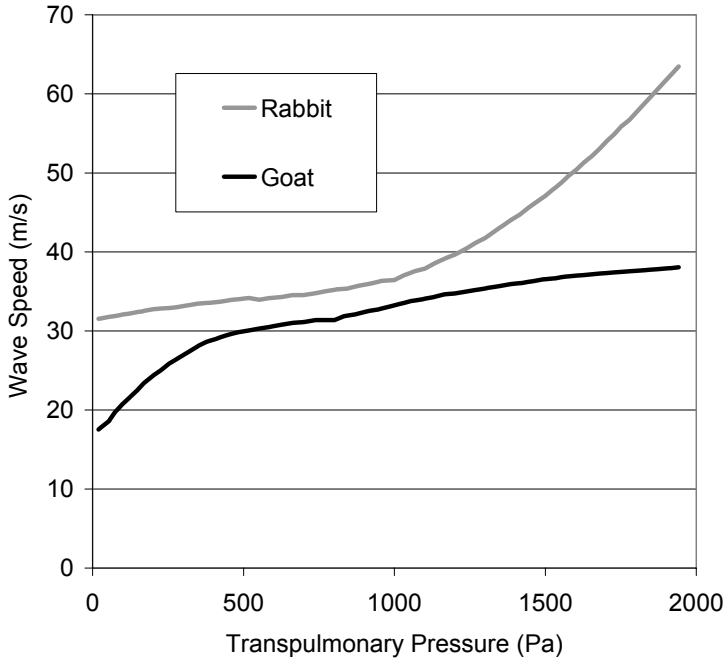

Figure 3.11: Wave speeds in the lungs of rabbit and goat at varying transpulmonary pressures [Stuhmiller, 1988].

The parameters derived above permit a reasonably accurate representation of the volumetric and stress wave transmission behaviour of lung tissue, and can be directly applied to the finite eleent model using the parameters listed below, in Table 3.13.

An experimental value for the dynamic viscosity of lung was not found, but Abe and Hayashi [Abé, 1996] state that, depending on shear rate, blood has a dynamic viscosity ranging from 0.01-0.1 Pa·s, and Von Gierke [1968] found that soft tissue has a viscosity of approximately 15 Pa·s. A brief sensitivity study was undertaken to find whether the dynamic viscosity of lung tissue would result in changes to the pressure wave, and hence the predicted injury. By changing the viscosity of the lung from 0.1, to 1.0 Pa·s, a reduction of approximately 10% in the peak lung element pressures was seen. A similar reduction was seen when the value was changed from 1.0 to 10 Pa·s.

Given that lungs are a combination of soft tissue, blood and air, a value of 1.0 Pa·s was prescribed for the dynamic viscosity of lung, representing an order of magnitude above the viscosity of blood, and an order of magnitude below that of tissue. 1.0 Pa·s has been chosen as a conservative estimate, but if an increase in the amount of deviatoric strength being simulated by viscosity is desired, a higher value could be used, bearing in mind the anticipated effect on the pressure wave.

Table 3.13: Material model parameters for lung tissue.

Material	ρ (kg/m3)	Dynamic Viscosity (Pa·s)	C (m/s)	S_1
Lung	200	1.0	30.1	1.295

Injury prediction to the thorax currently focuses on tracking parameters of interest in specific organs, such as peak pressure in the lung, to identify the degree of predicted damage or injury. Although the current modeling approach is providing a good degree of predictability related to primary blast injury, this approach requires the tracking of all lung elements, followed by a filtering process to pull out the required information (peak

pressure, initial volume, etc.). Due to the transient nature of the solution this requires a significant amount of effort.

Chapter 4 Numerical Modeling of Blast Loading

With human and sheep thorax models created, the next step was to create a realistic and flexible blast environment. In addition, it is known that coupling between the blast flow and deformable body is significant. To expose the thorax to blast loading where it is able to actively interact with the incoming loads, a combination of Lagrangian and Eulerian formulations is necessary to represent the structural nature of the thorax, and the fluid flow of the explosive and air elements.

4.1 Arbitrary Lagrangian-Eulerian Formulation (ALE)

The LS-DYNA hydrocode [Halquist, 2003; Halquist, 1998] was selected to simulate the coupled human torso-blast problem due to the availability of fully coupled fluid-structure analysis and previous experience in biomechanical modeling with this code. LS-DYNA is an explicit, dynamic, nonlinear finite element code with a multi-material capability allowing the use of up to 12 different materials simultaneously within cells. The models are developed using an Arbitrary Lagrangian-Eulerian (ALE) formulation with the thorax modeled as a Lagrangian structure and the air and blast modeled as Eulerian fluids.

The Lagrangian formulation is based on a control mass where the elements distort over time, but the mass and composition of the elements remain constant. Lagrangian codes have the advantage of being fairly straightforward to implement, but they are not capable of very large strains (fluid flow) due to instabilities and greatly reduced timesteps resulting from element distortion. Eulerian codes are typically used in fluid flow problems, and are control volume based, where the material flows through a fixed mesh. Such a formulation permits turbulent flow calculation, large strains and the creation of free surfaces, and because of the fixed mesh, the timesteps remain relatively stable. Unfortunately, Eulerian codes cannot track the state variables for given elements over time as the material flows through the mesh.

The solution to these issues is to couple a Lagrangian structural model with an Eulerian representation of the fluid flow in a coupled ALE formulation. The LS-DYNA ALE implementation can be described as being composed of a Lagrangian timestep, followed by advection of the element state variables and remapping of the mesh. The first step, shown in Figure 4.1 (A-B) proceeds with element deformation as would be performed in a typical explicit Lagrangian code, with nodal forces calculated as the combined forces from deviatoric and volumetric deformation. Deviatoric stresses are calculated from strains in combination with either material specific constitutive models or viscosity. Volumetric stresses are calculated from the bulk strains in combination with a bulk modulus or an equation of state. After the Lagrangian timestep, the material and element state variables remain in place as the element boundaries are remapped to eliminate large scale element distortion, shown in Figure 4.1 (B-C). The remeshing of boundaries while allowing material to remain in place is referred to as advection. Advection can also be understood as material flowing through the element mesh. The Eulerian formulation can be seen as a special case of ALE where the mesh velocity is zero, or where after each timestep the elements are remapped onto the same, original mesh. This is the type of remeshing currently used, avoiding the need for mapping onto a new, arbitrary mesh.

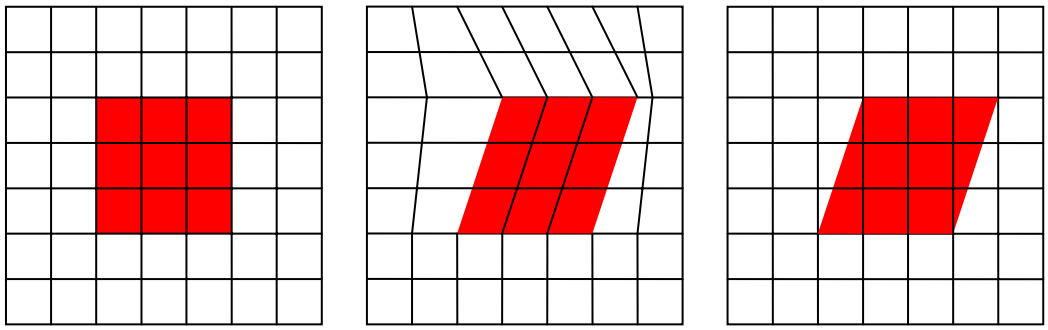

Figure 4.1: Showing steps of (A) original, (B) after Lagrangian step, and (C) advection.

A shortcoming of the code, however, has to do with the implementation of the advection scheme. Material can only advect through faces of the elements, and hence cannot transport material diagonally, as depicted in Figure 4.2. The effect of this is seen if the predominant direction of fluid flow is diagonal through a perpendicular mesh. For this reason, the axis of the air/blast mesh has been aligned with the predominant flow, as will be seen in 4.2 Modeling of Blast Environment.

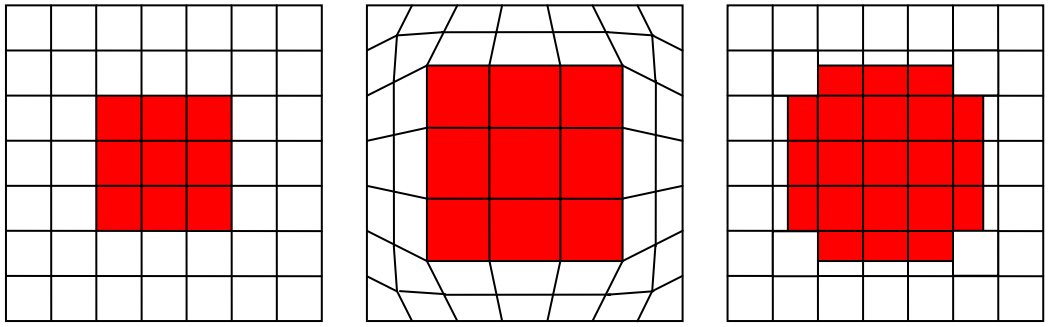

(A) (B) (C)

Figure 4.2: Showing disadvantage of code, can only advect through the faces of the elements, and hence cannot transport material diagonally.

4.2 Modeling of Blast Environment

Although the eventual goal of this research is the application of the model to complex blast loading, validation must first be undertaken in a more easily understood and repeatable environment. The most comprehensive published data for comparison are from Bowen et al. [1968a] in the form of the Bowen curves, and the most basic form of these would be the free field cases. To represent this scenario in a 2-dimensional environment, a rectangular air mesh was created, bounded on three sides by non-reflecting boundaries and on one side by a row of inflow elements providing the pressure wave input.

Once validated, the model can then be used with a reasonable level of confidence to predict trauma in more complex environments. Initially, however, these complex

environments should be kept fairly straightforward so that findings can be more easily interpreted. To introduce complex blast wave characteristics in this study, a flat rigid wall was inserted into the air mesh, or a corner (wedge) was inserted as seen in Figure 4.3. By varying the distance between the thorax and the reflecting surface, the blast environment surrounding the thorax can easily be modified.

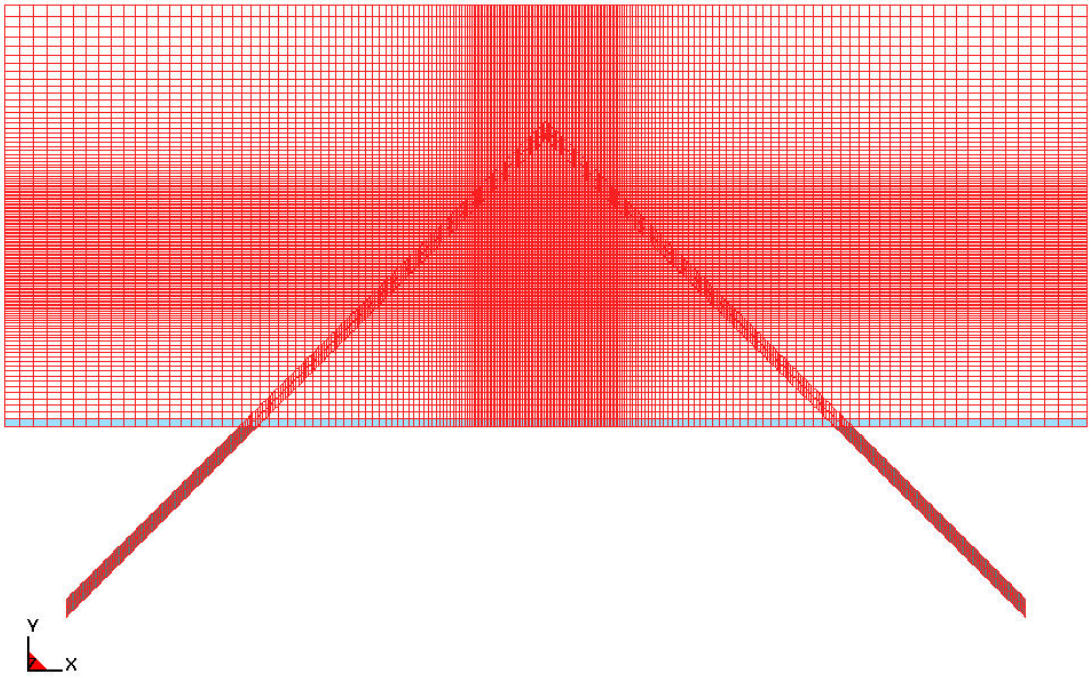

Figure 4.3: Air and ambient ALE element mesh with inserted Lagrangian wedge, showing biased mesh pattern, with smallest elements in central location where thorax would be inserted.

The four element thick finite element mesh of air and explosive was created using 8-node quadrilateral solid elements. Solid elements are necessary to apply the ALE technique in LS-DYNA, and multiple layers are required to accommodate the thickness of the thorax layers. The ALE mesh is 3.0 metres wide, 1.15 metres in length, and 1.4 centimetres in depth. These dimensions were chosen so that the same mesh could be used for all simple and complex scenarios, thereby easing comparison between the models. The width was chosen to ensure that the wave striking the thorax would be planar in all models, both initially and after reflection from the flat wall. As can be seen in Figure 4.4, because the

non-reflecting boundary conditions permit outflow of the blast, the pressures at the edges of the mesh decrease slightly and no longer form a planar blast wave. The length was determined so that the same air mesh could be used for all models, including those with the wall or wedge located the maximum distance behind the thorax.

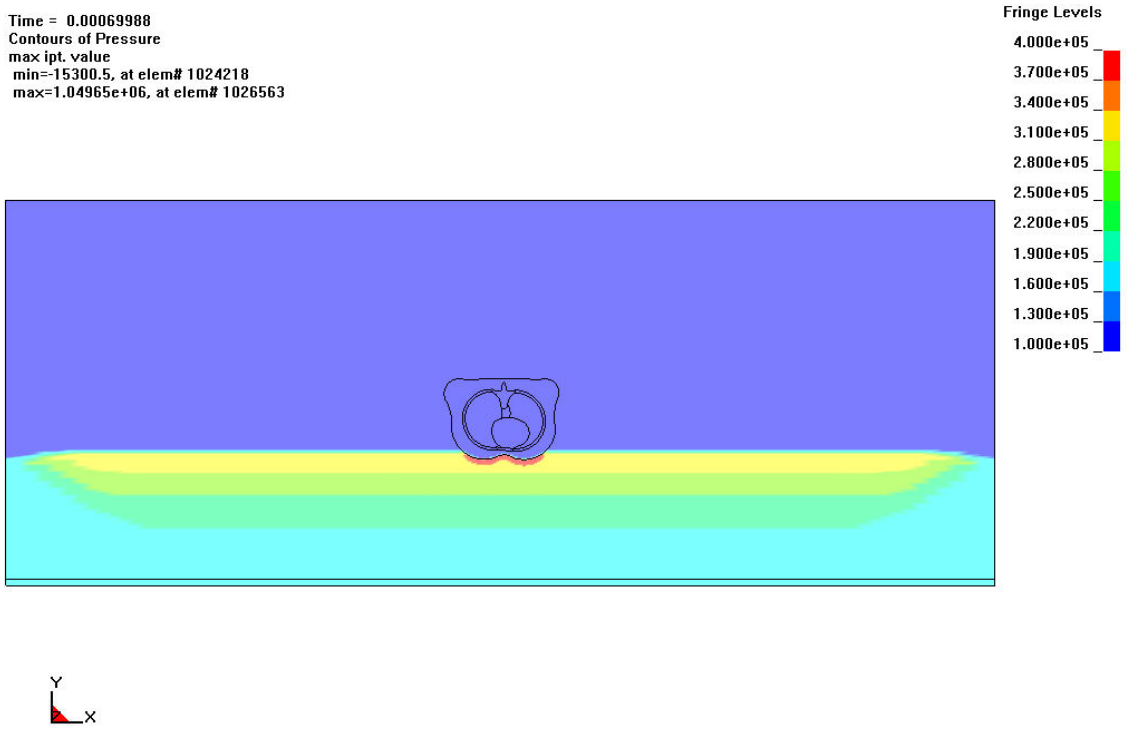

Figure 4.4: Blast showing planar wave as it strikes the torso, and lower pressures at the edge because of non-reflecting BC's allowing outflow.

Mesh density analyses showed that element dimensions in the torso should approach 2.5 mm in critical areas for accurate pressure wave transmission and measurement of peak pressures. However, to create an entire ALE mesh of such fine density would be prohibitive, and would provide limited improvement in the local behaviour around the torso. Various mesh designs were compared, each having advantages and disadvantages in terms of computational cost, accuracy, shock propagation etc. The final ALE mesh design selected for the study was biased through the centre region to allow a greater mesh density in the test area containing the thorax model, as seen in Figure 4.3. This enabled better fluid structure coupling while maintaining reasonable computation time. The coarse areas of the mesh correspond to a mesh size of 20mm while the fine mesh is 4mm

on a side. The spacing of the fine mesh in the central region is of approximately the same dimensions as the elements on the periphery of the torso model to improve coupling. Element dimensions in the lungs approach 2.0mm in order to better capture the peak pressures. If the elements of the lung are too large, the pressure is smeared over multiple elements, thereby reducing the peak value. The air mesh is composed of a total of 132,965 nodes and 105,040 elements.

4.2.1 Blast Loading

Several methods for creating blast overpressure applied to solids in the finite element hydrocode LS-DYNA were investigated. A layer of explosive material was initially used to generate the pressure pulse in the air mesh. However, it was found that this approach limited the pressure pulse magnitude, duration and impulses that could be achieved and a new approach using ambient elements with prescribed pressure-time histories was developed. For the final quasi 2-D thorax model, ambient elements with a prescribed internal energy history were used to create the desired overpressure and pulse duration.

For a general non-reacting material, the thermodynamic state can be defined by 2 thermodynamic variables. The ambient element properties are described by defining the boundary using a line of ambient elements in combination with an equation of state to define an ideal gas. By assigning a constant relative volume curve for the ambient elements, the pressure-time profile is then calculated using the ideal gas law based on a given temperature history curve, as shown in Figure 4.5. In this way, an experimental pressure-time history can be directly applied to a set of elements, enabling the model to simulate complex pressure environments as well as pressure histories from the detonation of more exotic explosives.

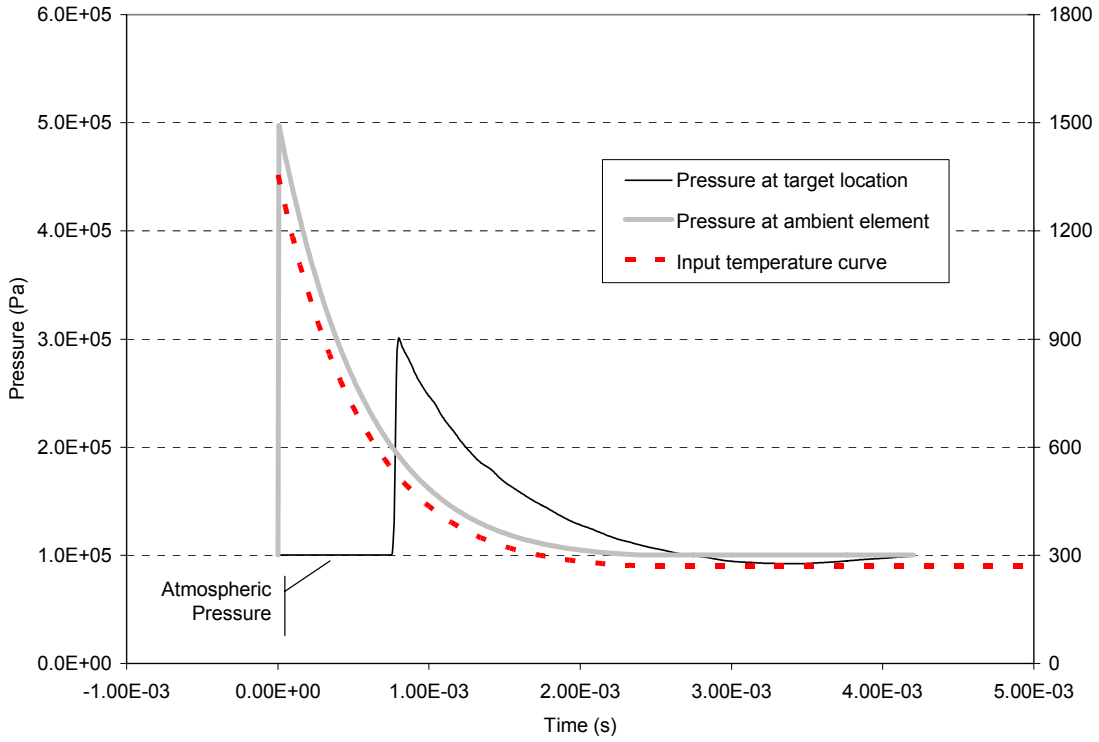

Figure 4.5: Pressure and temperature against time in a threshold level, free field blast.

Seven different peak pressure and duration pairs were chosen which correspond to points on the modified Bowen curves. The pressure-duration pairs chosen and the lethality as predicted by the modified Bowen curves are given in Table 4.1, and depicted in Figure 4.6.

Table 4.1: Blast pressure and duration for various test cases

Duration (ms)	Peak Overpressure (Pa)	Lung Damage
0.4	250	Threshold
2.0	200	Threshold
10.0	125	Threshold
2.0	500	LD1
10.0	300	LD1
2.0	700	LD50
10.0	400	LD50

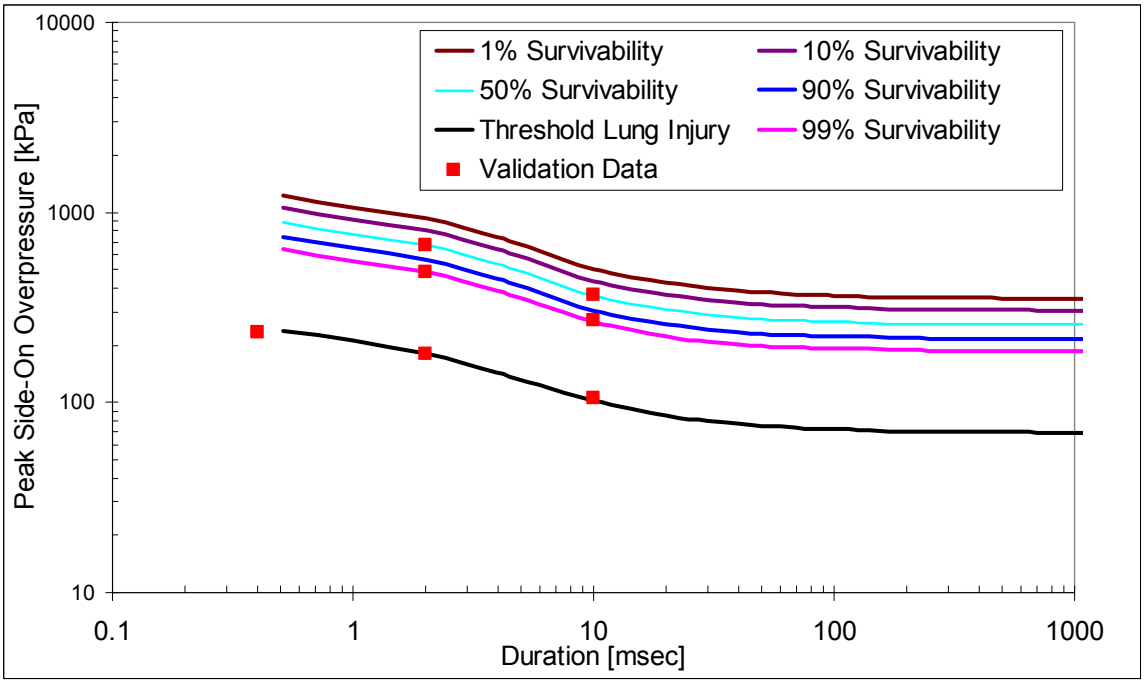

Figure 4.6: Modified Bowen curves showing data points selected for simple blast validation study.

The first three points were chosen to explore the effect of duration on the thorax. The remaining four points explore the effect of varying peak pressure, and hence higher lethality. In relative terms, the 0.4 ms duration would correspond to a small charge at a close range while the 10.0 ms duration would correspond to a large charge at a large distance or a volumetric type explosion. The 2.0 ms duration corresponds to a medium charge at near field distance. The creation of the pressure curves and research into explosive materials and ambient elements was conducted by Chris Salisbury at the University of Waterloo [Salisbury, 2004].

The ambient elements are located far enough away from the test region so that any reflections from the thorax that propagate back to the ambient elements prior to the end of the simulation are of relatively low pressure. Due to the dispersion and attenuation of the blast wave as it travels from the ambient elements to the thorax, the pressure time profile of the ambient elements had to be modified to generate the desired pressure

history at the thorax, as can be seen in Figure 4.5. In other words, the pressure profile generated within the ambient elements must compensate for any attenuation or dispersion of the wave so that the desired duration and peak pressure is achieved in the test section. A brief literature search for analytical methods to determine the blast wave peak pressure and duration as it propagates through air showed that there was no straightforward solution so an iterative method was used. It should be noted that the Bowen curves do not explicitly indicate the impulse or shape of the blast load curve. Therefore, a pressure profile following a Friedlander type response was assumed for these analyses. Several iterations were required to generate the required loading profile for each data point. Figure 4.7 shows the free field pressure history for the three different durations of blast causing threshold lung damage.

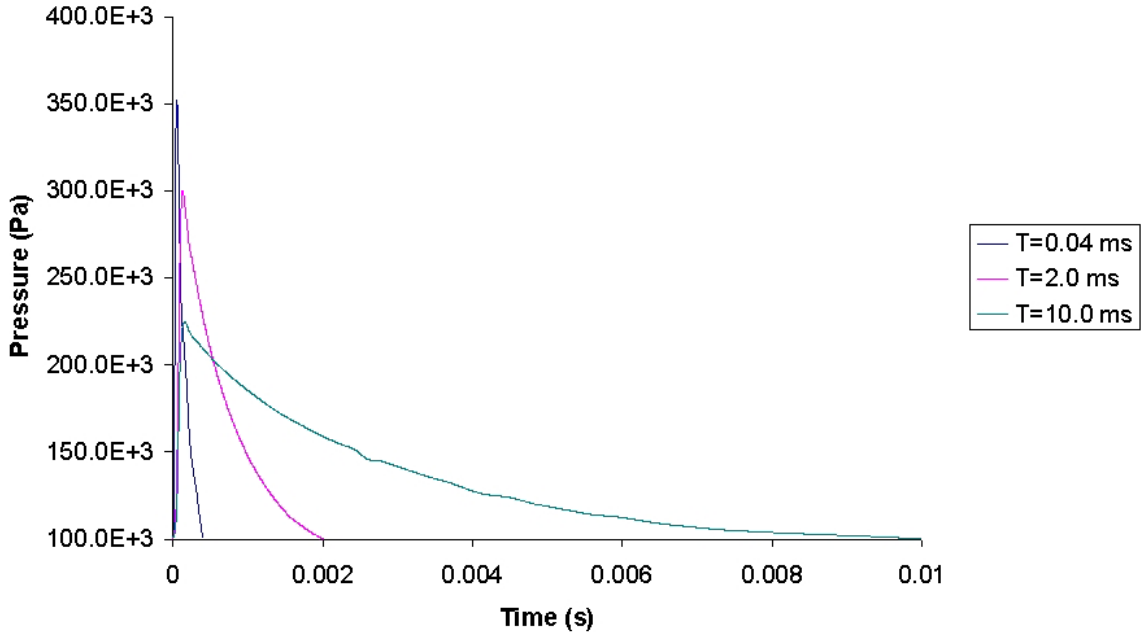

Figure 4.7: Threshold pressure-time histories.

As the peak pressure and duration vary for the three cases, so too does the impulse. Figure 4.8 shows the pressure time histories for the three levels of peak pressure at 2 ms. Once again, although the durations are the same, the impulse applied varies greatly.

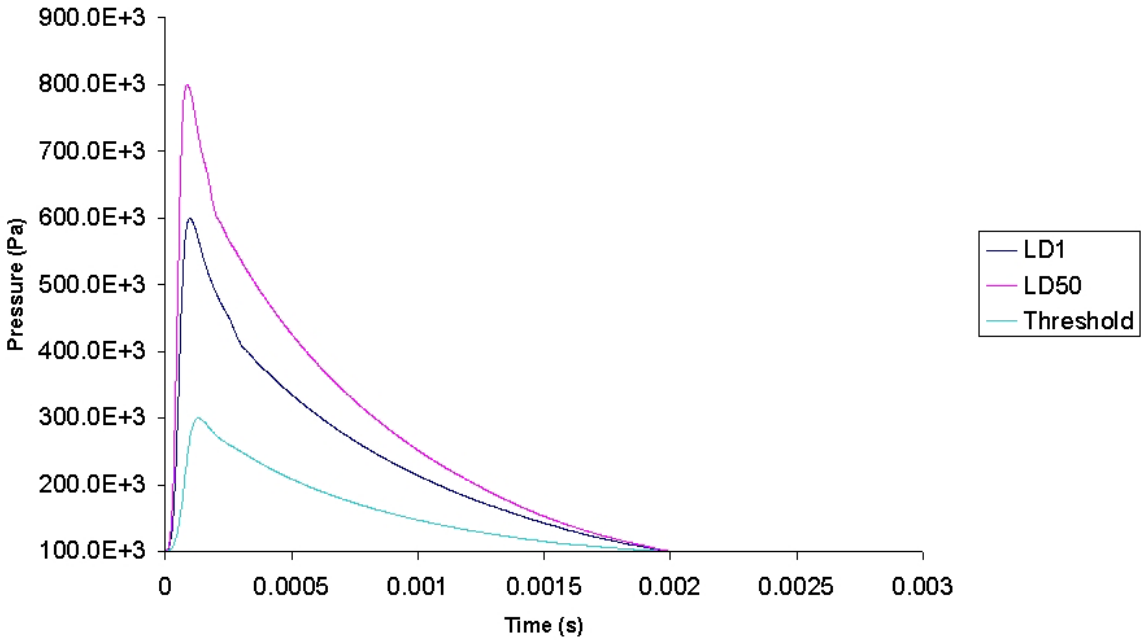

Figure 4.8: Pressure-time histories for three pulse magnitudes.

4.3 Material Models and Properties

Air was modeled as a null material because this material model allows equations of state (EOS) to be considered without computing deviatoric stresses, thereby providing a good representation of the behaviour of a gas. A dynamic viscosity coefficient, μ, can be defined for use with a more viscous fluid, but for air this value is set to zero resulting in a material with no shear stiffness. The density of air is required, as is a pressure cutoff, typically a small negative value; -100 Pa was used for these models. The pressure cutoff represents the point at which the material will numerically "cavitate," in other words the negative pressure at which any further dilatation is not increasingly resisted. Although there is no occurrence of such phenomenon in these models, the lack of a pressure cutoff could permit the pressure of air to drop below zero, or below a perfect vacuum. The properties for the material model and EOS for air can be seen in Table 4.2.

An EOS is required to accurately calculate the volumetric strains of the air and to correctly model wave propagation behaviour. The ideal gas EOS requires the definition

of specific heat capacities, initial temperature and initial relative volume. The pressure is then calculated from the ideal gas law as:

$$p = \rho\left(C_p - C_v\right)T \tag{4.1}$$

Ambient elements were modeled using the same properties as air which is logical given that they are simulating an air blast. Deviation from ideal gas behaviour, as denoted by the compressibility factor, was found to be insignificant even at the higher lethality pressures.

Table 4.2: Material values for the material model and equation of state for air and ambient elements.

Material	Air
Material Model	*MAT_NULL (*MAT_009)
Density, ρ	1.293 kg/m^3
Pressure Cutoff, PC	-0.100 kPa
Dynamic Viscosity Coefficient, μ	0.0 Pa·s
Specific Heat Capacity at Constant Pressure, C_p	1005
Specific Heat Capacity at Constant Volume, C_v	718
Initial Temperature, T_0	270 K
Initial Relative Volume, V_0	1

4.4 Eulerian Boundary Conditions

The 2-dimensional nature of the model requires a fairly straightforward symmetry boundary condition. This condition is applied through nodal constraints, where the nodes on the upper and lower surfaces of the model are not permitted to travel in the vertical, or z, direction. This ensures that material cannot flow out of the mesh, either upwards or downwards. The nodes in the central planes of the mesh are permitted to travel freely.

The final air mesh, shown in Figure 4.9 with boundary conditions, was much smaller than earlier models. Initially, a relatively large air mesh was required to simulate an infinite domain surrounding the torso in order to prevent reflected pressure waves from the edges

of the ALE model returning and interfering with the loading on the torso. To simulate a semi-infinite domain, the elements along the periphery of the air mesh were loaded with a constant ambient (atmospheric) pressure. Unfortunately, artificial reflected stress waves were created due to the impedance mismatch and the fact that the edges remain at ambient pressure, irrespective of the wave behaviour in the adjoining element. A non-reflecting boundary condition and nodal restraints were applied to the rear surface of the model allowing free flow of material out of the rear face of the mesh without causing reflections. The free outflow of material was ensured by permitting the nodes on the periphery of the mesh to translate in the horizontal plane (x and y directions). The non-reflecting boundary condition was applied to the exterior segments (element faces) where LS-DYNA internally computes an impedance matching function, based on the assumption of linear material behaviour. As such, the mesh was designed so that all significant non-linear behaviour was contained within the mesh, away from the boundaries.

To simulate a continuation of the planar wave at the left and right sides of the mesh, symmetry boundary conditions were required that did not permit flow in the normal direction. Unfortunately the reflections from the torso created artificial stress wave reflections when they reached the boundaries. To avoid this, the same boundary conditions were applied to the sides that were applied to the rear face. The ambient pressure applied at the edges, however, permitted some of the high-pressure wave to travel outwards, causing the planar wave to become bow shaped, with lower pressures at the edges. To solve this matter, the ALE mesh width was increased to ensure that the wave remained planar in the test section.

As previously mentioned, the front face of the mesh was bounded by ambient elements with a given pressure-time history. The nodes between the air and ambient elements must be coincident to allow flow of material from one ALE multi-material group to the next.

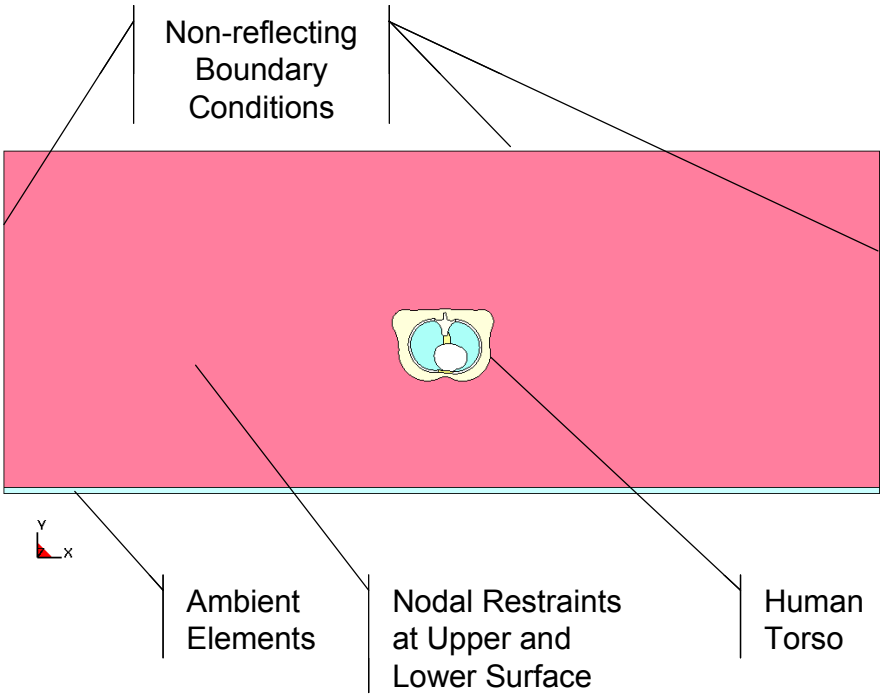

Figure 4.9: ALE air mesh and human torso showing ALE boundary conditions.

4.5 ALE/Lagrange Coupling

When two Lagrangian parts interact, a contact algorithm is necessary to transmit forces from one part to the other, and to prevent the two parts from occupying the same space. When a Lagrangian part interacts with an ALE mesh in LS-DYNA, this is referred to as coupling. Overall, the coupled LS-DYNA formulation provides a great deal of flexibility for solving complex problems involving fluid-structure interactions.

Coupling to Lagrangian parts (i.e. coupling the deformable human torso to the blast model) is accomplished by defining a master Eulerian or ALE entity and a slave Lagrangian entity [Halquist, 1998; Halquist, 2003]. Coupling is accomplished using a penalty method. This method calculates a force based on the distance between the fluid/solid interface and the stiffness based on the contacting material properties. Figure 4.10 shows a schematic of this process.

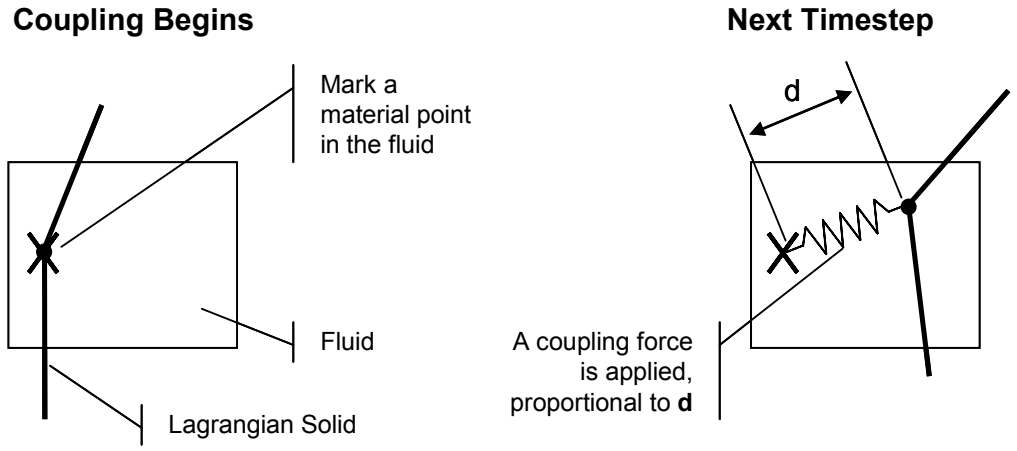

Figure 4.10: Penalty coupling method [Souli, 2004].

One of the more significant advances to the model is related to the constrained coupling method mentioned above, and the way in which it is implemented in the analysis. This modification was initiated following the observation that the predicted pressure in the lung was distributed between the lung elements and the ALE elements occupying the same volume. This is attributed to the low bulk modulus and density of the lung material relative to the air elements. The ALE coupling in LS-DYNA enables the Lagrangian torso to be placed inside the Eulerian air without changing the air mesh such that the torso and air elements occupy the same volume. This allows for a great deal of flexibility for various problems, but the physical reality of the model suffers because two materials are occupying the same space. When the density of the Eulerian material is much lower than that of the Lagrangian material, the error induced becomes negligible. However, when dealing with soft, lighter materials, such as lung tissue, the added presence of nodes representing air can have a marked influence on the results. In order to solve this issue, a very thin ring of shell elements was created between the ribs and the exterior soft tissue of the body, as seen in Figure 4.11.

The ring of shells was used to define the geometry of an ALE vacuum material allowing the volume inside the shells to be emptied of air upon initialization. This ensured that there was no other material interacting with the lung tissue and that energy was

transferred only to the lungs. The shell had to be situated at the rib/tissue interface instead of at the exterior surface of the torso model to avoid leakage of the vacuum material out of the torso. The vacuum material is defined using the vacuum material model, and has no properties associated with it. The volume that is defined as a vacuum has no density and the pressure is zero. Upon close inspection of the model, it was clear to see that no pressure waves were permitted in the vacuum and that there was no leakage of the vacuum material.

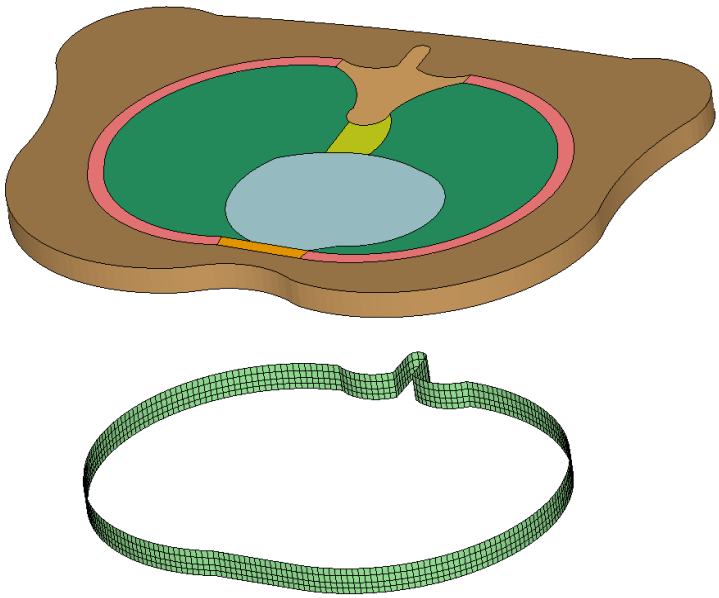

Figure 4.11: Human torso model and the ring of shells required to define the location of the vacuum material.

4.6 Lagrangian Boundary Conditions

The two-dimensional simplification for this model was chosen in order to make the model computationally viable while maintaining the accuracy of the stress wave transmission. The physical justification for a two-dimensional model is, as previously stated, that due to the central location of the lungs in the trunk of the body, the fluid flow around the thorax at that point can be reasonably approximated by two-dimensional flow

around a bluff body, with negligible vertical flow. Nodes in the thorax model were constrained in the same manner as those in the eulerian model, eliminating out of plane rotation and translation to simulate a two-dimensional model.

The human and sheep models include fatty tissue, intercostal tissue, muscle and the mediastinum modeled simply as "tissue," one continuous material within the model. The ribs, costal cartilage, sternum and vertebra are each treated as unique bone materials, and the heart and lungs are each treated as macroscopic continuums of "heart" and "lung" tissue, respectively. The interfaces of all parts of the human and sheep models use coincident nodes, meaning that the parts of the models are fixed to one another, and are not permitted to slide. Equivalencing the nodes in this fashion is reasonable assuming there is no significant relative sliding between the components. This approach reduces computational cost by reducing the number of nodes in the model, but more importantly, by reducing the number of material contact definitions required.

Since much of the tissue surrounding the ribcage is securely attached or even inserted into the ribs, and literature on pure PBI injuries don't typically speak of tissue stripping away, the joined interface is quite reasonable. Also, because stress wave transmission is of paramount importance, the coincident nodes method avoids any uncertainties associated with a penalty based contact definition. The ribs and costal cartilage are joined in the same manner, which is natural given that in reality, the two materials transition from one to the next.

At the mid-sternum level, the costal cartilage is joined to the sternum by a synovial joint with a thin joint capsule. This joint is reinforced by radiate sternocostal ligaments on both the anterior and posterior surfaces of the sternum, allowing limited motion [Gest, 1995; Rohen, 2002]. Attempting to accurately model the joint and the resistive forces of these ligaments would have been prohibitive, and it is believed that the extremely low strength of the costal cartilage provides sufficient mobility for the purposes of the current study. The rib-vertebral junction is known as the costovertebral junction, and is secured by ligaments in a similar manner. Once again, with the restrained motion of the thorax seen

in large animal studies, and the importance placed on wave transmission behaviour, it is believed that the setup of the current approach is sufficient to capture the required phenomena.

The sternum, heart, mediastinum and vertebra are also joined to one another keeping their relative positions somewhat fixed. The heart is contained within the pericardium, a membranous sac that also encloses the aorta and other large blood vessels. The pericardium is securely anchored within the thoracic cavity to the diaphragm, the deep cervical fascia, the great vessels and the posterior surface of the sternum. Generally speaking, the posterior mediastinum contains soft tissue, veins, arteries, the aorta and esophagus, and connective tissue, and is attached to the vertebral column [Gray, 1989]. Therefore, given the fixed nature of the heart and mediastinum within the thoracic cage, coincident nodes are required to keep the organs correctly aligned in the absence of 3-dimensional boundaries. Also, it is highly unlikely that organ realignment would occur in pure PBI incidents. Although most organs are linked to one another through connective tissue, it is possible that the assumption of coincident nodes overestimates the tensile stress wave transmission in the later stages of the simulation in order to accurately predict the earlier stages of compressive wave transmission.

The lungs float freely within the pleura, and can slide easily, lubricated by pleural fluid. Initially, a standard penalty-based contact was used, where the static and dynamic friction coefficients were set to zero. This contact definition allowed the two parts to separate and should accurately represent the near-frictionless, lubricated contact between pleural surfaces within the thoracic cavity. However, due to the lack of deviatoric strength, the lungs underwent significant, unrealistic deformation when exposed to higher blast loads. Comparing the pressure transmission within the lungs of models using contacts to those with merged nodes, two observations were made:

- The contact based model shows compressive lung pressures 10-15% higher than in merged node model.
- Tensile lung stresses are rarely seen in the contact based model, but commonplace in the merged node model.

Having studied the results from these two approaches, it was found that the increase in pressure seen when contact was used is related to the method in which the software handles contact. The contact algorithms in FE programs are generally poor at accurately transmitting forces when very soft materials contact hard materials with different bulk moduli. It is possible that the penalty based contact is over-estimating the required put-back (resistive) force, thereby pushing the lung away from the rib cage with more force than would truly be produced at the interface.

The lack of tensile waves in the lung of the contact based model can likely be explained by the fact that the contact interface cannot sustain a tensile load, and thus cannot allow tensile waves to enter the lung. The tensile loading first occurs when the initial compressive wave in the tissue strikes the low impedance lung, and returns as a tensile wave. When the lung interface is joined to the ribs, the tensile loads can be transferred to the lung. It is assumed that the tensile waves produced by the merged node model are erroneous since they occur only because of the artificial union between the lungs and the rib cage. However, the merged node model was chosen because of its ability to predict the compressive waves that form the basis for the lung damage prediction, and because the merged nodes maintain the shape of the lungs. In the future, it would be advisable that one of the first steps in improving the model would be to create an elastic user material model for the lung tissue capable of being coupled to an equation of state. The prediction of compressive waves in a non-linear lung material model is of paramount concern, therefore the merged node model was deemed appropriate for the current application.

4.7 Experimental Validation of Blast Loading

The University of Waterloo participated in a series of blast tests at DRDC Valcartier in June 2004. The goal of these tests was to generate data that could be used to validate the numerical modeling approach used in the current project.

4.7.1 Experimental Test Setup

A series of experimental tests were undertaken with the goal of validating the numerical modeling approach. To address this goal a simple representation of the thorax was designed using ballistic gelatin with internal and surface mounted pressure transducers to record pressures during the blast testing. Ballistic gelatin was selected because the wave transmission properties are relatively well known and it is accepted as a reasonable simulant for soft tissue.

The surrogate thorax was cast in gelatin containing no cavities or discontinuities, the simplest structure for validation of the models, with one face mounted pressure transducer on the front surface and one embedded inside the thorax. The transducers were offset from one another in the vertical direction to avoid any wave interference generated by the presence of the front sensor. Figure 4.12 shows the test fixture and sensor locations. The surrogate thorax was placed on a stand so that the middle of the thorax was 1.25m from the ground, roughly corresponding to the mid sternum of a standing 50th percentile male. The thorax was 450mm tall.

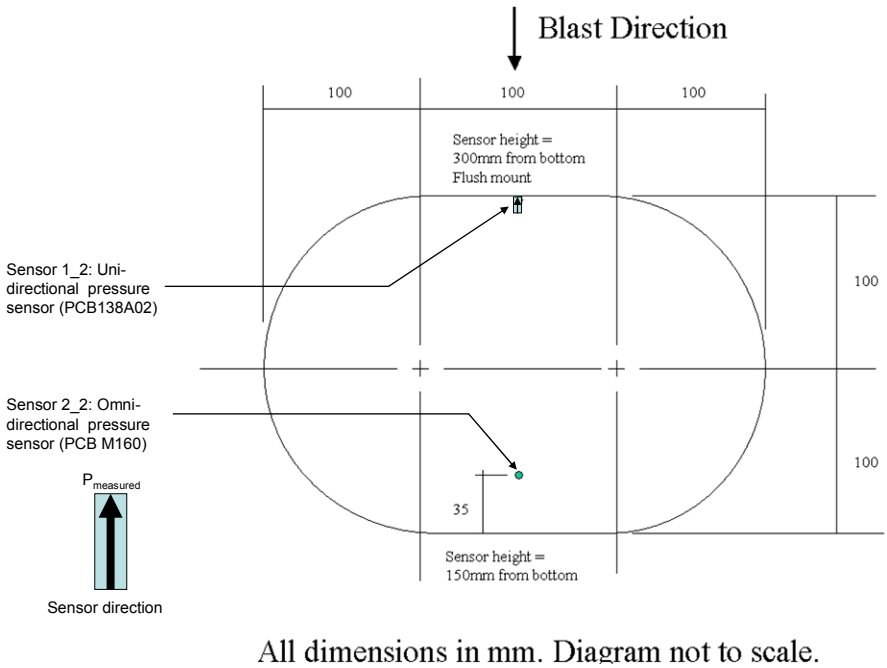

Figure 4.12: Solid thorax.

In addition to the gelatin thorax, a blast test device (BTD) was instrumented and fielded by DRDC Valcartier. The BTD was included in the study due to the simplicity of the model, availability of data, and wide use of BTD-like surrogates in blast testing. The BTD used in testing consisted of a PVC cylinder instrumented with four uni-directional pressure gauges, one in each quadrant. The BTD was oriented so that the front gauge was pointing directly at the blast. Figure 4.13 is a diagram of the BTD showing the sensor locations. Gauges 2 and 4 should provide similar results as a result of symmetry. Gauge 1 should have the highest pressure since it is directly exposed to the incident pressure pulse.

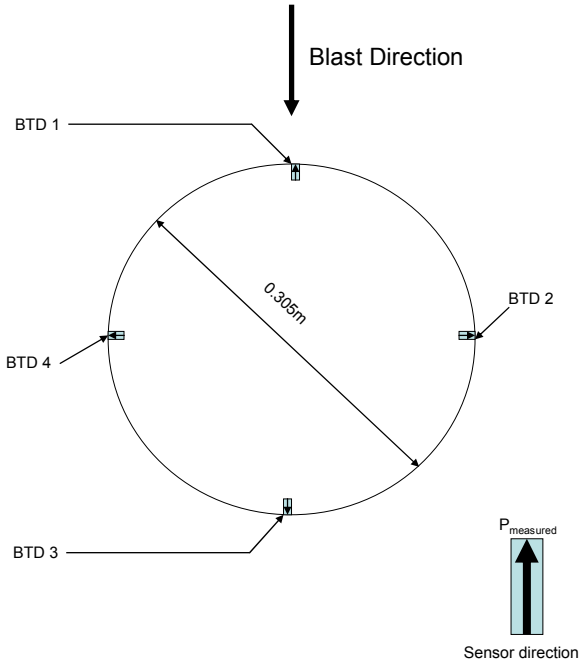

Figure 4.13: BTD and pressure sensors.

Given the arrangement of the sensors, sensor 1 measures the stagnation pressure with sensors 2-4 measuring both the static pressure and some component of the dynamic pressure, based on the flow around the region.

For each experimental blast test, seven lollipop sensors were placed at 1m intervals starting 2m from the charge. The sensors were placed inline with one another and at a

height of 1.27m. Lollipop sensors are designed with a knife edge to provide an undisturbed measurement of the side-on (incident) pressure in the flow field. This allowed a free field pressure time history at various locations to be recorded. Figure 4.14 is a diagram of the lollipop sensor and physical layout.

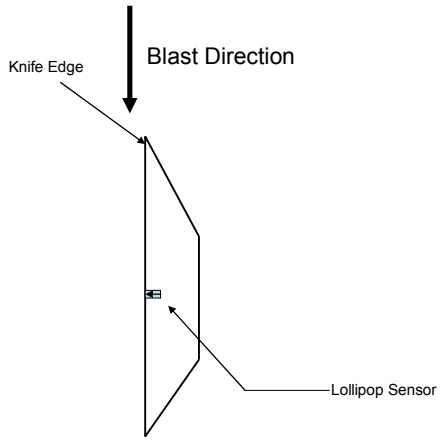

Figure 4.14: Lollipop sensor.

Numerous tests were conducted with various heights of burst (HOB) and locations of the thorax and BTD. By varying the HOB, the shape of the ground reflection varies, changing the incident pressure pulse history. Table 4.3 shows the test matrix, including the location of the test fixtures, HOB. For the tests of interest, the charges of C4 were cylindrical with a height to diameter ratio of one, and a mass of 5 kilograms.

Table 4.3: Experimental test matrix [Williams, 2004].

Test No.	Charge Height	BTD Location	U of Waterloo Rig Location
1-6	1.5 m	4.0 m	5.0 m
7-11	0.2 m	4.0 m	5.0 m
12-17	1.5 m	3.5 m	4.0 m
18-22	0.2 m	3.5 m	4.0 m
23-28	1.5 m	3.0 m	3.0 m

4.7.2 Data Analysis

Prior to modeling the specific conditions and thorax rigs used in the blast testing, a preliminary analysis of the experimental data was undertaken and compared to existing numerical modeling results. One important aspect of the modeling approach considered in this project is the ability to numerically couple the blast loading with a model of the human torso. The peak pressure and the pressure history measured at the front of the thorax is known to be geometry dependant and represents a useful quantity for assessing the performance of the coupling method.

For this analysis, the peak pressure - as measured by the forward flush mounted pressure transducer in the solid gelatin thorax - was used as the peak pressure applied to the thorax. This data is plotted for three different distances from the charge, corresponding to different peak overpressures (shown on the x-axis) in Figure 4.15. The error bars indicate one standard deviation and show that there was a significant amount of variability in the test data, as would be expected in a blast environment. Note that the peak pressure (y-axis) has been normalized by the free field peak pressure to provide an estimate of the amplification by the geometry of the gelatin thorax.

Also shown in Figure 4.15 is the corresponding data from the human torso numerical model. It can be seen that on average the results are in good agreement (within the experimental scatter of the experiments). Although there is a slight difference in geometry between the physical gelatin model and numerical human model, these differences should have only a minor effect on the predicted pressure. In any case, the reversed curvature of the human model at the location of interest would be expected to lead to slightly higher pressures as seen in Figure 4.15. This shows that, based on peak pressures, the coupling method is producing realistic loadings on the numerical thorax.

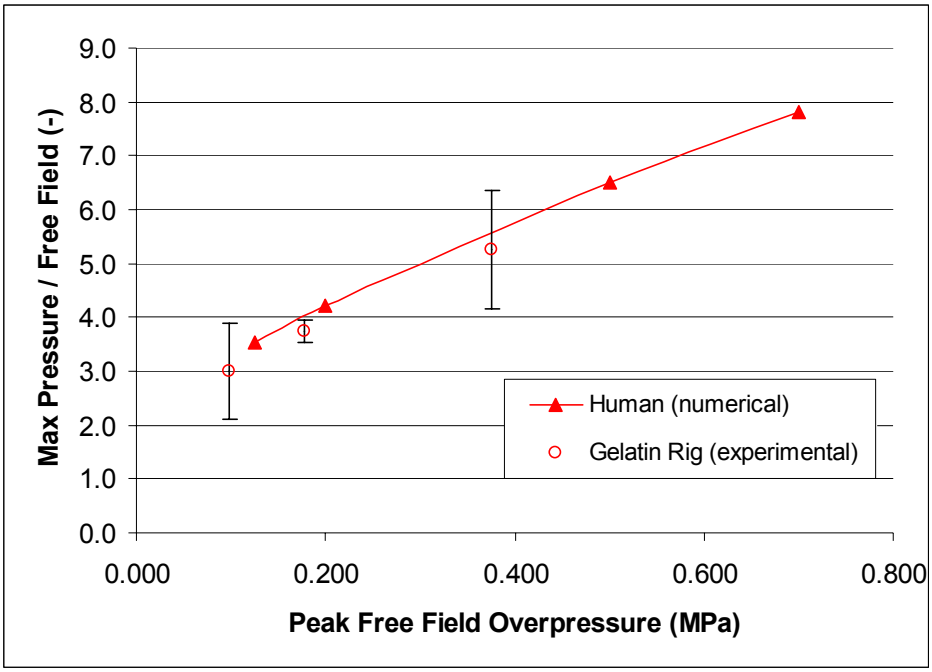

Figure 4.15: Dynamic pressure increase (front of thorax) for numerical and experimental tests

A numerical model of the BTD was generated to further evaluate the modeling approach used in this study. In order to make the analysis computationally feasible, a slice model, similar to those used to model sheep and human torsos, was generated. Figure 4.16 shows the BTD in the ALE mesh. The mesh lines have been removed for clarity.

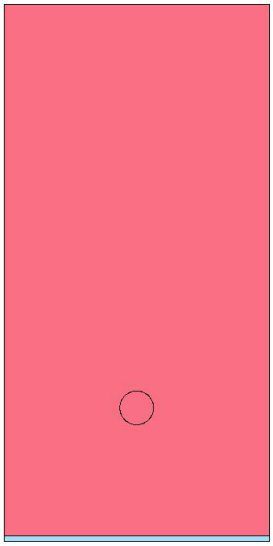

Figure 4.16: Gelatin thorax (left) and BTD (right) surrounded by ALE mesh.

It should be noted that the focus of this study was to validate the modeling approach and as such, some tests were not considered. Tests 12-17 and 18-22 for the BTD were not modeled since there was no corresponding free field pressure history measured at 3.5m. The pressure history cannot be inferred from the reading at 3m and 4m since the movement of the blast wave is nonlinear and would have to include an analysis of the ground reflection.

Figure 4.17 shows results from the numerical models for the human torso, sheep thorax, and one result from the BTD. As expected, the dynamic pressure decreases as the presented frontal area of the model decreases. This is also related to the shape of the objects.

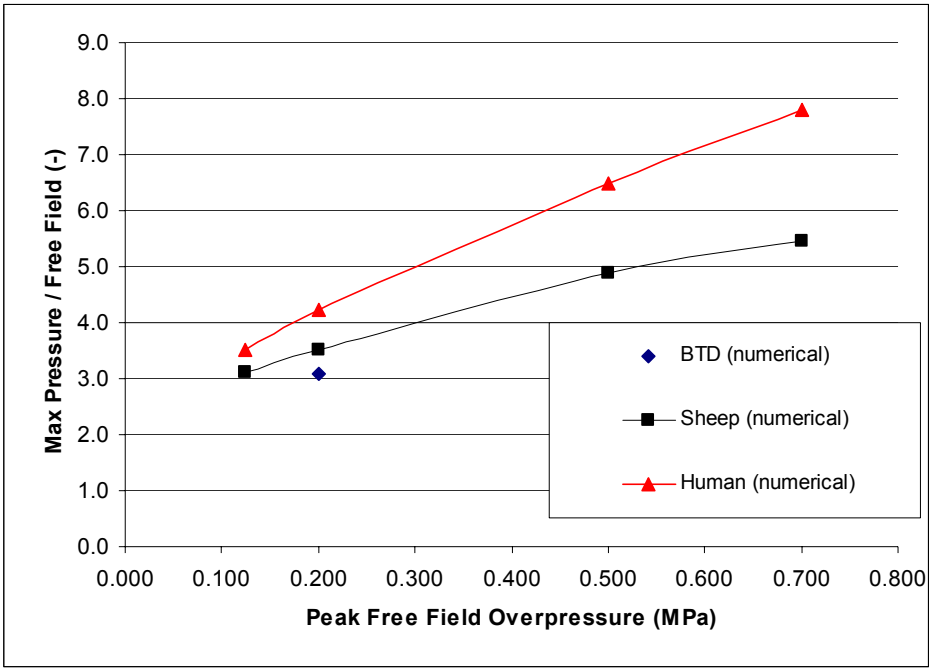

Figure 4.17: Dynamic pressure increase (front of thorax) for numerical models of the human, sheep and BTD

The work reported in the current section is based on work detailed in the Phase II (2004) and Phase III (2005) reports: Numerical Modeling of Blast Injuries, by Christopher Salisbury, Alexander Greer, and Duane Cronin. With assistance from the above mentioned individuals and the staff at Defence Research and Development Canada, this

author contributed to the experimental testing and numerical modeling. Christopher Salisbury and Duane Cronin carried out much of the analysis for this series of experiments.

Chapter 5 Evaluation of Thorax Model for Simple Blast Loading

The basic requisite components for this finite element model are: part geometries, material properties, boundary conditions and loading conditions. Testing and validation of the general modeling approach and coupling mechanism were successfully demonstrated in Section 4.7 (Experimental Validation of Blast Loading). In cases where experimental data is unavailable, a scientifically derived and justified finite element model such as the one developed in this study might be considered satisfactory. Fortunately, however, there exists a significant amount of experimental and theoretical data for the simple blast environment, on both the loading and resulting injuries. The model was first compared to the Bowen curves to establish a trauma criterion and to associate the magnitude of the criterion with known injury outcomes. Once established, the model was then compared to Axelsson's chest wall velocity model, and the mathematical model developed by Stuhmiller et al. in order to evaluate the consistency of the results.

5.1 Bowen – Curves

The primary goals of this section are to evaluate the thorax model by showing its concurrence with the modified Bowen injury tolerance curves and to propose peak lung pressure as a simple, relative measure of lung injury in the FE model. The volume of lung exceeding a given pressure, as well as the distribution of peak pressures around the lung can be used as a more in-depth comparison of lung injury.

The modified Bowen curves are iso-injury curves, that is they predict a given level of injury based on the peak free field overpressure, and the positive phase duration. Therefore, given various points along an iso-injury curve, the finite element model should predict a somewhat constant level of injury, in this case measured as peak pressures in the

lung elements. Three loads corresponding to the lung damage threshold were investigated to determine if any relationship could be found between lung response and the published injury thresholds. By subjecting the model to pressure-time points along a higher level iso-injury curve (1% or 50% lethality), there should be a significant and consistent increase in trauma, or peak pressure, predicted in the lung elements. Seven points on the modified threshold, LD_1 and LD_{50} iso-injury curves were used to propose the magnitudes of lung pressures associated with the three distinct levels of injury. The original and modified Bowen curves, as well as the peak pressure-duration points used can be seen in Figure 5.1.

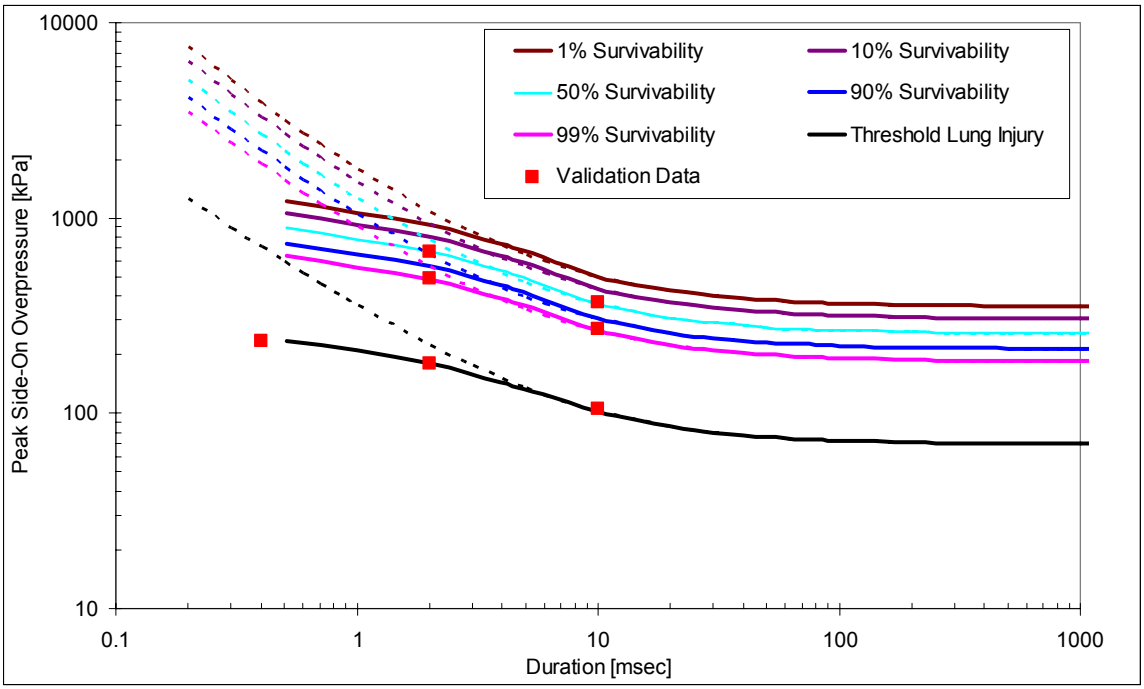

Figure 5.1 Bowen curves representing lethality predictions in the free field for a 70 kg man. Original curves are shown as dashed lines, solid lines represent the modified curves.

Plots of the blast pressure loading on the thorax model can be seen in Figure 5.2. The increased pressure in front of the thorax can be seen clearly in the second plot where the pressure exceeds the free field blast pressure. In this case, the peak free field overpressure was 200 kPa and the positive phase duration was 2.0 ms.

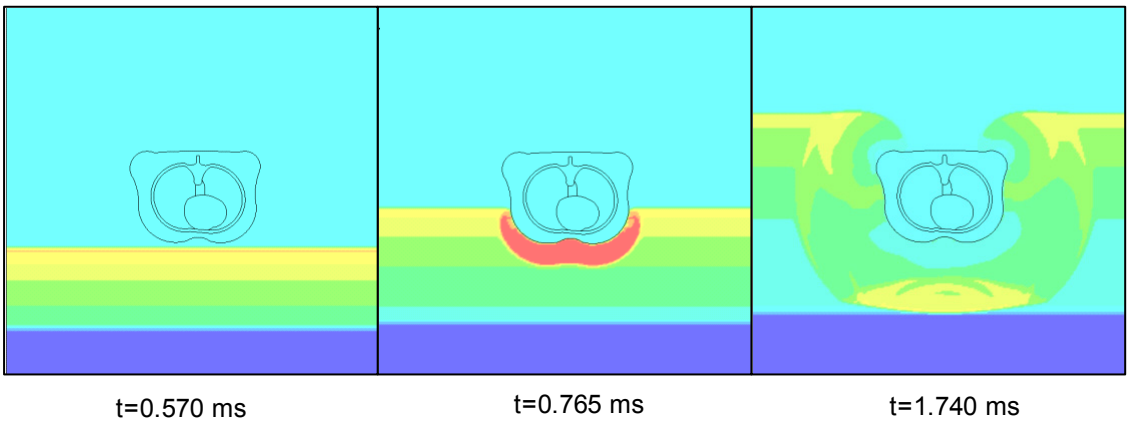

Figure 5.2: Blast loading on the human torso model, contours of pressure.

Although the actual mechanism of injury at the alveolar level is not fully understood, the transmission of stress waves and the pressure history within the lungs is of great interest. Trauma evaluation for the numerical models was focused on pressure within the lung. In particular, the peak pressure was considered. This parameter is known to be associated with lung damage, in addition to the frequency or rise time of the pressure pulse and exposure time [O'Brien and Zachary 1996],[Cooper 1996]. The use of pressure in the lung as a trauma indicator follows the work of Josephson et al. and Stuhmiller et al, who have also suggested the existence of a threshold lung pressure level above which trauma will occur [Stuhmiller, 1988; Josephson, 1988]. However, much of the information on actual pressure within the lung is based on pressure measured outside of the alveoli, and may not be representative of the local pressures within the alveoli since there is negligible air flow between the various areas of the lung during blast loading. At present, actual trauma thresholds at this level are inferred from models, or measured experimentally within larger structures (i.e. the bronchial tubes) in the lung. A mass-spring-damper analytical model has inferred the damage threshold pressure in the lung to be approximately 240 kPa [Josephson and Tomlinson 1988]. However, experimental measurements of intrathoracic pressure have suggested a threshold between 70 and 110 kPa [Stuhmiller et al. 1988] for blast loading.

Both the sheep and human finite element models were subjected to the seven simple blast load cases. As primary blast injury to the lung is believed to be a pressure dominated

phenomenon, the peak pressure measured in the elements of the lung are used to gauge the level of injury sustained. The values of peak pressures are somewhat normally (Gaussian) distributed (by pressure, not location in the lung), and hence the mean value was chosen as a representation of the overall severity of injury to the lungs. Figure 5.3 and Figure 5.4 compare the mean of the peak lung element overpressures in the human and sheep models, respectively, for various simple blasts. When subjected to threshold injury blasts of varying overpressures and positive phase durations, the lung overpressures remain reasonably constant. These results indicate that, while the loadings represent blast durations of three different orders of magnitude (0.4, 2.0 and 10.0 ms), the model predicts a relatively consistent level of trauma in agreement with the modified Bowen curves. When subjected to LD_1 and LD_{50} blast doses, the mean lung pressures are approximately three to eight times higher than in threshold blasts, correctly predicting a significant increase in severity of trauma.

The shortest duration blast, tested only at the threshold level, appears to show pressures that are consistently lower. This finding seems, initially, contradictory to a preliminary study using an earlier version of the human FE model and Bowen's original curves (Cronin et al. 2004). It was found that with increasing blast pressure along an iso-injury curve, in general, the pressure in the lung increased and high pressures were noted over larger areas of the lung. It was assumed that this effect was primarily due to the inability of the lung material to deform during such short loading times resulting in higher pressures. However, the main difference between the original and the modified curves, as seen in Figure 5.1, is that the pressure required for a given injury is significantly lower in the short duration region – the area where the discrepancy is seen. These findings may indicate that the true pressures required for injuries from a short duration blast lie somewhere in between the original and the modified curves. Some of the most recent literature would indicate that this is, in fact, the case [Bass, 2006], and the short duration threshold blast should be significantly higher than 250 kPa. That would then explain the low pressure findings at the 0.4 ms threshold blast. It must also be kept in mind that the values suggested for such short durations are based on extrapolated data, as shown in

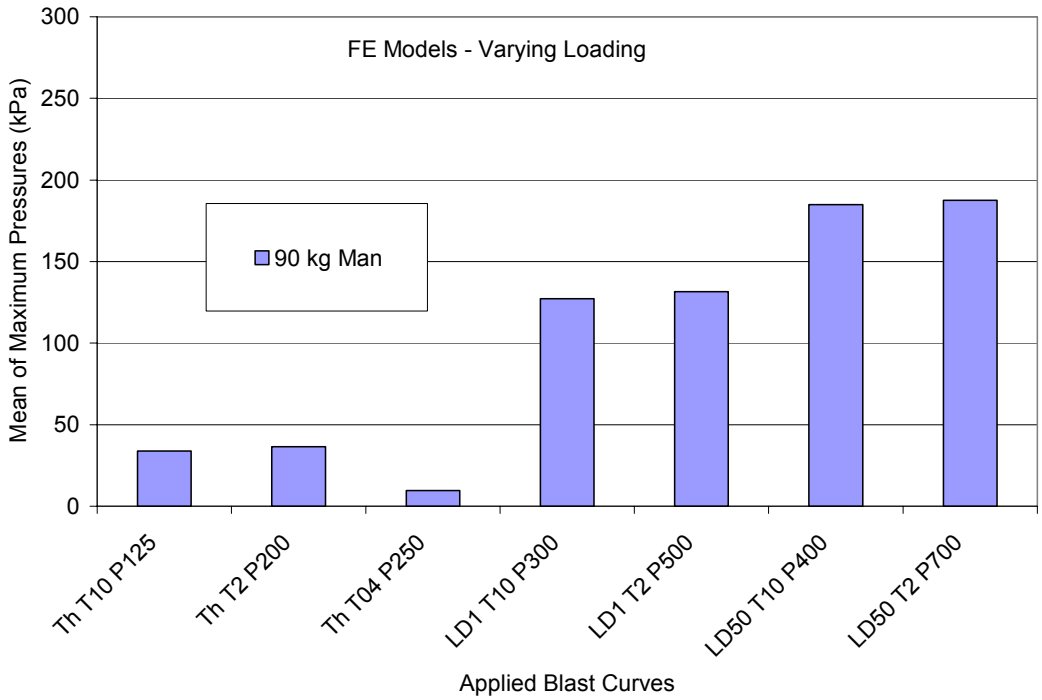

Figure 5.3: Mean lung overpressure predicted by the finite element model of the human for seven simple blast loads.

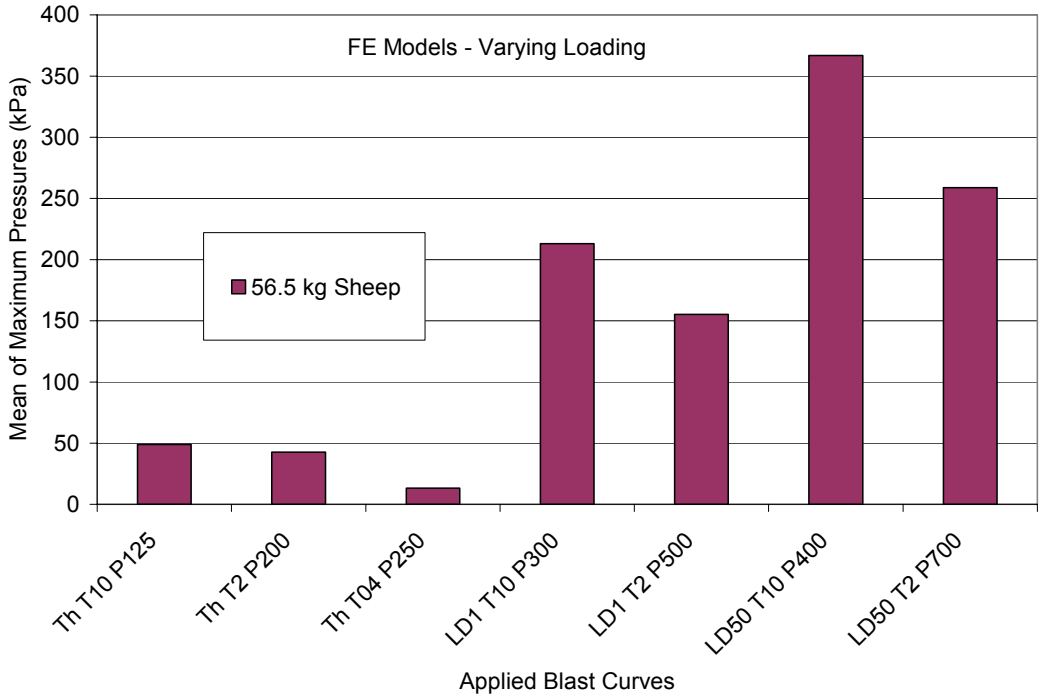

Figure 5.4: Mean lung overpressure predicted by the finite element model of the sheep for seven simple blast loads.

Figure 2.10, and these values represent a very small blast at extremely close range, and could be drastically affected by positioning of the blast relative to the body.

It is interesting to note that while the human model predicts a constant level of injury for the LD_1 cases, and a constant level for the LD_{50} loading cases, the long duration blasts appear to cause the sheep more injury – a phenomenon also seen in the model by Stuhmiller (see section 5.3 Stuhmiller – Injury 8.1). It is possible that the differences in geometry and orientation between the two models/species are responsible. By rotating the sheep model by varying degrees, it was noted that the orientation of the body has a significant effect on the intrathoracic pressure. When the right side of the sheep thorax is oriented facing the blast (as in the shock tube portion of the Bowen experimental data), the lung overpressure is nearly doubled in comparison to the same blast wave contacting the ventral surface of the thorax. When the sheep is positioned with its side facing the blast, the lung overpressures in the sheep model more closely reflect those of the human model. For the purposes of simulating a human in experimental testing, it would be recommended that the sheep be placed side-on to the blast. These findings may also bring into question the assumption in the Bowen curves that the orientation of the human body in the vertical axis makes negligible difference to the trauma outcome. This author believes that the orientation of the body would have an appreciable effect on the pressure buildup, and resulting trauma, when in the free field. However, if the experimentation were carried out in front of a reflecting wall (which much of it was), the orientation would likely cause less variation. It can be assumed that the orientation in front of the wall would have little effect on the build-up of pressure and also trauma, as the wall would cause a similar type of pressure buildup, regardless of the body's orientation.

As shown in the differently scaled Figure 5.3 and Figure 5.4, although the sheep and human models were exposed to the same blast loading, the pressures in the lungs of the sheep were somewhat higher compared to the human when subjected to LD_1 and LD_{50} blasts. As blast tolerance is typically scaled by scaling the time axis by the cube root of the body mass [Stuhmiller, 1996], and the human model is based on a 90 kg man, while

the sheep model is based on a 56.5 kg sheep, the higher levels of pressure predicted in the lungs of the sheep are to be expected.

The seven pressure and duration points selected for comparison represent injury predictions for a 70 kg man. Figure 5.5 shows the data points after they have been scaled for mass and species according to Equations (2.6) and (2.7) to represent a 90 kg man and a 56.5 kg sheep. Making the blast waves of longer duration for the human while decreasing the duration for the sheep, there would likely have been some change in the trauma outcome, potentially bringing the results slightly closer to one another. Overall, the sheep and human thorax models reacted predictably under varying loading conditions indicating that appropriate scaling of blast data from sheep to humans is reasonable.

Also of note is that the original research by Bowen et al. assigns the sheep a higher tolerance for blast, as seen in Figure 5.5. This is simply coincidence, as the human was given the average for all large animals, and sheep happened to be above the average. For this work, it was decided that rather than introduce even more variables to the testing, it was best to compare all models based on the modified Bowen tolerance curves for a 70 kg man.

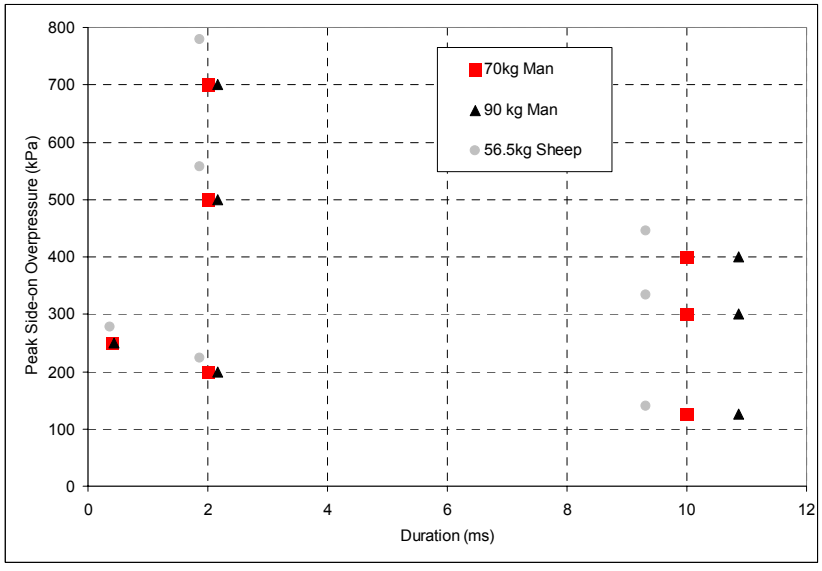

Figure 5.5: Pressure-time points of various lethalities scaled for mass and species.

After studying the pressure wave propagation it also became evident that the high pressures found in the right lung of the sheep are due primarily to its orientation normal to the blast and its unprotected location. The ventral section of the left lung is protected by the heart, whereas pressures in the left-dorsal section are higher, a result of the pressure wave flowing easily from the right to the left lung. Damage to anterior portions of the human lungs would be severe as the lungs are compressed between the dense tissues of the heart and thoracic cage. The lower pressures in the human lungs as compared to the sheep are likely also due to the anterior-posterior orientation of the lungs presenting a lower cross-sectional area for the blast wave, as well as the shielding effect of the heart. Overall, injury levels to the lungs appear to be quite comparable between the two models, when the difference in mass is considered.

Figure 5.6 shows time-pressure history data from elements at the front, middle and rear regions of the lung in the human FE model subject to a short and a long duration blast of LD_{50} severity. The curves show that lung pressure, and hence injury, are extremely dependent on the blast wave parameters and the location in the lung. In terms of predicted pressure within the numerical model, the lungs generally showed the highest pressures (and therefore the highest likelihood of damage) at the location nearest the point of load (blast) application. This is consistent with published findings [Stuhmiller et al. 1996]. However, an interesting trend was observed while studying the pressure pulses in the lungs subject to short and long duration blasts. Comparing the pressure traces in Figure 5.6, it can be seen that the high pressure/short duration blasts produce higher pressures at the front of the lungs, which is reasonable. In contrast, the long duration blast causes more damage at the rear of the lung, applying sustained transmission of energy from all around the body and focusing the pressure pulse in the vicinity of the vertebrae. This phenomenon may explain - as Bowen [Bowen 1968] noted – the fact that lung injuries in short duration blasts were more significant on the blast side of the animal, whereas long duration blasts typically resulted in injuries on the opposite side of the animal. However, this is partially due to the single, high pressure peak that the opposite side of the body will see as the pressure is reflected off the wall at the end of the shock tube; the side of

the body farther from the wall would see a stepped pressure increase, with the second pressure increase coming from the reflection off the wall, refracting around the body.

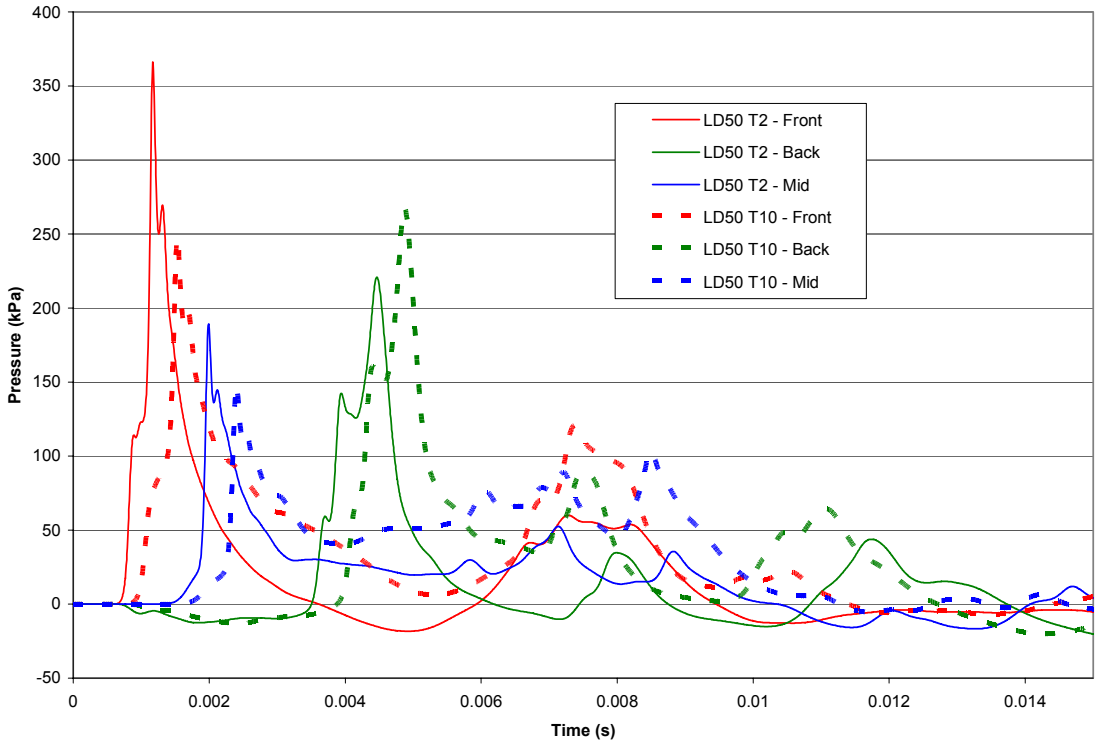

Figure 5.6: Pressure-time histories from elements at the front, middle and back regions in the lung of the human FE model comparing a short and a long duration LD_{50} blast scenario.

By examining the distribution of peak pressures in the lungs of the FE models subject to the seven free field blasts, it was possible to estimate the pressure levels responsible for varying degrees of injury. Pressure ranges for no injury, trace, slight, moderate and severe can be seen in Figure 5.7, with the lung damage predicted due to a 2 ms blast of threshold, LD_1 and LD_{50} severity. These values are bounded by the range of pressures suggested by researchers as a threshold for lung injury, quoted earlier in this section (70-110 kPa, and 240 kPa).

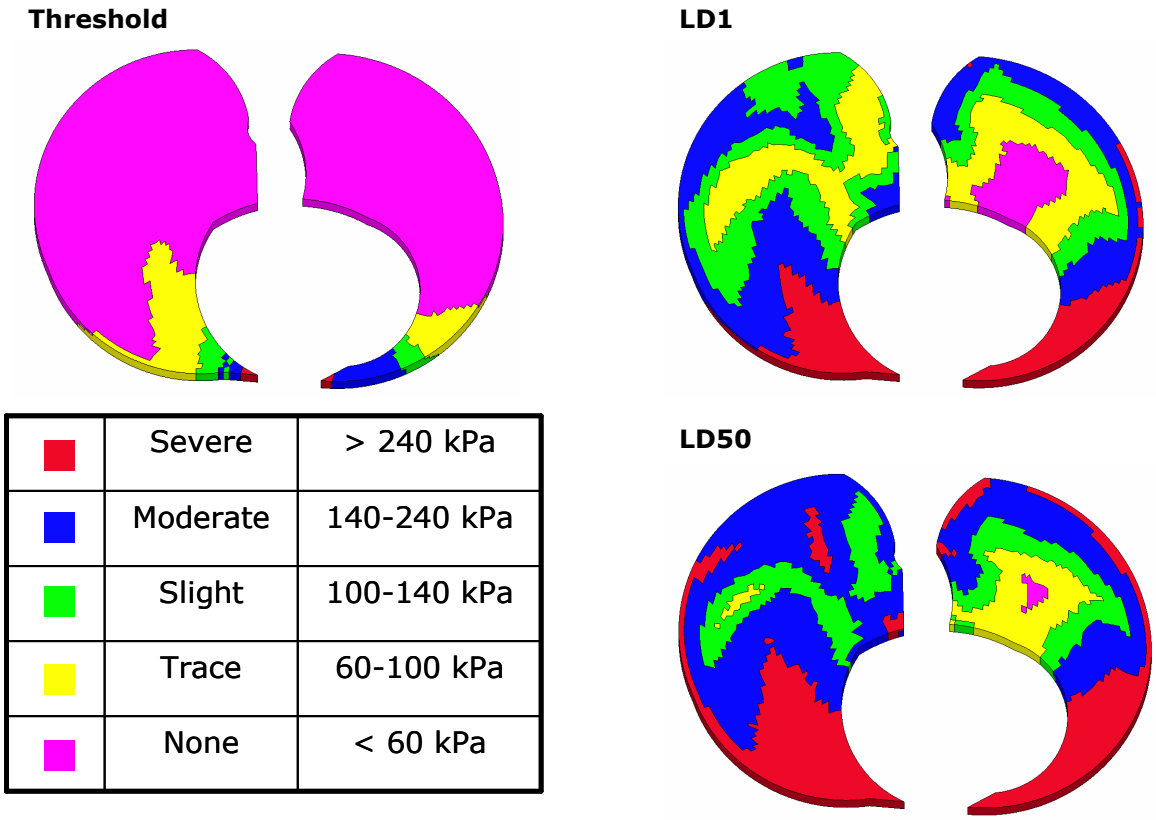

Figure 5.7: Pressure ranges for different levels of injury, and lungs showing damage from blast waves of increasing severity.

The regions of highest predicted pressure coincide with locations where blast injury has been observed in blast experimentation, such as along the ribs, around the heart, and near the vertebra [Bellamy, 1991]. As compressive waves reflect off the high density heart, the pressures in the lung are magnified, causing damage at the front of the lungs. However, due to the high density of the heart, the lung region behind the heart is largely protected. The periphery of the lungs is damaged as the compressive wave travels rapidly around the thorax in the ribs and muscle tissue, and inward at the lungs. The region in proximity to the vertebra is significantly damage as the ribs and vertebra combine to create a geometric focal point for the waves in the lungs.

5.2 Axelsson – Chest Wall Velocity

The mathematical model by Axelsson et al. [Axelsson, 1994] requires pressure-time curves recorded by four sensors on the Blast Test Device (BTD) in order to predict injury. To accurately compare the mathematical models with the human FE model, a finite element BTD was created, as discussed in Section 4.7 (Experimental Validation of Blast Loading). To limit variability, the same multi-layer air/blast model was used, with the same parameters and boundary conditions as described for the human and sheep FE models. Pressure-time histories at each of the four pressure sensor locations on the BTD were recorded for all of the simple blast loading cases, and input to the predictive models. The Axelsson model parameters were input as those specified in the literature by Axelsson et al. [Axelsson, 1994] for a 70 kg mammal. As previously discussed, the mathematical model was validated based on the average of the maximum velocities calculated from the four pressure histories.

The chest wall velocities predicted by the mathematical model for simple loading based on Bowen's threshold, LD_1 and LD_{50} curves can be seen in Figure 5.8. The predicted magnitudes correlate well to the ASII scale proposed by Axelsson, seen below in Table 5.1, and overlayed on Figure 5.8. The relatively constant velocity within each lethality suggested by Bowen et al., and the stepped increase in velocity with an increase in the lethality shows that the model is correlating well to experimental data. These values also show that the FE BTD model is in agreement with the experiments carried out by Axelsson.

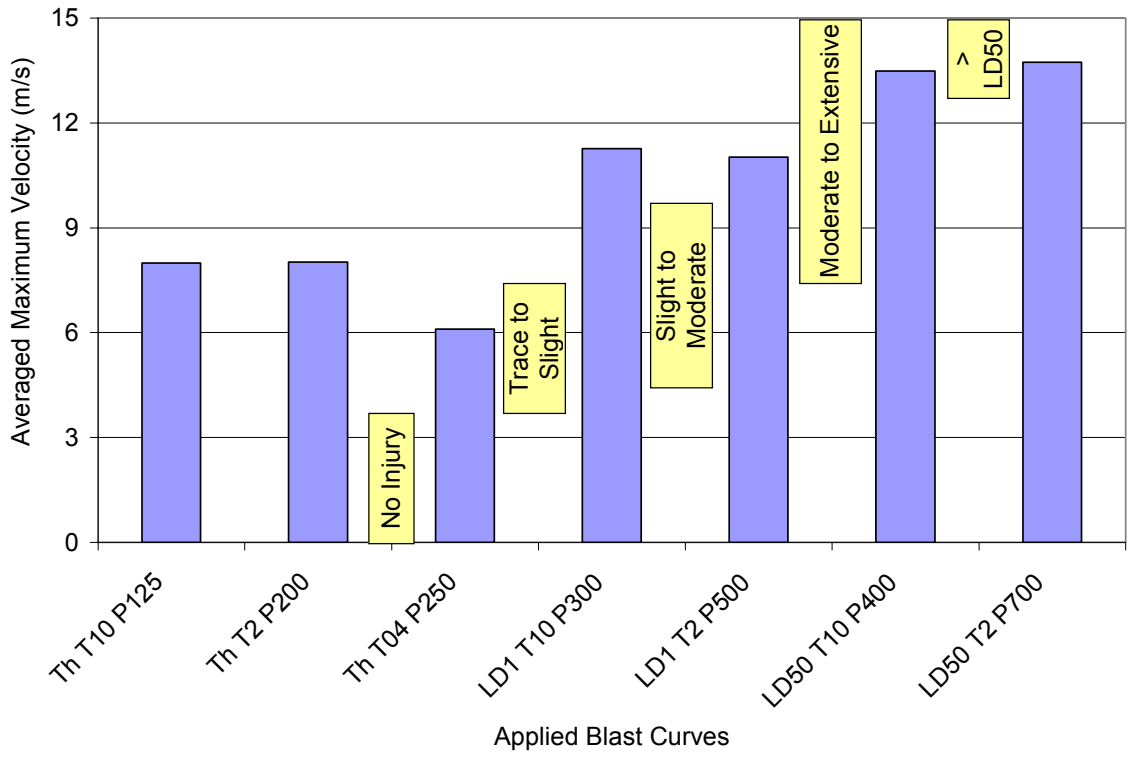

Figure 5.8: Axelsson model prediction based on BTD simulations for a 70 kg mammal, showing levels of trauma related to chest wall velocity.

Table 5.1: Injury levels with corresponding ASII and peak inward chest wall velocity [Axelsson, 1994].

Injury level	ASII	Velocity (m/s)
No injury	0.0 – 0.2	0.0 – 3.6
Trace to slight	0.2 – 1.0	3.6 – 7.5
Slight to moderate	0.3 – 1.9	4.3 – 9.8
Moderate to extensive	1.0 – 7.1	7.5 – 16.9
>50% lethality	> 3.6	> 12.8

The overall trends and performance of the sheep and human FE models closely follow those calculated by the validated Axelsson model, as can be seen by comparing Figure 5.3, Figure 5.4 and Figure 5.8 . Similar to the phenomenon noted in the previous section, this model suggests that the threshold level blast of 0.4 ms duration is likely to cause less

damage than the other data points suggested by Bowen et al. as representing threshold levels of injury.

As an additional exercise, the chest wall velocities predicted by the sheep and human FE models were compared to those calculated by the Axelsson model. It is important to keep in mind, however, that the velocities calculated by Axelsson are for the velocity of a mass scaled to represent the chest wall in a mathematical spring-mass-damper model. Axelsson et al. correlated the velocity of the mass to the trauma seen in animals subject to blast. They did not, however, directly measure the chest wall velocity of the animals to validate this aspect of the model.

The chest wall velocity values for the FE models were gathered from representative nodes on the exterior surface of the rib cage, as indicated in Figure 5.9. For the human, nodes on the anterior portion of the ribcage were used, while on nodes on the right side of the sheep were used, as these locations saw the highest inward velocities. Nodes on the opposite side of the thorax were also tracked to ensure that the maximum velocity being measured was an inward motion, and not a gross motion of the entire body.

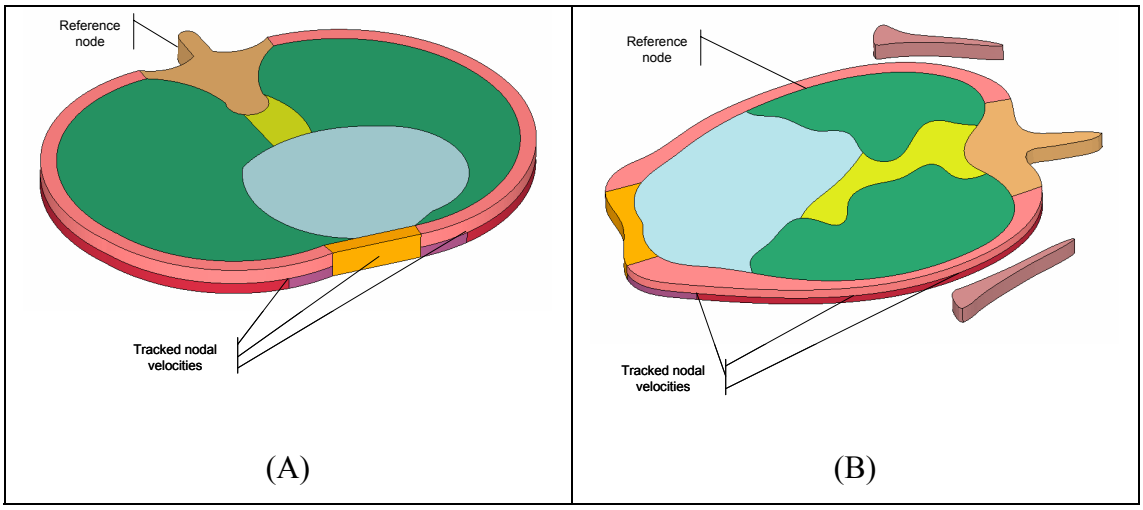

Figure 5.9: Human (A) and sheep (B) FE models showing locations of nodes used for calculating inward chest wall velocity.

The measured and calculated velocities are summarized in Figure 5.10. Subject to threshold blast levels of varying duration, the model predicts relatively constant chest wall velocities, and hence similar resultant trauma. A lower velocity is recorded at the shortest duration, as found with the other methods. The LD_1 and LD_{50} blast waves clearly show a significant increase in chest wall velocity in relation to the threshold curves. The chest wall velocities predicted by the sheep and human thorax models subject to blast loading generally correlate to the injury index scale proposed by Axelsson et al., but overlap exists between the two higher lethality loading cases. Axelsson correlated a peak inward chest wall velocity range of 3 – 4.5 m/s for threshold lung damage, 8 – 12 m/s for LD1 and 12 – 17 m/s for LD50. As can be seen in Figure 5.10, these velocity ranges correspond well to the sheep and human chest wall velocity ranges predicted in the finite element models. These trends indicate that the model generally shows higher inward chest wall velocities for higher levels of blast, but the chest wall velocity cannot be used as a predictor of trauma, as the longer duration blasts don't appear to cause as much damage, in contrast to the findings of Bowen et al. As an aside, although the velocities predicted by Axelsson's model correlate well to injury, the actual velocities measured at the chest wall of the FE models do not.

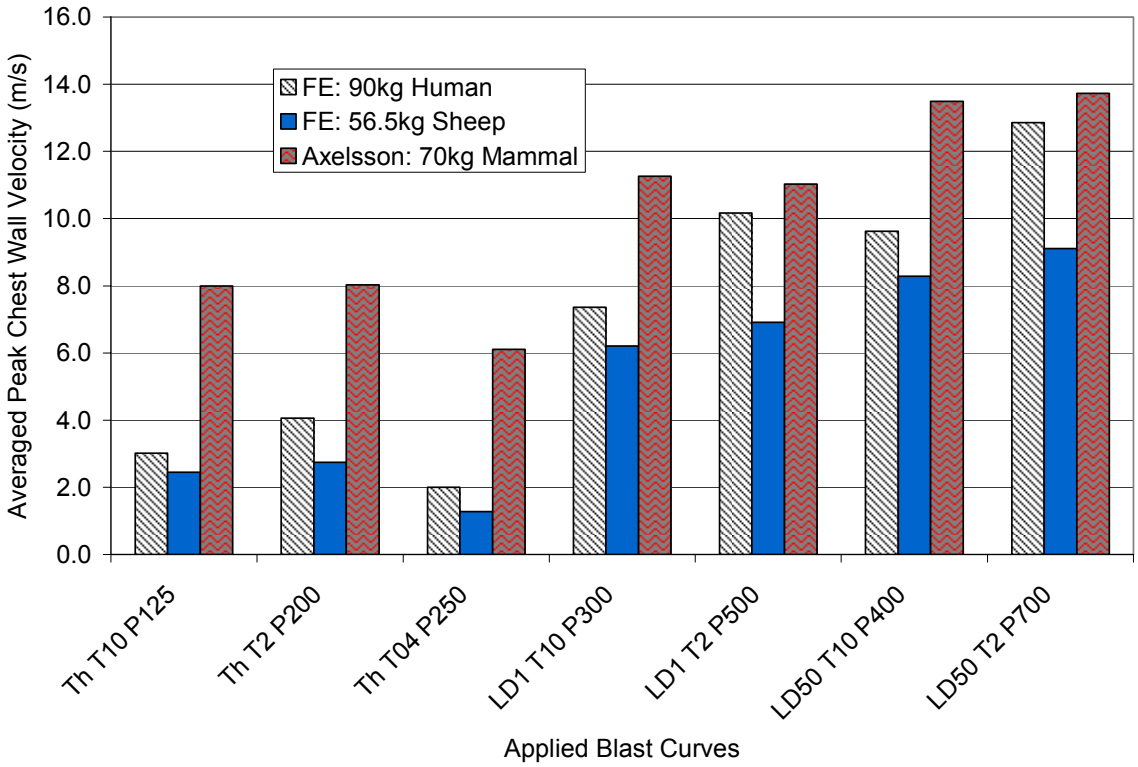

Figure 5.10: Predicted chest wall velocities of FE models and calculated velocity from Axelsson model.

Another interesting finding shown in Figure 5.10 is that, although the sheep model predicted higher lung pressures for a given loading, the human model shows a tendency towards higher inward chest wall velocities. After studying the overall motion of the thoraces, the difference between the two models appears to be overstated, and is partly a result of the chest wall velocity being reported only as an average of three nodal velocities. It is also suspected that the significant mass of soft tissue toward the dorsal region of the side of the sheep (see Figure 3.5) resists acceleration and hence does not permit as high a velocity in that area.

Studying the values calculated by Axelsson's model, this author would agree that the velocity of the mass in the mass-spring-damper system is a reasonable predictor of trauma in the simple blast environment. However, while higher chest wall velocities of the FE models generally indicate higher levels of injury, the peak inward chest wall velocity cannot be reliably used to predict the level of trauma. From the correlations

between the two methods (FE versus Axelsson) when subject to blast loading conditions specified in Bowen's curves, it can be seen that the use of peak lung pressure in the FE model is an appropriate predictor of injury from simple blast loading.

5.3 Stuhmiller – Injury 8.1

The Injury 8.1 software was run with two different subjects to better compare with the sheep and human FE models: (1) a 90 kg man representing the Visible Human Project, and (2) a 56.5 kg sheep as in Davies' CT data of the sheep. As previously mentioned in Section 2.7.5, Injury 8.1 requires the input of pressure profiles measured by the sensors located on a blast test device. As in the Axelsson study, pressure profiles from seven simple blast loading scenarios were loaded into the software, while specifying either sheep or human characteristics. Stuhmiller's model predicts injury levels based on the total normalized work of the pressure wave in the lung.

Figure 5.11 shows the total normalized work calculated by Stuhmiller's Injury 8.1 software for the man and sheep subject to simple blast loading. The shaded band is centred about 0.0208, and represents approximately 50% lethality as found experimentally by Stuhmiller et al. [1996]. The normalized work stays relatively constant within each level of lethality and increases significantly from one level to the next. The 0.4 ms threshold level blast produces appreciably less work than the other threshold level blasts, indicating concurrence with the findings of both the sheep and human FE models, as reported in Section 5.1. The long duration blasts tend to create more total work (and hence higher levels of injury), a phenomenon also shown by the sheep FE model, and seen in Figure 5.4. As much of the Injury 8.1 blast research was carried out using sheep, it is possible that this concurrence between the models indicates a higher level of lethality for sheep in longer duration blasts. When the sheep is loaded from the side, as in most studies, the higher level of injury may be a result of the bluff body of the sheep causing significant pressure build-up over longer durations.

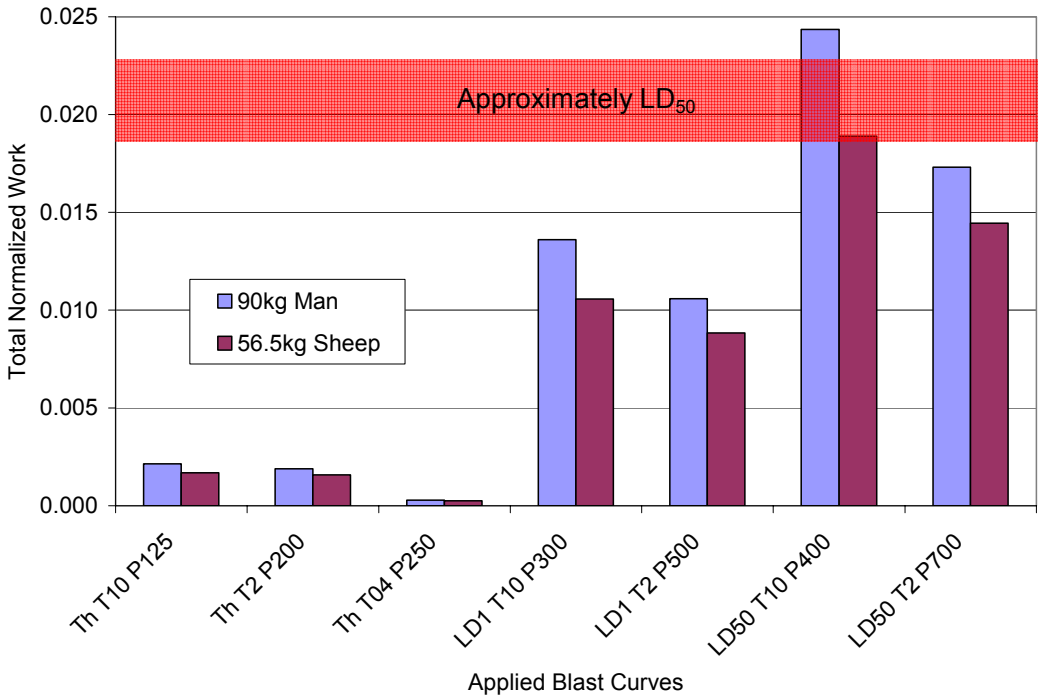

Figure 5.11: Total normalized work computed by the Injury 8.1 software for seven simple blast loading cases – shaded band shows LD_{50} level centred on 0.0208.

An anomaly of significance seen in Figure 5.11 is that the method predicts a lower level of injury for a 56.5 kg sheep than for a 90 kg man. This finding would tend to disagree with the predictions of the FE model, Bowen's scaling with the cube root of body mass, and the limited research with monkeys that indicates primates may have a higher blast tolerance than other large mammals [Bowen, 1968b]. Upon closer inspection of the mathematics behind Stuhmiller's software for predicting probability of injury for sheep and man, a likely explanation was uncovered. Figure 5.12 shows the graphical user interface of Injury 8.1 where the user can input such parameters as species, mass and atmospheric pressure. The image under "Input Files" is a representation of the blast test device, where the user can input four pressure-time curves for the chest, left side, right side, and back. The software calculates the effective work of each sensor, multiplies those values by the respective fractional surface loading areas, and sums the results. The values for the fractional surface loading areas can be seen in Table 5.2 for both the human and sheep. For the man, a value of 0.50 is used as the scaling factor for the frontal BTD sensor, and 0.25 for each of the side sensors. This would place a higher level of

importance on the frontal sensor which correlates to the human chest having a higher cross sectional area in breadth than in depth. However, it is important to keep in mind that this sensor typically is the location of highest pressure in simple blast. The sheep values tend to place much more emphasis on the large area at the sides of the sheep, represented by the left and right sensors. These sensors, however, record significantly lower pressures than the frontal sensor. The mathematics in the software assume that the sheep is being struck while standing on its hind legs, with the ventral surface being directly struck by the blast. As mentioned previously in Section 3.2 (Geometry): analysis of ventrally loaded sheep models showed significantly lower air pressures on the ventral surface of the sheep and significantly lower pressures in the lungs, as compared to laterally loaded sheep models and ventrally loaded human models. The assumption of orientation, and hence the assumed mathematical scaling factors alone could fully explain the lower levels of injury for the sheep predicted by Injury 8.1. It is also interesting to note that while the fractional surface loading area for the back of the BTD is 0, the pressure trace at the rear sensor still affects the predicted injury. Only limited information on this method and software has been published.

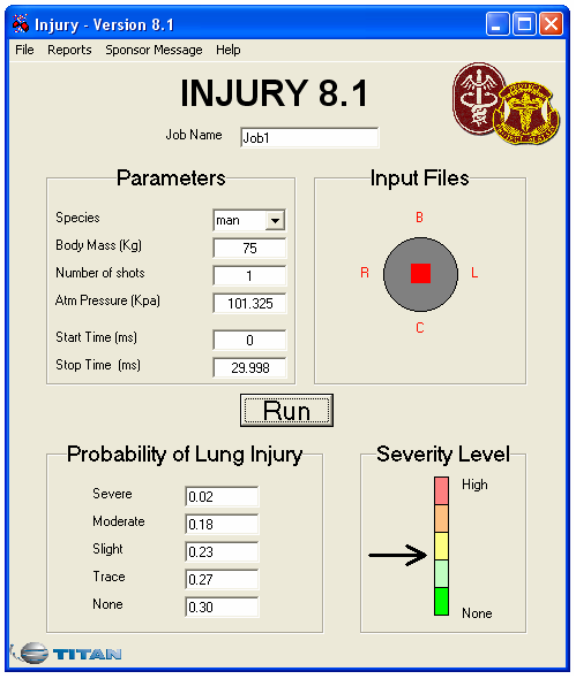

Figure 5.12: Graphical user interface for Injury 8.1 showing input parameters, BTD sensor locations and predicted severity of injury.

Table 5.2: Fractional surface loading areas for chest, left, and right locations on the human and sheep subject for the Injury 8.1 mathematics.

Subject	f_c	f_l	f_r
Man	0.50	0.25	0.25
Sheep	0.20	0.40	0.40

The overall trends and predictions of Injury 8.1 correlate well with the FE models. The performance of the FE model can be qualitatively assessed by visually comparing the trauma predictions and trends from each of the models. The model can then be quantitatively assessed by comparing the consistency of the predicted outcome within each injury level. To compare the results in more detail, Figure 5.13 shows the probability of various levels of injury for a 90 kg man, as predicted by Injury 8.1. Recapping from Section 2.7.5, lung injuries were defined based on the area of injury as: trace (appearance of small petechiae), slight (up to 10%), moderate (10-50%), and severe (above 50%). As the severity of the loading increases, the chances of no lung injury decreases, and the chances of moderate or severe injury increase. Figure 5.14 shows the volume of lung injured to various levels of severity as predicted by the human FE model. Comparing the two figures, it becomes apparent that the two models are quantifying a closely related parameter, by two completely different methods, and providing very similar predictions. Some distinct advantages of the FE models over Injury 8.1 are that the FE models can provide insight into the injury physics and phenomena, can be used for analysis in conjunction with personal protective equipment, and can provide predictions related to the locations of injury.

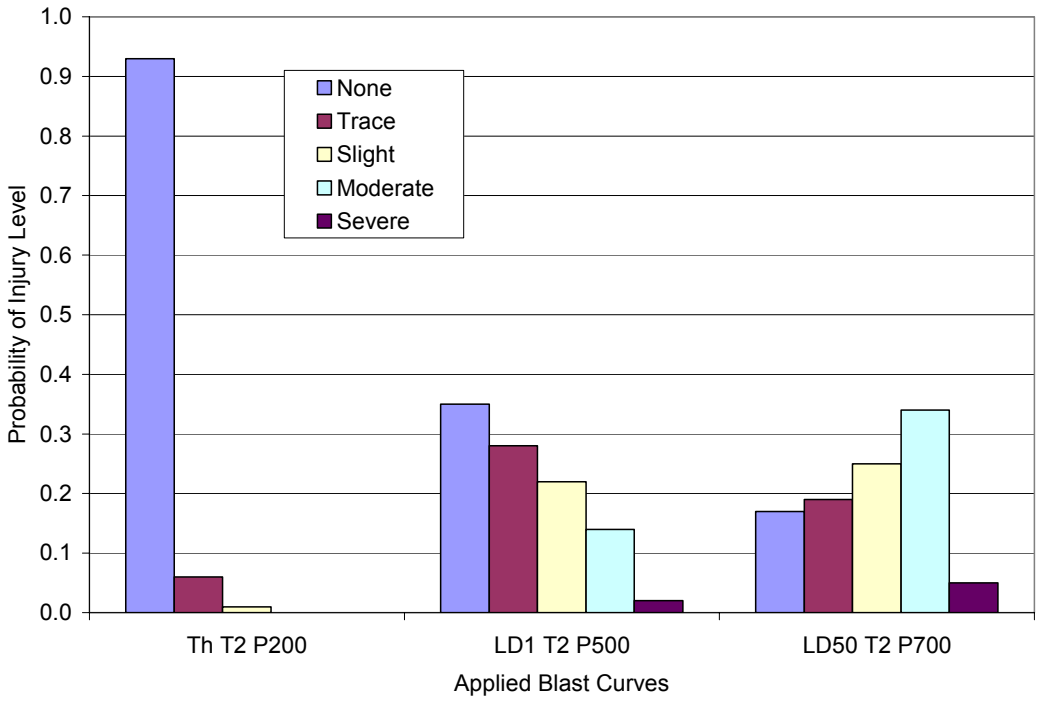

Figure 5.13: Probability of different injury levels predicted by Injury 8.1 for a 90 kg man.

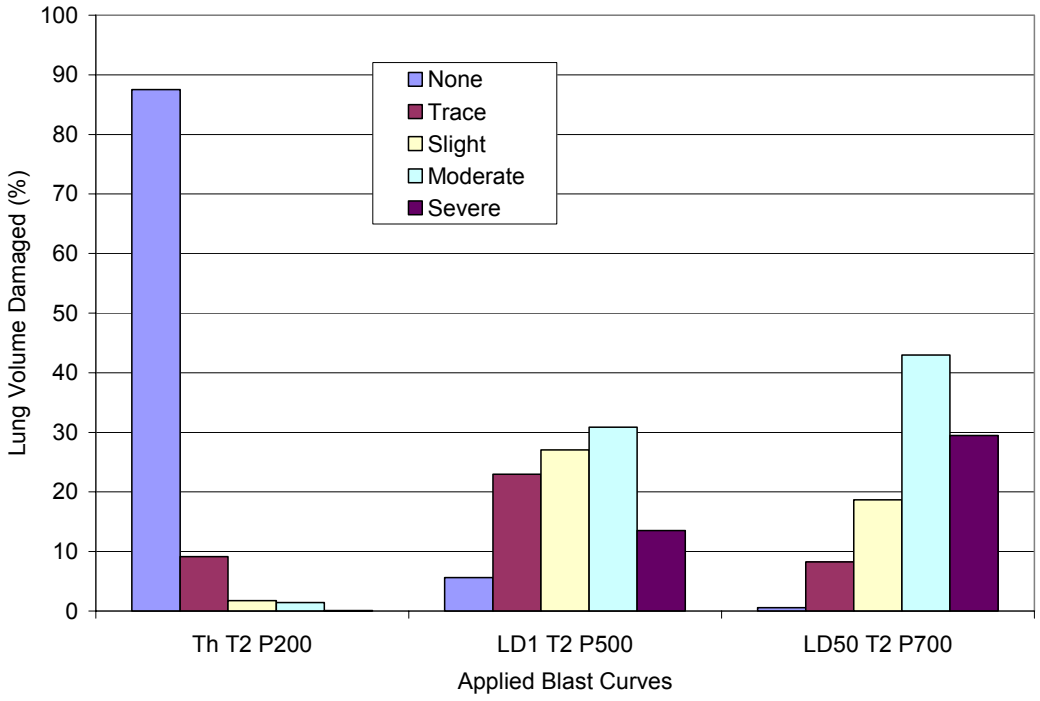

Figure 5.14: Percentage of lung volume damaged to varying degrees, as predicted by the human FE model.

Figure 5.15 shows the results from the Stuhmiller, Axelsson, and the human FE model, showing their respective predictions for each of the seven simple blast loading cases. The three models, including the FE model clearly show a marked increase in lung pressure going from threshold to LD_1 and LD_{50} loading cases. The predictions are also relatively constant within each of the three severity levels, described in detail below. For the short duration (0.4 ms) threshold value, the results of all three models indicate lower levels of trauma compared to the two other threshold values. This short duration value was significantly lowered in the modified Bowen curves, and perhaps should be treated with caution. Figure 5.15 also shows how high the threshold values in the Axelsson model are, leading to possible cases of overlap between trauma levels.

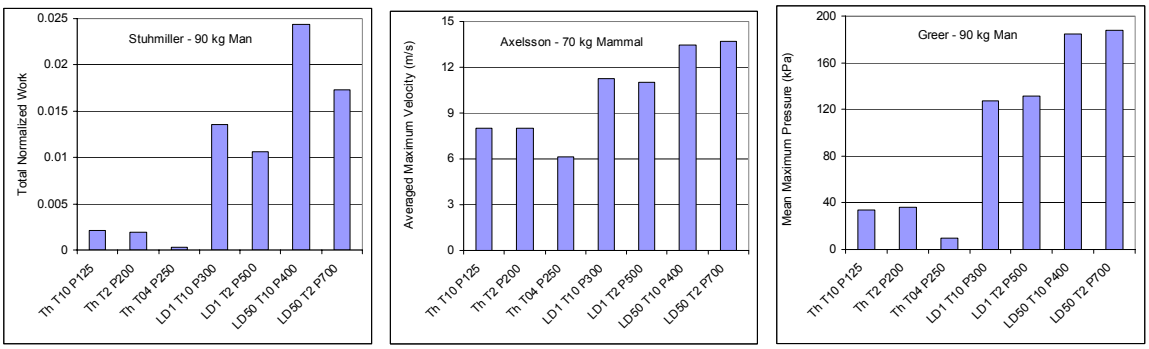

Figure 5.15: Results from Stuhmiller (Injury 8.1), Axelsson, and the human FE model show similar trends with distinct increases from threshold, to LD_1 and LD_{50} and relative consistency within each iso-injury level.

As the three models calculate completely different physical parameters, normalizing the data must somehow be done in order to compare the models on a single scale. Although the magnitudes of the values cannot be directly used to compare the performance of the models, the relative similarities can be used to assess whether the FE model is correctly predicting the same trends and phenomena as the previously validated models by Axelsson and Stuhmiller.

Figure 5.16 and Figure 5.17 show encouraging results. The data was normalized by the average of the two longer duration threshold level values. The short duration threshold value was not used for normalizing as previous examination of that blast curve appears to

indicate that it is an anomaly, causing injury levels significantly below the others. The FE model of the man follows the trends of the Stuhmiller and Axelsson models, but also shows a very stable prediction for the LD_1 and LD_{50} blast loadings. The FE model of the sheep generally follows the predictions of Axelsson as shown in Figure 5.17, and very closely replicates the behaviour of the Stuhmiller model. One visible downfall of the Axelsson model is the relative closeness of all predictions, from threshold to fifty percent lethality. This behaviour is also shown in Table 5.1 where the velocity is tied to a particular level of injury. Unfortunately, some of these levels overlap significantly, which can lead to undecipherable results.

Assuming that the modified Bowen curves correctly show iso-injury levels, the FE and mathematical models should show relatively constant levels of injury within each loading severity. To provide a more quantitative comparison of the accuracy of the models, the relative change in injury prediction within each loading severity is shown in Table 5.3. Once again, the short duration threshold level value was not included, due to its suspect nature as shown by each of the mathematical models, and in light of the recent information from Bass [2006].

The consistency of the model predictions can be expressed by calculating the range of predictions within one iso-injury level as a percentage of the average value within that injury level. The consistency as predicted by the FE models is quite comparable to that of the model by Stuhmiller. Although the Axelsson model appears extremely constant, it must be noted that there is very little variability in the Axelsson model from one level of severity to the next, making it difficult to differentiate between injury levels. By averaging the animal and human predictions from the FE model and the Stuhmiller model, variations of 15% and 20%, respectively, can be seen. An average of 4.1% change within the iso-injury level predictions for the human FE model indicates extremely good consistency in relation to the modified Bowen curves. With each of the levels indicating a consistent level of pressure in the lung, this value can be tied to the overall prediction of injury in the lung.

Table 5.3: Percentage change in trauma predictor value within each iso-injury level

Model	Threshold (%)	LD_1 (%)	LD_{50} (%)	Average (%)
Stuhmiller – 90kg Man	12.5	24.9	33.8	23.7
Axelsson – 70 kg Mammal	0.4	2.1	1.8	1.4
Greer – 90 kg Man	7.5	3.4	1.4	4.1
Stuhmiller – 56.5 kg Sheep	6.5	17.8	26.7	17.0
Axelsson – 70 kg Mammal	0.4	2.1	1.8	1.4
Greer – 56.5 kg Sheep	14.2	31.3	34.6	26.7

Having compared the predictions of the finite element models to the mathematical models, a reasonable level of confidence has been established. As previously indicated, an overall assessment of injury can be found by using the mean value of the peak lung pressures. Calculated as the average of the mean values for each injury severity shown in Figure 5.3, the values shown in Table 5.4 are proposed for overall lung injury prediction. As done in the previous calculations of variation, the short duration threshold value was not considered.

Table 5.4: Proposed mean values for the prediction of overall lung injury severity.

Level of injury severity	Mean of maximum lung pressures (kPa)
Threshold	35 kPa
LD_1	129 kPa
LD_{50}	186 kPa

A limitation of both mathematical models is the limited flexibility to account for differences between sheep and man. Although the mathematical models attempt to scale the parameters to reflect the inter species differences, the FE models were built from the foundations to account for the geometric and material differences, while providing detailed results to compare the effects on the two species.

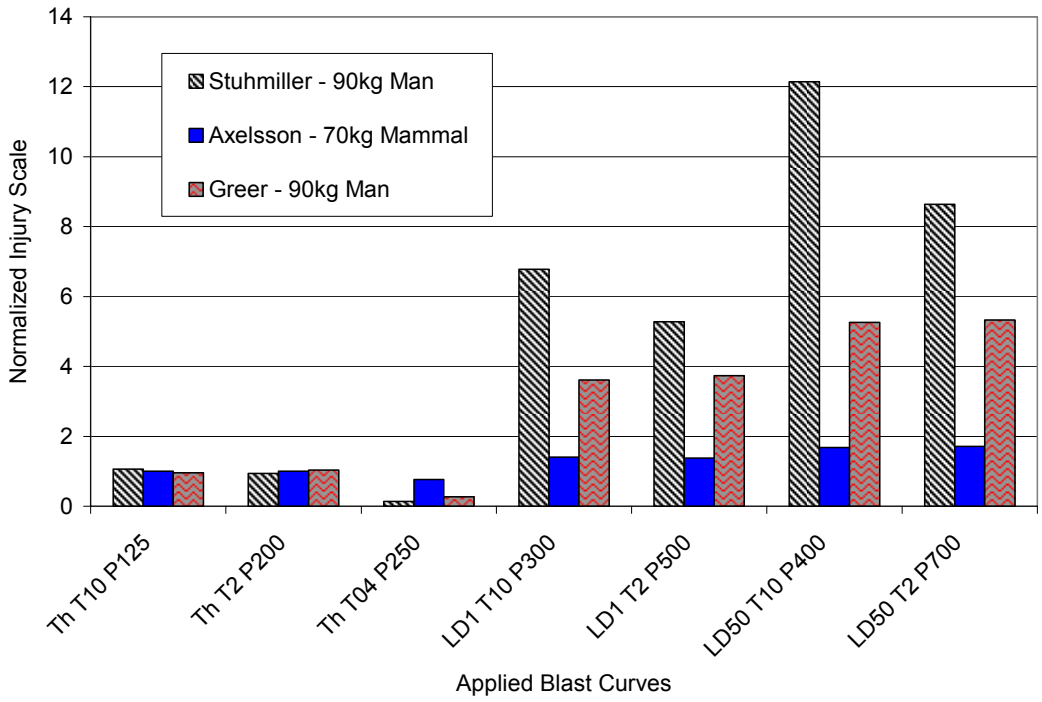

Figure 5.16: Prediction of injury to man/mammal by three models normalized to the average threshold injury prediction.

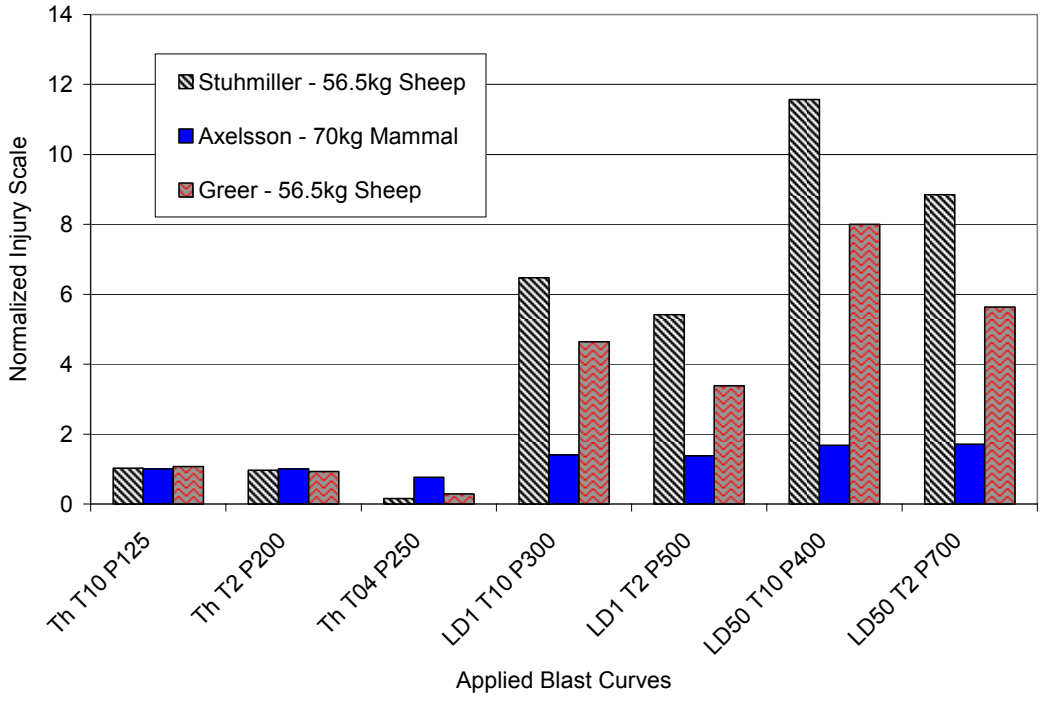

Figure 5.17: Prediction of injury to sheep/mammal by three models normalized to the average threshold injury prediction.

By comparing the behaviour of all models side by side, it becomes evident that the models generally follow the same trends. This finding provides evidence that the FE models are, in fact, predicting the same type of injuries as the two mathematical models calibrated to experimental test data, and that the FE models also correlate to the modified Bowen curves. These findings, however, are not entirely independent, as the Axelsson and Stuhmiller models were also extensively correlated to Bowen's experimental data. The FE models also indicate that, although mass scaling is a logical and appropriate scaling method, sheep and human bodies do react differently to blast inputs. Further attempts should therefore be made to examine the true behaviour and tolerance of human subjects to blast loading.

Chapter 6 Human Torso Model in a Complex Blast Environment

Thus far in this thesis, simple blast exposure has been depicted as a standing body being subjected to a planar, Friedlander type blast wave while situated in an open environment. In the literature, however, a much broader description is sometimes adopted, where the body orientation may vary, the wave may not be planar, or a reflecting wall may be situated next to the subject, as in a blast tube. Although these situations may be described as simple due to the initial blast wave having a Friedlander type profile, the resulting interaction with different parts of the body is anything but simple.

Complex blast loading can be described as any loading that does not fall under the description of simple blast. For this report, seven complex blast-loading environments have been investigated by placing walls or corners at varying distances behind the torso. Such an arrangement was chosen in order to provide a variety of loading, and to study the effects of surrounding geometry on the predicted injury. These situations, themselves, are quite relevant because the described geometry can be found in any urban area, and such scenarios could reliably be reproduced for experimental testing. The blast wave was applied using ambient boundary elements, as in the previous section. Each model was subjected to the same applied *threshold* blast of 200 kPa peak overpressure and 2 ms overpressure duration, and each model was located the same distance from the applied loading in order to isolate the geometry as the only variable. Comparing the lung pressures in these complex cases to those seen in the validated simple blast enables the model to estimate the effects on injury of complex blasts, and geometry.

6.1 Effect of Reflecting Wall

Three scenarios were modeled to simulate a human torso subjected to a Friedlander type blast while facing away from a flat, rigid wall. The distance between the torso and the

wall was varied in order to study the influence of the wall on the resulting blast loading and injury. The distances from the back of the torso to the wall were: 0.0m, 0.25m, and 0.5m, representing a separation of approximately 0, 1, and 2 chest depths, respectively.

Simulating a wall was accomplished by modeling a straight section of wall two-elements in depth, and inserting it into the air mesh at the appropriate position, as shown in Figure 6.1. A contact interface was introduced to ensure that both the air and body could interact with the wall. Nodal constraints were placed on all nodes of the wall, ensuring that it remained stationary and rigid. Although the wall was rigid with constrained nodes, the elements had to be modeled as a material with reasonable properties to avoid time step and contact interface issues. The wall was defined with an elastic material model with the properties of steel (ρ = 7860 kg/m^3; E = 200GPa; ν = 0.3). The elements were sized similar to those of the surrounding elements to reduce the chance of leakage in the ALE analysis. Increased distance to the wall was accomplished by maintaining the position of the torso in the air mesh while placing the wall progressively further back. The models of the air, wall and torso can be seen below, in Figure 6.1.

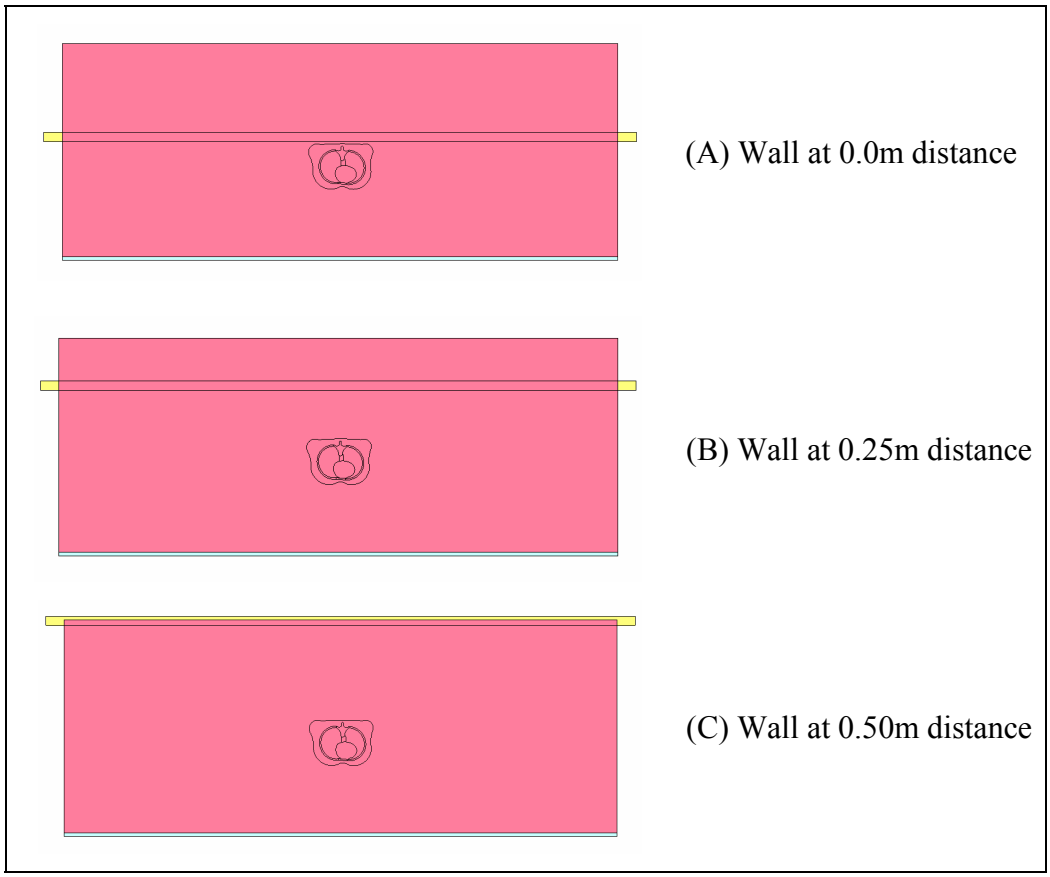

Figure 6.1: Flat wall inserted at various distances to compare the effects of complex blast on trauma outcome.

To compare the results with other validated predictive models, a finite element model of the Blast Test Device was inserted into the same three scenarios shown above using the same procedure as outlined in the previous chapter. Recording the pressure in air elements at locations of the four pressure sensors in the BTD, and running these pressure-time curves through Stuhmiller's Injury 8.1 software and Axelsson's mathematical model allows a direct comparison to the results of the human FE model. Although the three models calculate and output different physical parameters, the models can be compared by normalizing data to the threshold, free field results of each model. The effect of the body's proximity to a flat wall can be seen in Figure 6.2, as predicted by the FE model, Stuhmiller's Injury 8.1, and Axelsson's mathematical model. Approaching the wall or the corner, an increase in severity of injury can clearly be seen. Comparing the curves in Figure 6.2 it is clear that the three models are providing similar results. The change in slope of the curves with distance, however, shows a marked difference between the

Stuhmiller and Axelsson predictions, with Stuhmiller indicating a much more significant increase in trauma with decreasing distance. As a frame of reference, the human FE model would require a normalized value of approximately 3.7 to reach LD_1 lethality.

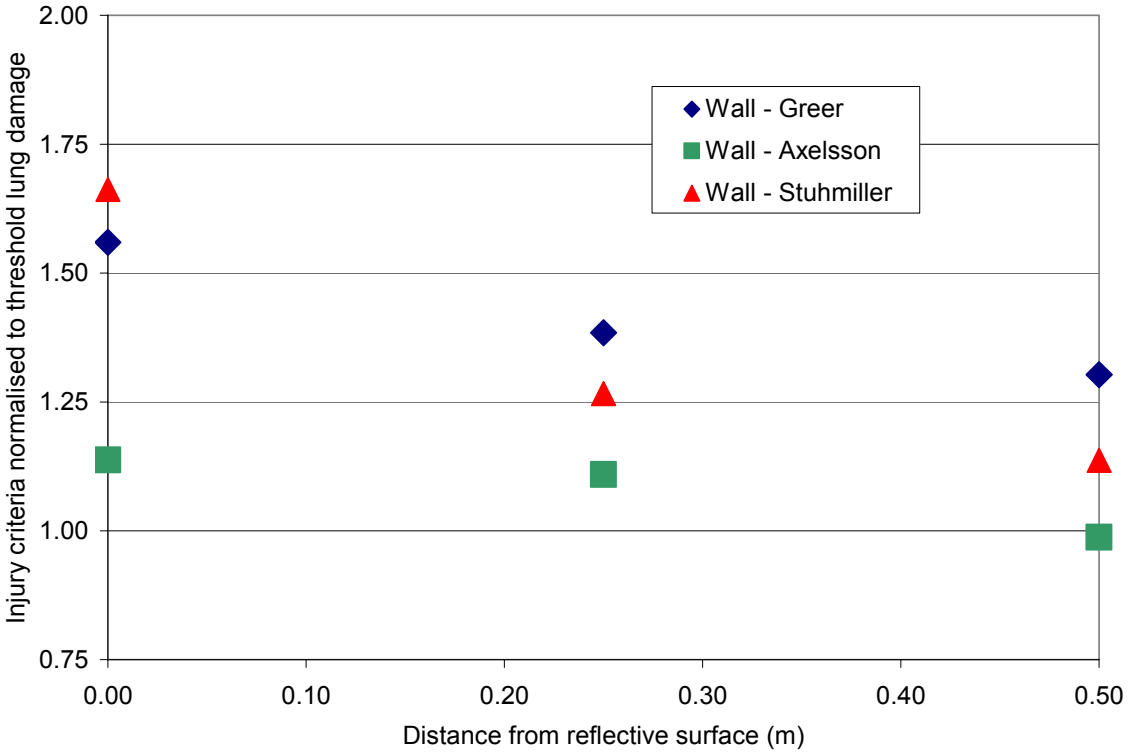

Figure 6.2: Injury criteria from three different models normalised to the injury predicted in the free field shows the effect of a wall at varying distance on the severity of injury.

As the body approaches the flat wall (from 0.5m to 0.25m), the injury is increased relative to the free field due to the pressure reflecting off the wall and striking the body from behind, effectively providing an extended loading, or even a second assault. If the torso is farther from the wall, the wave has more time to dissipate and causes less damage, explaining the decrease in injury with distance from the wall. Also, when the torso is situated relatively close to the wall, the loading is both of higher pressure and longer duration due to the reflection and superposition of the blast wave. When in contact with the wall, although the wall may provide a small degree of protection from the blast, the rest of the torso is much more aggressively loaded, resulting in higher levels of trauma. Such findings explain why Bowen et al. used the pressure-time curve measured

at the reflective end of the blast tube instead of using the Friedlander curve initially impinging upon the end of the blast tube, which was of significantly lower pressure and duration.

6.2 Effect of Reflecting Corner

Another common geometric feature that can create a complex blast-loading environment is a corner. Three models were investigated to identify trends in the level of injury sustained while located at various distances from a corner. The three scenarios had the torso at a 45-degree angle to the corner (appears as a wedge), with the planar blast wave traveling directly toward the torso, at a 45-degree angle to each wall. Once again, the three models varied by changing the distance between the walls and the torso from 0, to 1 and 2 torso distances, as shown in Figure 6.3 A, B, and C, respectively.

Application of nodal constraints at 45-degrees on the air mesh to simulate a wall was not considered as these conditions would have created a jagged edge. Therefore a smooth Lagrangian part representing the wall was inserted in the ALE mesh. The distance from the blast to the torso remained constant, and the same threshold blast loading was used.

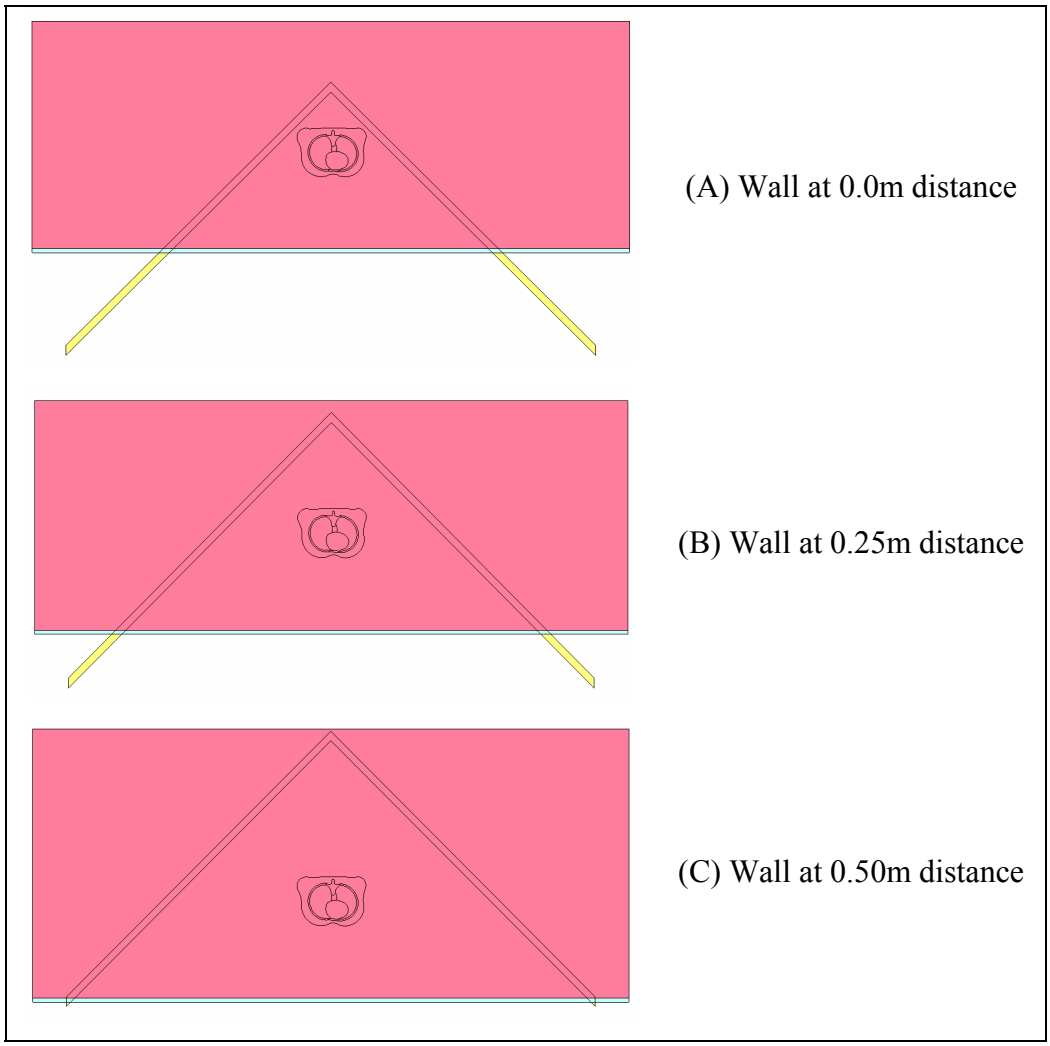

Figure 6.3: Corner wall inserted at various distances to compare the effects of complex blast on trauma outcome.

Figure 6.4 shows contours of pressure as the blast is applied to the human torso while located 0.25 metres from the wedge. Regions of high pressure can be found: (1) at the wall where the pressure wave is superimposed and concentrated by the decreasing width, (2) in front of the torso (as seen in the free field case), (3) in the wedge where the flow from the two sides of the torso superimpose on one another, and (4) against the back of the torso where the concentrated blast returns and builds against the body. As a result of these pressure concentrations, the corner causes an ever greater level of injury than the wall, focusing the blast pressure towards the body, and providing a reflective surface to cause a sustained loading or a second pressure strike on the body.

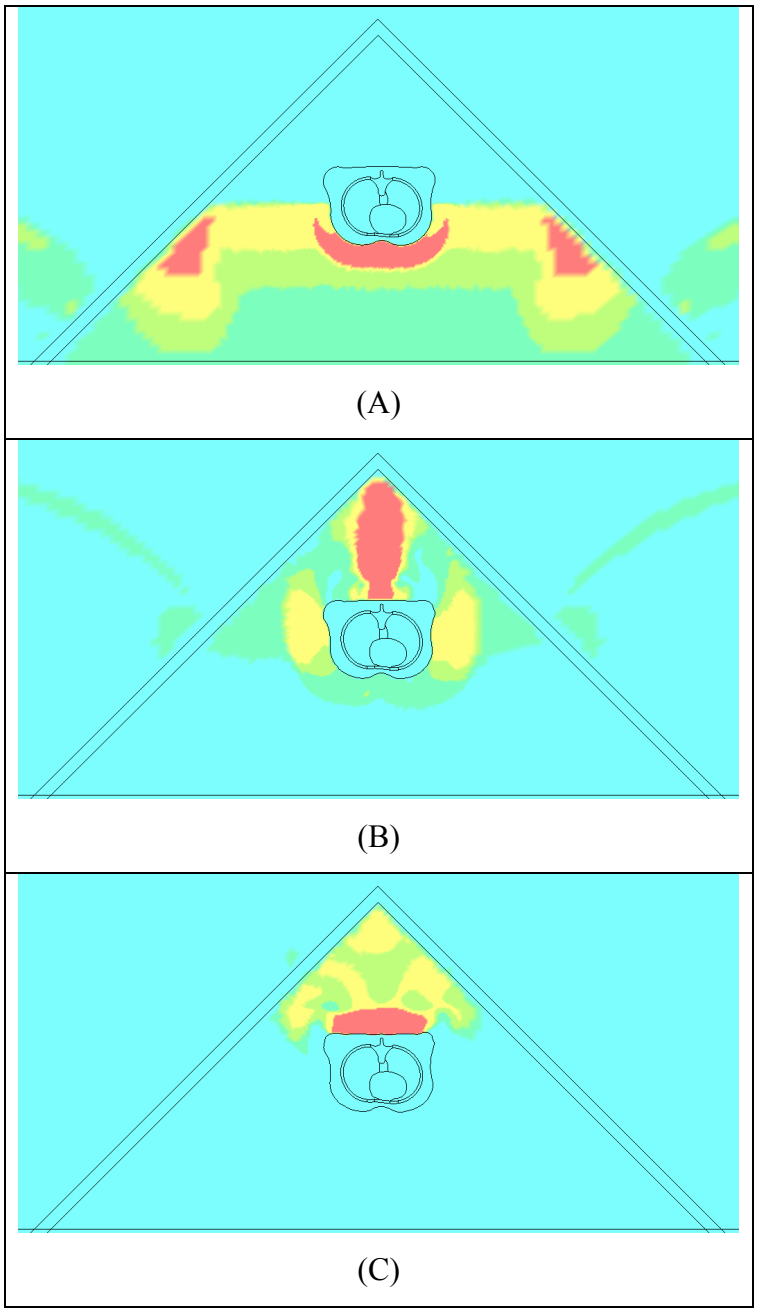

Figure 6.4: Contours of pressure showing the human torso located 0.25m from the wedge, subjected to a threshold level blast wave at (A) 9.0 ms, (B) 21 ms, (C) 32 ms.

The higher lethality with decreasing distance is displayed in Figure 6.5, where normalized results from the three models are compared. Without further examination, one could conclude that the results are quite comparable, with the finite element model simply predicting a lower relative increase in injury when the torso is directly against the wall. However, after studying the pressure flow around the FE torso, the results could be

even more closely related. When the torso is placed directly against the walls in the corner, as shown in Figure 6.3 (A), the pressure wave is not able to penetrate behind the body. This phenomenon arises as a result of the ALE advection algorithm not allowing the pressure to flow readily in a diagonal direction. This could be partially alleviated with smaller air elements, or a larger gap between the wall and the body. Such a situation does not occur with the BTD, as it is smaller than the FE torso, allowing more of a channel for the pressure to flow behind the BTD. Low flow behind the FE torso is also not realistic in a three dimensional environment, as pressure would readily flow above, below and around the body in front of a reflecting surface. With smaller elements, or a slightly greater distance to the corner, it is likely that the FE model would correlate even more closely with the Axelsson and Stuhmiller models.

The significant effect of the corner on trauma outcome can clearly be seen in Figure 6.6, comparing the normalized results of the torso in a corner to those of being in front of a flat wall. In the worst case, where the body is located directly in the corner, the mean lung overpressure is nearly twice as high as that predicted for the free field environment, subject to the same blast wave.

Further examination of the results for wall and corner blast environments can be seen in Figure 6.7, where the percentage volume of the lung damaged to varying degrees is presented for each of the scenarios. Figure 6.9 shows the locations of the trauma in the lung, as well as the level of injury. Figure 6.8 is shown in order to relate the trauma outcome in complex blast to the free field blast of threshold and LD_1 lethality.

An interesting finding seen in Figure 6.6, Figure 6.7 and Figure 6.9 is that the FE models predict a similar level of injury for a body directly against a flat wall, or 0.5m from a corner. Studying the distribution of lung injury, it is also interesting to note that the front of the lungs in all complex environments show an almost constant level of injury, while the majority of the increases in injury occur in the back of the lungs. This is a result of the front of the chest being loaded similarly in all scenarios, but the pressure waves on the back and sides being significantly altered by the environment. Such a situation is a good

example of why it is necessary to study the pressure field around the entire body, and not simply measure the free field pressure, or the location of highest pressure.

Figure 6.7 indicates that the level of injury is higher when located at 0.5m than at 0.25m, contradicting Figure 6.6. Studying the entire distribution of pressures, however, showed that the higher mean value predicted the level of injury. The contradiction stems from the 0.5m scenario showing higher levels of pressure recorded along the periphery of the lungs, but the 0.25m scenario applying more energy to the torso, with higher levels of pressure penetrating throughout the lung volume. Overall, Figure 6.7 shows a decrease in the uninjured volume of lung, with all other levels of injury increasing in volume as the body approaches the reflective surface.

The locations of trauma shown in Figure 6.8 and Figure 6.9 correlate well with experimental observations in free field and complex blast. Pulmonary contusions are typically more severe on the side facing the blast when in the free field, but tend to be bilateral and diffuse in a confined environment [Wightman, 2001]. Bowen et al. [Bowen, 1968] have also shown that the regions of injury were different in free field and blast tube experiments. The long duration blasts in the shock tube typically produced severe injury at the reflective surface, which can be explained by the pressure waves superimposing at that point. By comparing Figure 6.8 and Figure 6.9, the increasing level of injury at the back of the lungs can be seen as a direct result of the complex environment.

Comparing the results of the complex blast scenarios with those of the threshold and LD_1 cases in the free field, one can clearly see that the level of lung damage is increasing with decreasing distance to the reflective surface, but an LD_1 level of injury was not sustained, even when directly in the corner. For comparison purposes, threshold level injury is predicted as a mean value of 35 kPa and LD_1 is predicted as 129 kPa. When the torso was closest to the wall, the mean value was 57 kPa, and in the corner it was 69 kPa. These results show good correlation to the previously validated Axelsson and Stuhmiller models, but also provide far greater insight into the origins of the trauma, the locations of injury, and the effect of complex blast on the level and characteristics of lung injury. In

addition to these advantages, the human FE model is extremely flexible, and can be used to compare and develop personal protective equipment.

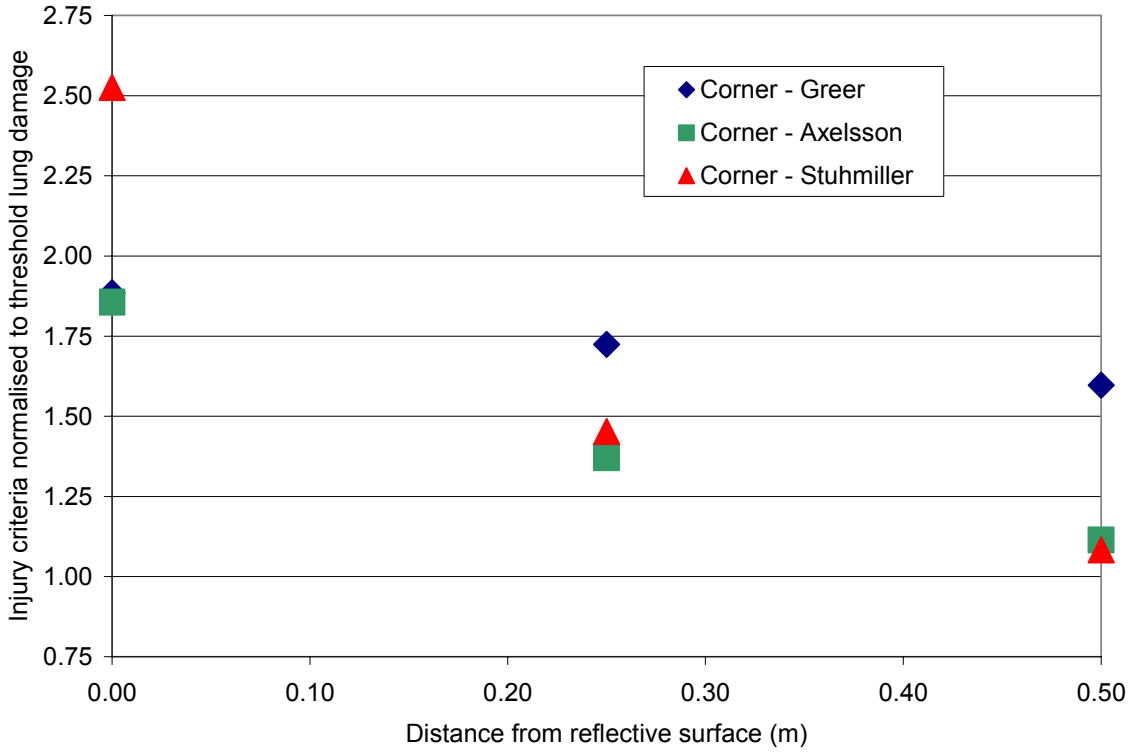

Figure 6.5: Injury criteria from three different models normalised to the injury predicted in the free field shows the effect of a corner at varying distance on the severity of injury.

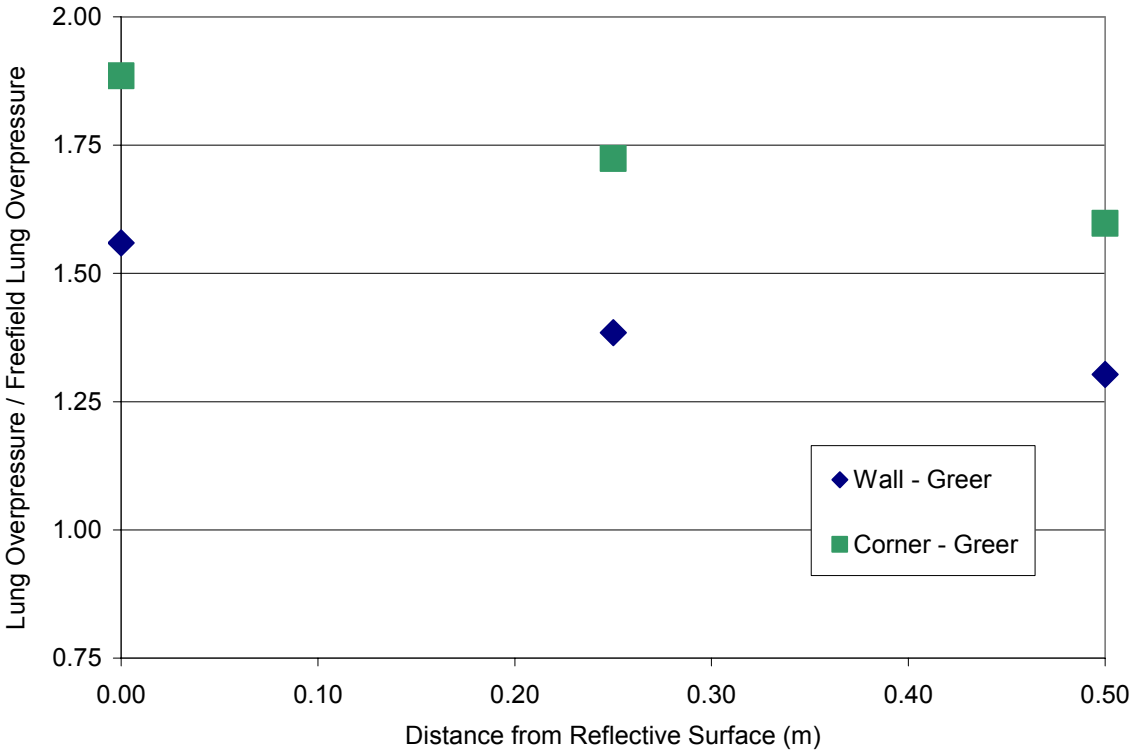

Figure 6.6: Mean lung overpressure predicted by the human FE model, normalised with the overpressure predicted subject to a free field blast.

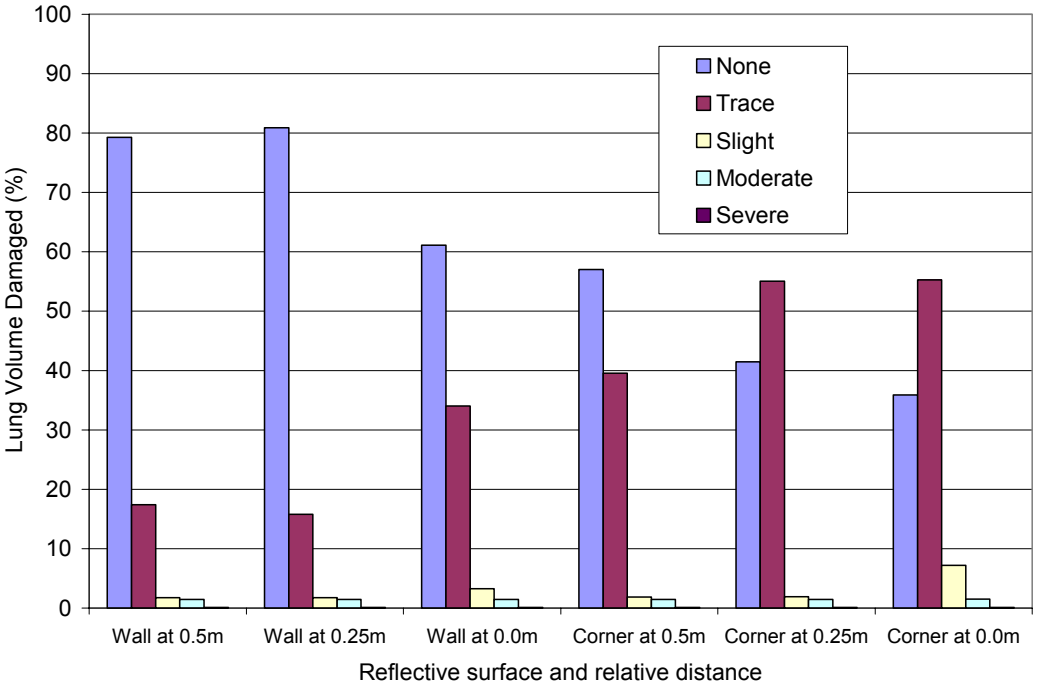

Figure 6.7: Percentage of lung damaged at each level, shown for each reflective surface and relative distance.

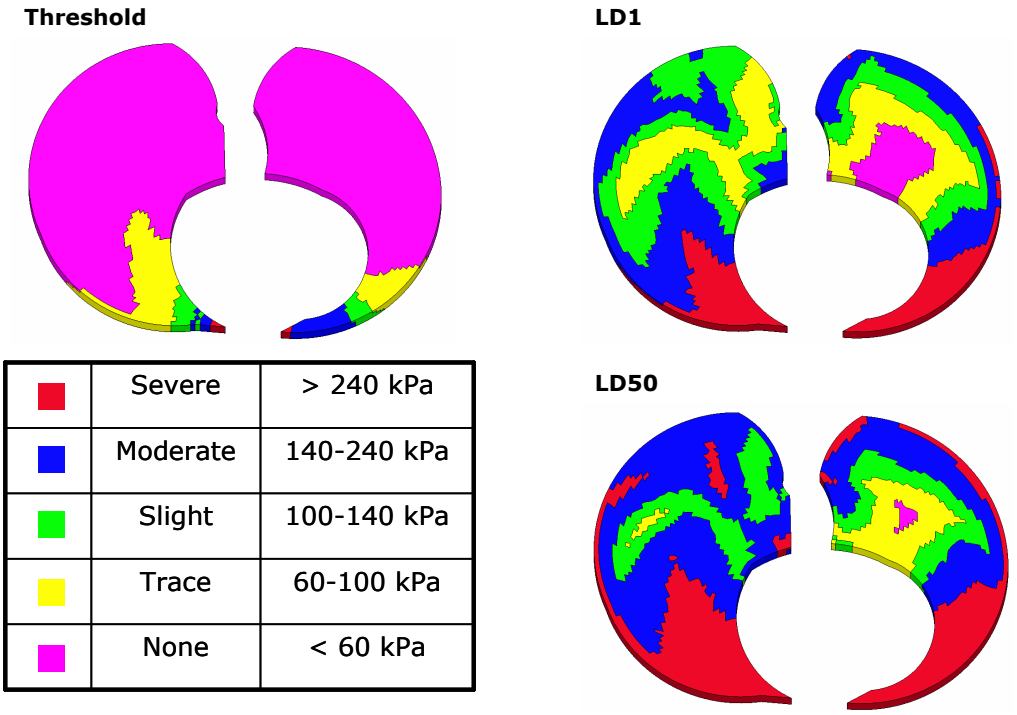

Figure 6.8: (Shown here for reference, also shown in Chapter 5) Pressure ranges for different levels of injury, and lungs showing damage from blast waves of increasing severity in the free field.

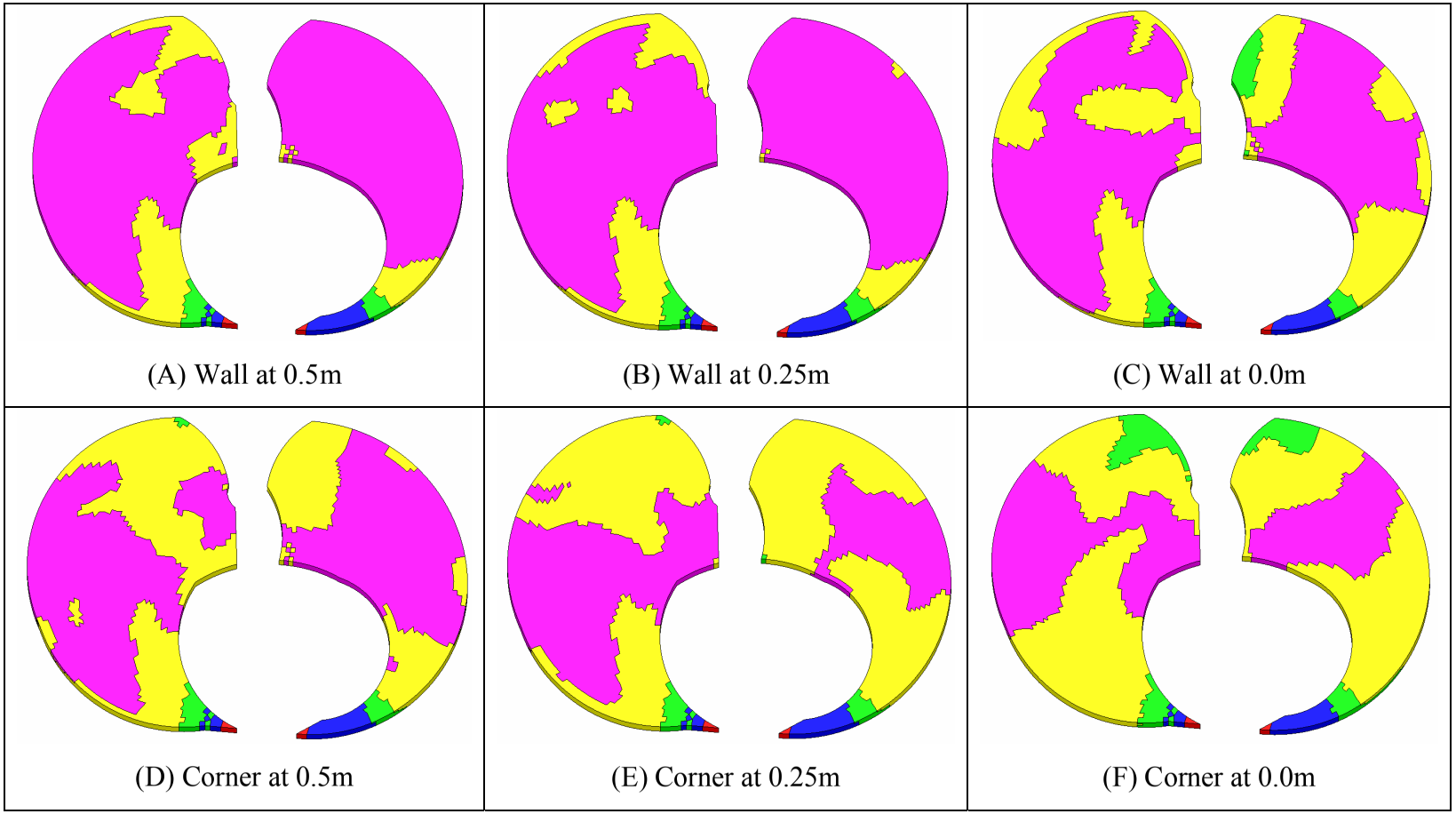

Figure 6.9: Lung damage shown for a human subject to a threshold level blast of 200 kPa overpressure and 2 ms duration while in front of a flat wall (C,D,E), and in front of a corner (F,G,H).

Chapter 7 Conclusions and Future Considerations

In both the civilian and military environment, blast injury has resulted in significant casualties, and a fundamental understanding of primary blast injury is needed. A finite element model has been created in order to provide insight into the origins of trauma, as well as to provide an engineering tool for the development of personal protective equipment. A human torso model and a sheep thorax model were created from detailed anatomical images and experimentally defined material properties. Approximations for lung material properties were derived from the shock properties of air and water in order to satisfy high-rate requirements of the model. The fluid-structure coupling modeling approach was successfully validated by comparing the predictions to experimental blast studies carried out at DRDC-Valcartier.

The performance of the models was then correlated to animal studies carried out by Bowen et al. in the simple blast environment. Based on the correlation between the animal blast results and the performance of the models, an injury criterion based on peak lung pressure was proposed. Overall lung injury was predicted using the mean of the peak lung pressure values where a mean of 35 kPa indicates threshold level injury, 129 kPa indicates LD_1 and 186 kPa indicates LD_{50}. The models and injury criterion compared quite favourably with two well-known blast injury prediction models, those of Axelsson et al. [Axelsson, 1994] and Stuhmiller et al. [Stuhmiller, 1996] by showing similar trends and by predicting consistent levels of injury for the threshold, LD_1 and LD_{50} loadings.

For a more detailed analysis of the injury pattern in the lung, local lung injury can be categorized by the peak level of pressure recorded in each finite element, according to the following scale: no injury (< 60 kPa), trace (60-100 kPa), slight (100-140 kPa), moderate (140-240) and severe (> 240 kPa).

Relatively consistent values were seen within each level of injury severity when compared with the model by Stuhmiller: 15% variation for the FE model, and 20% for Stuhmiller. These numbers are greater than those predicted by Axelsson (1.4%), but the variation in that model from one level of severity to the next is extremely small. An average variation of only 4.1% within levels of severity for the human FE model indicates extremely good correlation to the modified Bowen curves. The finite element models were also able to predict the locations of injury reported in experimental studies, namely, at the periphery of the ribs, around the heart, and in the vicinity of the vertebrae.

The performance of the human finite element model in complex blast was then compared to the two predictive models. Complex environments were simulated by inserting either a flat wall or a corner, and varying the distance between the reflective surface and the torso. The models predicted similar increases in the level of trauma, and similar trends were noted as the distance between the torso and the reflective surface was varied. The finite element model was also able to demonstrate how the wall or corner affects the blast flow, and how that ultimately affects the level of injury.

The current method of calculating the mean of the maximum pressures in the lung elements requires an enormous amount of memory and post-processing. It is for this reason that the implementation of a user material model in LS-DYNA was undertaken to allow for the tracking of damage in the lungs. At this time, the model is still under development, but such a model could allow for a consistent means of damage evaluation, reduced data analysis time, and most importantly the investigation of alternate injury criteria.

The finite element model of the human is now being used to compare the effectiveness of personal protective equipment, and to further study the mechanisms of primary blast injury. To further improve the performance of the model, it is suggested that deviatoric strength be added to the lung model in combination with a frictionless contact definition at the lung/rib interface. This change would permit the accurate modeling of long-term deformation in the lung. As computer performance increases, a finer mesh and a truly

three-dimensional model of the torso would allow a more in-depth study of the complex wave interactions that cause injury within the lungs.

REFERENCES

[Abé, 1996] Abé, H., Hayashi, K., Sato, M., Data book on mechanical properties of living cells, tissues, and organs, Springer-Verlag, New York, 1996.

[American Lung Association, 2004] American Lung Association: www.lungusa.org/learn/resp_sys.html, 2004.

[Axelsson, 1994] Axelsson, H., Yelverton, J.T., "Chest wall velocity as a predictor of non-auditory blast injury in a complex wave environment," 7th International symposium of weapons traumatology and wound ballistics, St. Petersburg, Russia, 1994.

[Bass, 2005] Bass, C.R., "Injury biomechanics of blast: known and unknown," DSRC Mitigation of blast injury: modeling and simulation workshop, DARPA – Defense Sciences Research Council, Arlington, Virginia, April 2005.

[Bass, 2006] Bass, C.R., Rafaels, K., Salzar, R., "Pulmonary Injury Risk Assessment for Short-Duration Blasts," Personal Armour Systems Symposium (PASS) 2006, Leeds, United Kingdom, September 2006.

[Bellamy, 1991] Bellamy R.F., Zajtchuk R., "Conventional Warfare: Ballistic, Blast, and Burn Injuries." In: Bellamy RF, Zajtchuk R, eds. Textbook of Military Medicine, Part 1, Volume 5. Washington, DC: Office of the Surgeon General of the US Army; 1991; pp. 1-51.

[Bowen, 1965] Bowen, I.G., Holladay, A., Fletcher, E.R., Richmond, D.R., White, C.S., "A fluid-mechanical model of the thoracoabdominal system with applications to blast biology, Technical report DASA-1675, Defense Atomic Support Agency, 1965.

[Bowen, 1968a] Bowen, I.G., Fletcher, E.R., Richmond, D.R., "Estimate of man's tolerance to the direct effects of air blast," Technical progress report no. DASA-2113, Department of Defense, Defense Atomic Support Agency, Washington, D.C., 1968.

[Bowen, 1968b] Bowen, I.G., Fletcher, E.R., Richmond, D.R., Hirsch, F.G., White, C.S., "Biophysical mechanisms and scaling procedures applicable in assessing responses of the thorax energized by air-blast overpressures or by nonpenetrating missiles," Annals of the New York Academy of Sciences, 1968, Vol. 152, pp. 122-146.

[BUPA, 2003] BUPA Health Information Team, Hearing Loss, www.bupa.co.uk, October, 2003.

[CDC, 2005] Centers for Disease Control and Prevention – Department of Health and Human Services (www.CDC.gov): Emergency Preparedness & Response: "Explosions and Blast Injuries: A Primer for Clinicians," April, 2005.

[Chuong, 1985] Chuong, C.J., "Modeling of wave dynamics near lung pleura during airblast incidence," Advances in Bioengineering, 1985, pp. 99-100.

[Clemedson, 1956] Clemedson, C.J., "Blast Injury", 1956, Physiol. Rev. 36, pp. 336-354.

[Clemedson, 1968] Clemedson, C.J., Hellstrom, G., Lindgren, S., "The Relative Tolerance of the Head, Thorax, and Abdomen to Blunt Trauma," Annals New York Academy of Sciences, 1968, 152, pp. 187-198.

[Clifford, 1984] Clifford, C.B., Moe, J.B., Jaeger, J.J., Hess, J.L., "Gastrointestinal lesions in lambs due to multiple low-level blast overpressure exposure." Military Medicine, 1984; 149: pp. 491-5.

[Cooper, 1989] Cooper, G.J., Taylor, D.E.M., "Biophysics of impact injury to the chest and abdomen," Journal of the Royal Army Medical Corps, 1989, Vol. 135, pp. 58-67.

[Cooper, 1991] Cooper, G., Townend, D, Cater, S., Pearce, B., "The role of stress waves in thoracic visceral injury from blast loading: modification of stress transmission by foams and high-density materials", Journal of Biomechanics, 1991, Vol. 24, pp. 273-285

[Cowin, 2001] Cowin, S.C., (editor), Bone mechanics handbook, second edition, CRC Press, New York, 2001.

[Cronin, 2000a] Cronin, D.S., Worswick, M.J., Pick, R.J., "DREV simplified physical leg model: phase I literature review and preliminary numerical analysis", DREV contract #W7701-9-1941, 2000.

[Cronin, 2000b] Cronin, D.S., Salisbury, C., Worswick, M.J., Pick, R.J., Williams, K.V., Bourget, D., "Appropriate material selection for surrogate leg models subjected to blast loading," Explomet 2000, Albuquerque, New Mexico.

[Cronin, 2004] Cronin, D., Salisbury, C., Greer, A., "Numerical Modeling of Blast Injuries: Phase 1 – Final Report," Contract report for Defence R&D Canada – Valcartier, March 2004.

[Davies, 1987] [Davies et al. 1987] Davies, A.S., Garden, K.L., Young, M.J., Reid, C.S.W., An atlas of X-ray tomographical anatomy of the sheep, Science Information Publishing Centre, Wellington, New Zealand, 1987.

[Deal, 1957] Deal, W.E.,"Shock Hugoniot of Air," Journal of Applied Physics, Vol. 28, No. 7, July 1957, pp. 782-784.

[Deng, 1999] Deng, Y.C., Kong, W., Ho, H., "Development of a finite element human thorax model for impact injury studies," SAE International congress & exposition, Detroit, MI, USA, 1999.

[Dodd, 1990] Dodd, K.T., Yelverton, J.T., Richmond, D.R., Morris, J.R., Ripple, G.R., "Nonauditory injury threshold for repeated intense free field impulse noise," Journal of Occupational Medicine, Vol. 32, No. 3, March 1990.

[Dowsett, 1998] Dowsett, D.J., Johnston, R.E., Kenny, P.A., The Physics of Diagnostic Imaging, Arnold Publication, 1998.

[DuBois, 2003] DuBois, PA, "A simplified approach to the simulation of rubber-like materials under dynamic loading," 4th European LS-DYNA Users Conference, May 2003.

[Elsayed, 1997] Elsayed, N.M., "Toxicology of blast overpressure," Toxicology, Vol. 121, 1997, pp. 1-15.

[Fung, 1985] Fung, Y.C., Yen, M.R., Zeng, Y.J., "Characterization and modeling of thoraco-abdominal response to blast waves – Volume 3: Lung dynamics and mechanical properties determination," University of California, San Diego, Contract No. DAMD17-82-C-2062, supported by U.S. Army Medical Research and Development Command, Maryland, 1985.

[Fung, 1988] Fung, Y., Yen, R., Tao, Z., Liu, S., "A hypothesis on the mechanism of trauma of lung tissue subjected to impact load", Journal of Biomechanical Engineering, ASME, 1988.

[Fung, 1993] Fung, Y.C., Biomechanics: mechanical properties of living tissues – second edition, Springer-Verlag, New York, 1993.

[Garth, 1997] Garth, R.J.N., "Blast Injury to the Ear,"in: Scientific Foundations of Trauma, Butterworth-Heinemann, Jordan Hill, Oxford, 1997, pp. 225-235.

[Gest, 1995] Gest, T.R., Schlesinger, J., "MedCharts Anatomy," ILOC Inc., New York, 1995.

[Goss, 1978] Goss, S.A., Johnston, R.L., Dunn, F., "Comprehensive compilation of empirical ultrasonic properties of mammalian tissues," Journal of the acoustical society of America, Vol. 64, No. 2, August 1978, pp. 423-457.

[Gray, 1989] Gray, H., Gray's anatomy, 37th edition, Edinburgh; New York, Churchill Livinstone, 1989.

[Grimal, 2002] Grimal, Q., Watzky, A., Naili, S., 2002, "A one-dimensional model for the propagation of transient pressure waves through the lung", Journal of Biomechanics 35, pp. 1081-1089.

[Guelph, 2005] University of Guelph, Department of Integrative Biology, http://www.uoguelph.ca/zoology/devobio/210labs/endol.html, Guelph, Ontario, Canada.

[Guyton, 1996] Guyton A.C., Hall J.E., 1996, Textbook of medical physiology – 9th edition, W.B. Saunders Company, Toronto.

[Halquist, 1998] Hallquist, J.O., "LS-DYNA Theory Manual," Livermore Software Technology Corporation, Livermore, California, 1998.

[Halquist, 2003] Livermore Software Technology Corporation, "LS-DYNA Keyword User's Manual – Version 970," Livermore Software Technology Corporation, April 2003.

[Ho, 2002] Ho, A.M.-H., "A Simple Conceptual Model of Primary Pulmonary Blast Injury," Medical Hypotheses, Elsevier Science Ltd, 2002, Vol. 59, Issue 5, pp. 611-613.

[Januszkiewicz, 1997] Januszkiewicz, A.J., Mundie, T.G., Dodd, K.T., "Maximal exercise performance-impairing effects of simulated blast overpressure in sheep," Toxicology, Vol. 121, 1997, pp. 51-63.

[Johansson, 1970] Johansson, C.H., Persson, P.A., Detonics of High Explosives, Academic Press, New York, 1970.

[Jönsson, 1979] Jönsson, A., "Experimental investigations on the mechanisms of lung injury in blast and impact exposure." Ph.D. dissertation, No. 80, Department of Surgery, Linköping University and National Defence Research Establishment, Stockholm, Sweden, 1979.

[Josephson, 1988] Josephson, L., Tomlinson, P., "Predicted thoraco-abdominal response to complex blast waves", The journal of trauma, Vol. 28, No. 1 Supplement, 1988.

[Junkui, 1996] Junkui, Z., Zhengguo, W., Huaguang, L., Zhihuan, Y., "Studies on lung injuries caused by blast underpressure," The Journal of Trauma: Injury, Infection, and Critical Care. Vol. 40, No. 3, 1996.

[Kinney, 1962] Kinney, G.F., Explosive Shocks in Air, The Macmillan Company, New York, 1962.

[Mayorga, 1997] Mayorga, M.A., "The pathology of primary blast overpressure injury," Toxicology, Vol. 121, 1997, pp. 17-28.

[McConville, 1980] McConville, J.T., Churchill, T.D., Kaleps, I., Clauser, C.E., and Cuzzi, J., 1980, "Anthropometric relationships of body and body segment moments of inertia", Wright-Patterson AFB, Aerospace Medical Research Laboratory, AMRL-TR-80-119.

[McElhaney, 1966] McElhaney, J.H., "Dynamic response of bone and muscle tissue," Journal of applied physiology, Vol 21, pp.1231-1236.

[Mellor, 1992] Mellor, S.G., "The relationship of blast loading to death and injury from explosion," World Journal of Surgery, Vol. 16, pp. 893-898, 1992.

[Meyers, 1994] Meyers, M.A., Dynamic Behavior of Materials, John Wiley & Sons, Inc., Toronto, 1994.

[Motuz, 2001a] Motuz, J., Cronin, D., Worswick, M.J., "Arbitrary lagrangian eulerian modeling of a landmine explosion coupled to a lagrangian leg mesh," Defence Research Establishment Valcartier, Contract Report: DREV CR # 2001-01-23.

[Motuz, 2001b] Motuz, J., Cronin, D.S., Worswick, M.J., Williams, K., Bourget, D., Pageau, G., "Numerical modeling of a simplified surrogate leg subject to an anti-personnel blast mine," 2001, 19th International Symposium of Ballistics, Interlaken, Switzerland.

[Mow, 1991] Mow, V.C., Hayes, W.C., Basic orthopaedic biomechanics, Raven Press, New York, 1991.

[NLM, 2004] National Library of Medicine (NLM), The Visible Human Project, National Institutes of Health, www.nlm.nih.gov/research/visible/visible_human.html.

[NPL, UK, 2005] National Physical Laboratory, Acoustics: www.npl.co.uk/acoustics/techguides/beginnersguide/, Teddington, Middlesex, UK.

[Phillips, 1988] Phillips, Y.Y., Mundie, T.G., Yelverton, J.T., Richmond, D.R., 1988, "Cloth ballistic vest alters response to blast", The journal of trauma, Vol. 28, No. 1 Supplement.

[Richmond, 1968] Richmond, D.R., Damon, E.G., Fletcher, E.R., Bowen, I.G., White, C.S., "The relationship between selected blast-wave parameters and the response of mammals exposed to air blast," Annals of the New York Academy of Sciences, 1968, Vol. 152, pp. 103-121.

[Richmond, 1989] Richmond, D.R., Yelverton, J.T., Fletcher, E.R., Phillips, Y.Y., "Physical correlates of eardrum rupture," Annals of Otology, Rhinology & Laryngology, Suppl. 1989 May; 140: 35-41.

[Richmond, 1991] Richmond, D.R., "Blast criteria for open spaces and enclosures," Scandinavian Audiology, 1991, Vol. 34, Suppl., pp. 49-76.

[Richmond, 1993] Richmond, D.R., Damone, E.G., "Biomedical Effects of Impulse Noise." Forsvarets bygningstjeneste, Fortfikatorisk notat nr 209/93, Section 7, Norway, 1993, pp 38-51.

[Ripple, 1997] Ripple, R., Phillips, Y., 1997, "Military Explosions", in: Scientific Foundations of Trauma, Butterworth-Heinemann, Jordan Hill, Oxford, pp. 247-257.

[Roberts, 1970] Roberts, S.B., Chen, P.H., "Elastostatic analysis of the human thoracic skeleton," Journal of Biomechanics, Vol. 3, pp.527-545, 1970.

[Robbins, 1983] Robbins, D.H., 1983, Anthropometric Specifications for the Mid-Sized Male Dummy, Volume 2, The University of Michigan Transportation Research Institute, U.S. Department of Transportation National Highway Traffic Safety Administration, UMTRI-83-53-2.

[Rohen, 2002] Rohen, J.W., Yokochi, C., Juetjen-Drecoll, E., Color Atlas of Anatomy: A Photographic Study of the Human Body, 5th Edition, Lippincott Williams & Wilkins, New York, 2002

[Rott, 1999] Rott, H.D., 1999, "EFSUMB: Tutorial – Acoustic cavitation and capillary bleeding – European Committee for Medical Ultrasound Safety (ECMUS)", European Journal of Ultrasound, 9, pp. 277-280

[Salisbury, 2004] Salisbury, C.P., Investigation of the Arbitrary Lagrangian Eulerian Formulation to Simulate Shock Tube Problems, 8th International LS-DYNA Users Conference, Dearborn, Michigan, May 2004.

[Souli, 2004] Souli, M., Advanced Course in ALE and Fluid/Structure Coupling, Livermore Software Technology Corporation, Livermore California, 2004.

[Spitzer, 1996] Spitzer, V., Ackerman, M.J., Scherzinger, A.L., Whitlock, D., The visible human male: a technical report, Journal of the American Medical Informatics Association, Vol. 3, No. 2, 1996.

[Stuhmiller, 1985] Stuhmiller, J.H. (Principal Investigator), "Characterization and modeling of thoraco-abdominal response to blast waves – Volume 1: Project Summary," 1985, Jaycor, California, Contract No. DAMD17-82-C-2062, supported by U.S. Army Medical Research and Development Command, Maryland.

[Stuhmiller, 1988] Stuhmiller, J., Chuong, C., Phillips, Y., Dodd, K., "Computer modeling of thoracic response to blast," The Journal of Trauma, Vol. 28, No. 1 Supplement, 1988.

[Stuhmiller, 1996] Stuhmiller, J., Ho, K., Vorst, M., Dodd, K., Fitzpatrick, T., Mayorga, M., "A model of blast overpressure in jury to the lung." Journal of Biomechanics, Vol. 29, No. 2, pp. 227-234, 1996.

[Stuhmiller, 1997] Stuhmiller, J., "Biological response to blast overpressure: A summary of modeling," Toxicology, Vol. 121 (1997) 91-103.

[Stuhmiller, 1998] Stuhmiller, J.H., Phillips, Y., et al., 1998, "Conventional Warfare: Ballistic, Blast, and Burn Injuries", In: Textbook of Military Medicine, Part I, Vol. 5. Office of the Surgeon General, Department of the Army, Washington, DC.

[Tamagawa, 1996] Tamagawa, M., Akamatsu, T., "Effects of shock waves on living tissues: Numerical analysis of a propagating pressure wave toward living tissue," JSME International Journal, Series B, Vol. 39, No. 4, 1996, pp. 714-720.

[Thuraisingham, 1998] Thuraisingham, R.A., "Sound speed in bubbly water at megahertz frequencies," Ultrasonics, Vol. 36, 1998, pp. 767-773.

[Van Sligtenhorst, 2003] Van Sligtenhorst, C.R., Cronin, D.S., Brodland, G.W., "High strain rate compressive properties of soft tissue," American Society of Mechanical Engineers, Bioengineering Division BED, Vol. 55.

[Vawter, 1979] Vawter, D., Fung, Y.C., West, J., 1979, "Constitutive equation of lung tissue elasticity", Journal of Biomechanical Engineering, ASME, Vol. 101.

[Viano, 1986] Viano, D.C., "Biomechanics of bone and tissue: a review of material properties and failure characteristics," Proceedings – Society of Automotive Engineers, pp. 33-63, 1986.

[von Gierke, 1968] von Gierke, H.E., "Response of the Body to Mechanical Forces - An Overview," Annals New York Academy of Sciences, 1968, Vol. 152, pp. 172-186.

[White, 1971] White, C.S., Jones, R.K., Damon, E.G., Fletcher, E.R., Richmond, D.R., "The biodynamics of air blast," Technical report DNA2738T. Defense Nuclear Agency, Washington, D.C., 1971.

[White, 1971] White, C.S., Jones, R.K., Damon, E.G., Fletcher, E.R., Richmond, D.R., (1971) "The biodynamics of air blast," Technical report DNA2738T, Defense Nuclear Agency, Washington, DC.

[Wightman, 2001] Wightman, J.M., Gladish, S.L., "Explosions and blast injuries," Annals of emergency medicine, Vol. 37, No. 6, June 2001.

[Wilbeck, 1978] Wilbeck, J.S., "Impact behavior of low strength projectiles," University of Dayton Research Institute for the Air Force Materials Laboratory, Wright-Patterson Air Force Base, OH. Technical Report AFML-TR-77-134, July 1978.

[Williams, 2004] Williams, K. "Mabil Phase III - June 04 Trials Plan", DRDC- Valcartier Document Number 3772-2RA03, 2004.

[Williams, 2005] Williams, K., Personal communication, Vulnerability/Lethality Weapons Effects Section, Defence R&D Canada – Valcartier, Canada, 2005.

[Wilson, 2005] Wilson, P.S., "Low-frequency dispersion in bubbly liquids," Acoustics Research Letters Online, Acoustical Society of America, 2005.

[Yamada, 1970] Yamada, H., Strength of biological materials, Evans, F.G., ed. Williams and Wilkins, Baltimore, 1970.

[Yen, 1985] Yen, R.T., Fung, Y.C., 1985, "Thoracic trauma study: rib markings on the lung due to impact are marks of collapsed alveoli, not hemorrhage", ASME - Journal of Biomechanical Engineering, Vol. 107.

[Yen, 1986] Yen, R.T., Fung, Y.C., Ho, H.H., Butterman, G., 1986, "Speed of stress wave propagation in lung", Journal of applied physiology.

[Yen, 1999] Yen, M., 1999, "Mechanical properties of human heart, lung and aorta for highway safety research" The university of Memphis, Memphis, U.S.A.

[Yoganandan, 1998] Yoganandan, N., Pintar, F.A., "Biomechanics of human thoracic ribs," Journal of biomechanical engineering, Transactions of the ASME, Vol 120, pp. 100-104, 1998.

[Yu, 1990] Yu, J.H.-Y., Vasel, E.J. and Stuhmiller, J.H., "Design and field test of a blast overpressure test module," Final report for USAMRDC Contract DAMD17-85-C-5238, JAYCOR, San Diego, CA.

[Zel'dovich, 1967] Zel'dovich, Y.B., Raizer, Y.P., Physics of shock waves and high-temperature hydrodynamic phenomena – Volume 2, Academic Press, New York, 1967.